P-wave quarkonium wavefunctions at the origin in the $\overline{\rm MS}$ scheme

Hee Sok Chung

Physik-Department, Technische Universität München,
James-Franck-Str. 1, 85748 Garching, Germany
Excellence Cluster ORIGINS,
Boltzmannstrasse 2, D-85748 Garching, Germany

E-mail: heesok.chung@tum.de

ABSTRACT: We compute *P*-wave quarkonium wavefunctions at the origin in the $\overline{\rm MS}$ scheme based on nonrelativistic effective field theories. We include nonperturbative effects from the long-distance behaviors of the potential, while the short-distance behaviors are determined from perturbative QCD. We obtain $\overline{\rm MS}$-renormalized *P*-wave quarkonium wavefunctions at the origin that have the correct scale dependences that are expected from factorization formalisms, so that the dependences on the scheme and scale cancel in physical quantities. This greatly reduces the theoretical uncertainties associated with scheme and scale dependences in predictions of decay and production rates. Based on the calculation of the *P*-wave wavefunctions at the origin in this work, we make first-principles predictions of electromagnetic decay rates and exclusive electromagnetic production rates of *P*-wave charmonia and bottomonia, and compare them with measurements.

https://doi.org/10.1007/JHEP09(2021)195

Contents

1 Introduction

Production and decay of *P*-wave heavy quarkonia have played important roles in studies of nonrelativistic effective field theories of QCD. An early triumph of rigorous QCD analyses of heavy quarkonia based on the nonrelativistic QCD (NRQCD) effective field theory is the resolution of the problem of infrared divergences in *P*-wave heavy quarkonium production and decay rates [1–4]. The infrared divergences in perturbative QCD calculations are removed through renormalization of NRQCD long-distance matrix elements (LDMEs), which are well-defined universal quantities that encode the nonperturbative nature of heavy quarkonium states. This way, nonrelativistic effective field theory methods eliminate the need for ad hoc remedies for cutting off singularities, and make possible computations of production and decay rates of *P*-wave heavy quarkonia based on first principles. Ongoing experimental activities in lepton and hadron colliders call for continued theoretical efforts for making accurate QCD-based predictions of *P*-wave quarkonium production and decay [5–9].

NRQCD describes hard processes like decays of quarkonia into light particles in terms of factorization formulae, which separate the perturbative short-distance contributions from the nonperturbative physics that the LDMEs describe [4]. The LDMEs have known scalings in v, the typical heavy-quark velocity inside the quarkonium, and the factorization formulae are organized in powers of v. First-principles calculations of decay and production rates can be made by computing the short-distance coefficients and LDMEs in QCD. The short-distance coefficients can be determined perturbatively by matching the factorization formulae with perturbative QCD amplitudes. Infrared divergences in perturbative QCD amplitudes are absorbed into the LDMEs, and leave their trace in the short-distance coefficients as dependences on the scheme and scale at which the LDMEs are renormalized. The scheme and scale dependences cancel between the LDMEs and short-distance coefficients in the factorization formulae, as long as the LDMEs are renormalized in the same scheme. The scale at which the LDMEs are renormalized is often called the NRQCD factorization scale. In order to make accurate predictions of heavy quarkonium production and decay rates, it is crucial that we obtain LDMEs that have the correct dependences on the factorization scale, especially when the short-distance coefficients have strong scheme and scale dependences. Loop-level calculations of short-distance coefficients show that strong dependences on the factorization scale in the $\overline{\rm MS}$ scheme begin to appear from next-to-next-to-leading order in the strong coupling α_s in electromagnetic decay rates and exclusive electromagnetic production cross sections of heavy quarkonia [10–15]. Cancellation of the factorization scale dependence in the factorization formulae requires calculations of the LDMEs in the same scheme that has the correct dependence on the $\overline{\rm MS}$ scale. This has so far not been possible for *P*-wave heavy quarkonia, and most phenomenological studies have relied on model calculations of LDMEs, which are not accurate enough to reproduce their scheme and scale dependences correctly.

For *S*-wave heavy quarkonium states, a recent progress in ref. [16] has made possible first-principles calculations of LDMEs in the $\overline{\rm MS}$ scheme that correctly reproduce the factorization scale dependences at two-loop level. The factorization scale dependences in

the LDMEs arise from inclusion of the ultraviolet (UV) divergent effects that come from interactions in NRQCD that are suppressed by powers of $1/m$, where m is the heavy quark pole mass. This lead to accurate predictions of decay rates and decay constants of S-wave heavy quarkonia through exact cancellations of factorization scale dependences in the factorization formulas at two-loop accuracy, which has not been possible outside of perturbative QCD [17]. An unexpected consequence of this calculation is that large cancellations occur between the scheme-dependent finite parts of the two-loop short-distance coefficients and the finite parts in the LDMEs that remain after subtraction of the UV divergences, which improves the convergence of the corrections and enhances the reliability of the theoretical predictions that are based on fixed-order calculations of short-distance coefficients. As short-distance coefficients for electromagnetic decay and exclusive electromagnetic production rates of P-wave heavy quarkonia have recently become available to two-loop accuracy [14, 15], it is highly desirable to extend the calculation in ref. [16] to P-wave states.

In this paper, we compute NRQCD LDMEs of P-wave heavy quarkonia in the $\overline{\text{MS}}$ scheme by extending the calculation in ref. [16] to P-wave states. We focus on the LDMEs that appear at leading order in v, because short-distance coefficients associated with LDMEs beyond leading order in v are available only at tree level [18]. We compute the LDMEs by using the potential NRQCD (pNRQCD) effective field theory framework, which provides expressions of NRQCD LDMEs in terms of quarkonium wavefunctions and their derivatives at the origin [19–23]. The quarkonium wavefunctions are bound-state solutions of a Schrödinger equation, whose potential is obtained by matching NRQCD and pNRQCD order by order in expansion in powers of $1/m$. We work in the strong coupling regime, where $mv \gtrsim \Lambda_{\text{QCD}} \gg mv^2$, which is adequate for describing P-wave heavy quarkonia [22, 24]. Here, mv and mv^2 correspond to the typical sizes of the momentum and binding energy of the heavy quark Q and antiquark $\bar{Q}$ inside the quarkonium at rest, respectively. In this case, the nonperturbative long-distance behavior of the potential is important in calculation of quarkonium wavefunctions.

In pNRQCD calculations of NRQCD LDMEs, the UV divergences are reproduced by singularities in the wavefunctions or their derivatives at the origin. The singularities in the wavefunctions are generated by the corrections to the potential beyond leading power in $1/m$, which can diverge faster than the potential at leading power in $1/m$ in the limit where the distance between the Q and $\bar{Q}$ vanishes. Hence, we reproduce the UV divergences in the NRQCD LDMEs by including the corrections to the wavefunctions from the potentials at higher orders in $1/m$. The singularities are sensitive to the divergent short-distance behaviors of the potential, so that in the strong coupling regime, it is necessary to keep both the nonperturbative long-distance behavior and the perturbative short-distance behavior of the potential. In this case, a difficulty arises from the fact that the nonperturbative long-distance behavior of the potential is known only in position space, while renormalization of the UV divergence in the $\overline{\text{MS}}$ scheme is done in momentum space. This difficulty can be overcome by using the method adopted in refs. [16, 17, 25], where the singularities in the wavefunctions are first regularized in position space, which can then be converted to dimensional regularization (DR) by computing the scheme conversion. The scheme

conversion depends only on the divergent behavior of the wavefunctions at the origin, and can be computed in perturbative QCD. Then, the dimensionally regulated wavefunctions at the origin can be renormalized in the $\overline{\text{MS}}$ scheme. The result can be combined with the $\overline{\text{MS}}$ calculations of the short-distance coefficients to make predictions of decay and production rates of P-wave heavy quarkonia.

This paper is organized as follows. In section 2, we define the NRQCD LDMEs that appear in P-wave production and decay rates in forms that are suitable for calculations in DR. The pNRQCD expressions for the NRQCD LDMEs are given in section 3. We outline the position-space calculation of the wavefunctions in section 4, and compute the scheme conversion from position-space regularization to the $\overline{\text{MS}}$ scheme in section 5. Based on the calculations of the $\overline{\text{MS}}$ wavefunctions, we compute decay rates, production cross sections, and decay constants of P-wave charmonia and bottomonia in section 6. We conclude in section 7.

2 NRQCD long-distance matrix elements and their renormalization

Electromagnetic decay rates and exclusive electromagnetic production rates of P-wave heavy quarkonia at leading orders in v involve the following dimension-5 LDMEs [4]:

$$\langle\mathcal{Q}|\mathcal{O}(^3P_0)|\mathcal{Q}\rangle = \frac{1}{3}\left|\langle 0|\chi^\dagger\left(-\frac{i}{2}\overleftrightarrow{\boldsymbol{D}}\right)\cdot\boldsymbol{\sigma}\psi|\mathcal{Q}\rangle\right|^2, \tag{2.1a}$$

$$\langle\mathcal{Q}|\mathcal{O}(^3P_1)|\mathcal{Q}\rangle = \frac{1}{2}\left|\langle 0|\chi^\dagger\left(-\frac{i}{2}\overleftrightarrow{\boldsymbol{D}}\right)\times\boldsymbol{\sigma}\psi|\mathcal{Q}\rangle\right|^2, \tag{2.1b}$$

$$\langle\mathcal{Q}|\mathcal{O}(^3P_2)|\mathcal{Q}\rangle = \left|\langle 0|\chi^\dagger\left(-\frac{i}{2}\overleftrightarrow{D}^{(i}\right)\sigma^{j)}\psi|\mathcal{Q}\rangle\right|^2, \tag{2.1c}$$

$$\langle\mathcal{Q}|\mathcal{O}(^1P_1)|\mathcal{Q}\rangle = \left|\langle 0|\chi^\dagger\left(-\frac{i}{2}\overleftrightarrow{\boldsymbol{D}}\right)\psi|\mathcal{Q}\rangle\right|^2. \tag{2.1d}$$

Here, $|\mathcal{Q}\rangle$ is a nonrelativistically normalized heavy quarkonium state at rest, $|0\rangle$ is the QCD vacuum, $\boldsymbol{D} = \boldsymbol{\nabla} - ig_s\boldsymbol{A}$ is the covariant derivative with $\chi^\dagger\overleftrightarrow{\boldsymbol{D}}\psi = \chi^\dagger\boldsymbol{D}\psi - (\boldsymbol{D}\chi)^\dagger\psi$, $\boldsymbol{A}$ is the gluon field, $\boldsymbol{\sigma}$ is a Pauli matrix, and ψ and χ are Pauli spinor fields that annihilate and create the heavy quark and antiquark, respectively. $T^{(ij)}$ is the symmetric traceless part of a tensor T^{ij}, which we define in $d-1$ spatial dimensions by $T^{(ij)} \equiv \frac{1}{2}(T^{ij} + T^{ji}) - \frac{1}{d-1}\delta^{ij}T^{kk}$. The spectroscopic notation $^{2S+1}P_J$ denote the spin (S), orbital (P), and total angular momentum (J) of the $Q\bar{Q}$ in the leading $Q\bar{Q}$ Fock state of the quarkonium state $|\mathcal{Q}\rangle$. Hence, the LDMEs $\langle\mathcal{Q}|\mathcal{O}(^3P_J)|\mathcal{Q}\rangle$, where $J = 0$, 1, or 2, appear in processes involving heavy quarkonia with positive parity and charge conjugation with total spin J, such as χ_{cJ} and χ_{bJ}. The $\langle\mathcal{Q}|\mathcal{O}(^1P_1)|\mathcal{Q}\rangle$ appear in processes involving states with positive parity and negative charge conjugation with total spin 1, such as the h_c and h_b.

The LDMEs in eqs. (2.1) depend on the scheme and scale Λ at which they are renormalized. The anomalous dimensions of the NRQCD LDMEs at leading order in v are given

by [26]

$$\frac{d}{d\log\Lambda}\log\langle 0|\chi^\dagger\left(-\frac{i}{2}\overleftrightarrow{\boldsymbol{D}}\right)\cdot\boldsymbol{\sigma}\psi|\mathcal{Q}\rangle = \alpha_s^2\gamma_{^3P_0}^{(2)} + O(\alpha_s^3), \tag{2.2a}$$

$$\frac{d}{d\log\Lambda}\log\langle 0|\chi^\dagger\left(-\frac{i}{2}\overleftrightarrow{\boldsymbol{D}}\right)\times\boldsymbol{\sigma}\psi|\mathcal{Q}\rangle = \alpha_s^2\gamma_{^3P_1}^{(2)} + O(\alpha_s^3), \tag{2.2b}$$

$$\frac{d}{d\log\Lambda}\log\langle 0|\chi^\dagger\left(-\frac{i}{2}\overleftrightarrow{D}^{(i}\right)\sigma^{j)}\psi|\mathcal{Q}\rangle = \alpha_s^2\gamma_{^3P_2}^{(2)} + O(\alpha_s^3), \tag{2.2c}$$

$$\frac{d}{d\log\Lambda}\log\langle 0|\chi^\dagger\left(-\frac{i}{2}\overleftrightarrow{\boldsymbol{D}}\right)\psi|\mathcal{Q}\rangle = \alpha_s^2\gamma_{^1P_1}^{(2)} + O(\alpha_s^3), \tag{2.2d}$$

where[1]

$$\gamma_{^3P_0}^{(2)} = \frac{2}{3}C_F^2 + \frac{1}{6}C_F C_A, \tag{2.3a}$$

$$\gamma_{^3P_1}^{(2)} = \frac{5}{12}C_F^2 + \frac{1}{6}C_F C_A, \tag{2.3b}$$

$$\gamma_{^3P_2}^{(2)} = \frac{13}{60}C_F^2 + \frac{1}{6}C_F C_A, \tag{2.3c}$$

$$\gamma_{^1P_1}^{(2)} = \frac{1}{3}C_F^2 + \frac{1}{6}C_F C_A. \tag{2.3d}$$

Here, $C_F = (N_c^2 - 1)/(2N_c)$, $C_A = N_c$, and $N_c = 3$ is the number of colors. We display the evolution equations at the amplitude level, because matching calculations for electromagnetic decay rates and exclusive electromagnetic production rates can be done by comparing $Q\bar{Q}$ amplitudes in QCD and NRQCD. We note that, similarly to the S-wave case, the anomalous dimensions of the P-wave LDMEs begin at two-loop level (order α_s^2). We neglect the contributions to the right-hand sides of eqs. (2.2) that come from LDMEs of higher orders in v, because their contributions to decay and production rates have so far been computed only at tree level [18]. The nonvanishing of the anomalous dimensions at order α_s^2 imply that, in carrying out the perturbative matching at two-loop level, the NRQCD LDMEs contain UV divergences that must be renormalized. In order to renormalize the LDMEs in the $\overline{\text{MS}}$ scheme, we use DR in $d = 4 - 2\epsilon$ spacetime dimensions to regulate the UV divergences. In perturbative matching calculations, renormalization of the LDMEs in the $\overline{\text{MS}}$ scheme at two-loop level is carried out in the following form:

$$\langle Q\bar{Q}|\mathcal{O}(^{2S+1}P_J)|Q\bar{Q}\rangle^{\overline{\text{MS}}} = \left[1 - \frac{\alpha_s^2}{2\epsilon_{\text{UV}}}\gamma_{^{2S+1}P_J}^{(2)} + O(\alpha_s^3)\right]\langle Q\bar{Q}|\mathcal{O}(^{2S+1}P_J)|Q\bar{Q}\rangle_{\text{bare}}^{\text{DR}}. \tag{2.4}$$

Here the LDMEs are written in terms of perturbative $Q\bar{Q}$ states, and computed in perturbation theory as series in α_s. We use the subscript UV to emphasize the ultraviolet origin of the $1/\epsilon$ pole. The terms in the square brackets on the right-hand side correspond to the multiplicative renormalization factor to two-loop accuracy, and the bare LDME is computed in DR in $d = 4 - 2\epsilon$ spacetime dimensions. In computing the perturbative LDMEs, we associate a factor of $(\Lambda^2\frac{e^{\gamma_{\text{E}}}}{4\pi})^\epsilon$ for every loop integral, so that the LDME on

---

[1]Our expressions of the anomalous dimensions have opposite signs compared to refs. [14, 15, 26], because we define them from the scale dependences of the LDMEs, rather than the short-distance coefficients.

the left-hand side of eq. (2.4) is renormalized in the $\overline{\text{MS}}$ scheme at scale Λ. In case of the nonperturbative LDMEs that are computed on quarkonium states, the $\overline{\text{MS}}$-renormalized LDMEs can also be defined by using eq. (2.4) with the perturbative $Q\bar{Q}$ states replaced by quarkonium states $\mathcal{Q}$, provided that the UV divergences in the (nonperturbative) bare LDMEs on quarkonium states are regularized in DR and expanded in powers of α_s.

If we expand the right-hand side of eq. (2.4) in powers of α_s to two-loop accuracy, we obtain

$$\langle Q\bar{Q}|\mathcal{O}(^{2S+1}P_J)|Q\bar{Q}\rangle^{\overline{\text{MS}}} = \langle Q\bar{Q}|\mathcal{O}(^{2S+1}P_J)|Q\bar{Q}\rangle^{\text{DR}}_{\text{bare, two-loop level}}$$

$$-\frac{\alpha_s^2}{2\epsilon_{\text{UV}}}\gamma^{(2)}_{^{2S+1}P_J}\langle Q\bar{Q}|\mathcal{O}(^{2S+1}P_J)|Q\bar{Q}\rangle^{\text{DR}}_{\text{bare, tree level}}, \quad (2.5)$$

where the subtraction term in the second line removes the UV pole in the two-loop level bare LDME. The subtraction term can have finite parts of order ϵ^0, which comes from the order-ϵ contribution to the tree-level bare LDME. Hence, both the tree- and two-loop level bare LDMEs must be computed in d spacetime dimensions in order to obtain the correct finite parts. In both the spin triplet and spin singlet cases, the LDMEs defined in eqs. (2.1) do not generalize to d spacetime dimensions in a straightforward way; in the $S = 1$ case, the operators $\mathcal{O}(^3P_J)$ are defined by using the irreducible representations of a rank-2 tensor under rotation in 3 spatial dimensions, which do not generalize to arbitrary spatial dimensions. In the $S = 0$ case, matching calculations in DR using the standard threshold expansion method in refs. [27, 28] lead to the totally antisymmetric product of three Pauli matrices given by $\{\sigma^i, [\sigma^j, \sigma^k]\}$ that appear between the $\chi^\dagger$ and ψ fields. While in 3 spatial dimensions this matrix is proportional to the 2×2 identity matrix, this is not generally true in DR. A similar combination of Pauli matrices is obtained in the covariant spin projector method [29, 30], if one uses γ_5 in the t'Hooft-Veltman scheme. In principle, any scheme that defines the LDMEs in d spacetime dimensions is valid as long as the LDMEs reduce to the 3-dimensional expressions in eqs. (2.1) in the limit $d \to 4$, but the scheme dependence will cancel in decay and production rates only when the short-distance coefficients are computed in the same scheme.

We now define the scheme that we use in this paper to compute the LDMEs in d spacetime dimensions, which is the same scheme that is used in existing calculations of short-distance coefficients at two-loop level.

In the $S = 0$ case, the following definition is consistent with loop-level calculations of short-distance coefficients that employs the t'Hooft-Veltman scheme for γ_5:

$$\langle \mathcal{Q}|\mathcal{O}(^1P_1)|\mathcal{Q}\rangle^{\text{DR}} = \left|\langle 0|\chi^\dagger\left(-\frac{i}{2}\overleftrightarrow{\boldsymbol{D}}\right)\sigma_5\psi|\mathcal{Q}\rangle\right|^2, \quad (2.6)$$

where σ_5 is a 2×2 matrix that reduces to the identity matrix in the limit $d \to 4$, and commutes with σ^i with 3-dimensional indices, while it anticommutes with σ^i with $d-4$-dimensional indices. This definition is also consistent with the threshold expansion method in refs. [27, 28], as long as we assume $\{\sigma^i, [\sigma^j, \sigma^k]\}$ have same commutation and anticommutation properties as σ_5. This form of σ_5 has been used in calculations of short-distance

coefficients for S-wave spin-singlet quarkonia in refs. [12, 31]. We note that an explicit form of σ_5 is unnecessary in dimensionally regulated matching calculations and also in calculations in this paper.

In the $S = 1$ case, we use the fact that any rank-2 tensor in arbitrary spatial dimensions can be written as the sum of its trace, antisymmetric, and symmetric traceless parts; that is, we use the identity $T^{ij} = T_S^{ij} + T_V^{ij} + T_T^{ij}$, where

$$T_S^{ij} = \frac{\delta^{ij}}{d-1}T^{kk}, \tag{2.7a}$$

$$T_V^{ij} = T^{[ij]} \equiv \frac{1}{2}\left(T^{ij} - T^{ji}\right), \tag{2.7b}$$

$$T_T^{ij} = T^{(ij)} \equiv \frac{1}{2}\left(T^{ij} + T^{ji}\right) - \frac{\delta^{ij}}{d-1}T^{kk}. \tag{2.7c}$$

In 3 spatial dimensions, T_S^{ij}, T_V^{ij}, and T_T^{ij} are just the irreducible representations of T^{ij} under rotations with spin 0, 1, and 2, respectively. We note that the tensors T_S^{ij}, T_V^{ij}, and T_T^{ij} are orthogonal, in the sense that

$$T_S^{ij}T_V^{ij} = T_V^{ij}T_T^{ij} = T_T^{ij}T_S^{ij} = 0, \tag{2.8}$$

which is valid in $d - 1$ spatial dimensions. These relations imply that $T_S^{ij}T^{ij} = (T_S^{ij})^2$, $T_V^{ij}T^{ij} = (T_V^{ij})^2$, and $T_T^{ij}T^{ij} = (T_T^{ij})^2$. We define the $S = 1$ LDMEs by applying this decomposition to the rank-2 tensor $\overleftrightarrow{D}^i\sigma^j$ in $d - 1$ spatial dimensions. We begin with the expression

$$\sum_{J=0,1,2} \mathcal{O}(^3P_J) = \psi^\dagger\left(-\frac{i}{2}\overleftrightarrow{D}^i\right)\sigma^j\chi|0\rangle\langle 0|\chi^\dagger\left(-\frac{i}{2}\overleftrightarrow{D}^i\right)\sigma^j\psi, \tag{2.9}$$

which is valid in 3 spatial dimensions, and generalize it to $d - 1$ spatial dimensions. We decompose the tensor $\overleftrightarrow{D}^i\sigma^j$ into the trace, antisymmetric, and symmetric traceless parts, and define each contribution as the LDME of total spin 0, 1, and 2, respectively. We obtain, for $J = 0$,

$$\langle\mathcal{Q}|\mathcal{O}(^3P_0)|\mathcal{Q}\rangle^{\mathrm{DR}} = \langle\mathcal{Q}|\psi^\dagger\left(-\frac{i}{2}\overleftrightarrow{D}^i\right)\sigma^j\chi|0\rangle \times \frac{\delta^{ij}}{d-1}\langle 0|\chi^\dagger\left(-\frac{i}{2}\overleftrightarrow{\boldsymbol{D}}\right)\cdot\boldsymbol{\sigma}\psi|\mathcal{Q}\rangle$$

$$= \frac{1}{d-1}\left|\langle 0|\chi^\dagger\left(-\frac{i}{2}\overleftrightarrow{\boldsymbol{D}}\right)\cdot\boldsymbol{\sigma}\psi|\mathcal{Q}\rangle\right|^2. \tag{2.10}$$

For $J = 1$, we have

$$\langle\mathcal{Q}|\mathcal{O}(^3P_1)|\mathcal{Q}\rangle^{\mathrm{DR}} = \langle\mathcal{Q}|\psi^\dagger\left(-\frac{i}{2}\overleftrightarrow{D}^i\right)\sigma^j\chi|0\rangle\langle 0|\chi^\dagger\left(-\frac{i}{2}\overleftrightarrow{D}^{[i}\right)\sigma^{j]}\psi|\mathcal{Q}\rangle$$

$$= \left|\langle 0|\chi^\dagger\left(-\frac{i}{2}\overleftrightarrow{D}^{[i}\right)\sigma^{j]}\psi|\mathcal{Q}\rangle\right|^2. \tag{2.11}$$

It can be shown easily that this expression reduces to the 3-dimensional one by using the identity $\delta_{ik}\delta_{j\ell} - \delta_{i\ell}\delta_{jk} = \epsilon_{nij}\epsilon_{nk\ell}$, where ϵ_{ijk} is the totally antisymmetric tensor with $\epsilon_{123} = 1$ in 3 spatial dimensions. Finally, for $J = 2$, we obtain

$$\langle\mathcal{Q}|\mathcal{O}(^3P_2)|\mathcal{Q}\rangle^{\mathrm{DR}} = \langle\mathcal{Q}|\psi^\dagger\left(-\frac{i}{2}\overleftrightarrow{D}^i\right)\sigma^j\chi|0\rangle\langle 0|\chi^\dagger\left(-\frac{i}{2}\overleftrightarrow{D}^{(i}\right)\sigma^{j)}\psi|\mathcal{Q}\rangle$$

$$= \left|\langle 0|\chi^\dagger\left(-\frac{i}{2}\overleftrightarrow{D}^{(i}\right)\sigma^{j)}\psi|\mathcal{Q}\rangle\right|^2. \tag{2.12}$$

We note that these definitions of ^3P_J LDMEs are consistent with the calculations of short-distance coefficients in DR in refs. [14, 15, 32].

We have now established the definitions of NRQCD LDMEs that are suitable for calculations in DR. These definitions are consistent with the $\overline{\text{MS}}$ calculations of the short-distance coefficients for production and decay of P-wave heavy quarkonia. In this paper, we compute the $\overline{\text{MS}}$-renormalized LDMEs using these definitions, so that we can obtain theoretical predictions for production and decay rates of P-wave heavy quarkonia that are independent of the scheme and scale in which the NRQCD LDMEs are renormalized.

3 P-wave long-distance matrix elements in pNRQCD

We now compute the NRQCD LDMEs in eqs. (2.1) in pNRQCD [19–23]. In strongly coupled pNRQCD, the LDMEs are given by [22, 24]

$$\langle \mathcal{Q}|\mathcal{O}(^{2S+1}P_J)|\mathcal{Q}\rangle = \int d^3r \int d^3r' \int d^3R\, \Psi_\mathcal{Q}^*(\boldsymbol{r})$$
$$\times \left[-V_\mathcal{O}(\boldsymbol{x}_1,\boldsymbol{x}_2;\boldsymbol{\nabla}_1,\boldsymbol{\nabla}_2)\delta^{(3)}(\boldsymbol{x}_1-\boldsymbol{x}_1')\delta^{(3)}(\boldsymbol{x}_2-\boldsymbol{x}_2')\right]\Psi_\mathcal{Q}(\boldsymbol{r}'), \quad (3.1)$$

where the contact term $V_\mathcal{O}$ is the matching coefficient obtained by matching nonperturbatively to NRQCD in an expansion in powers of $1/m$. Here, $\boldsymbol{r} = \boldsymbol{x}_1 - \boldsymbol{x}_2$ and $\boldsymbol{r}' = \boldsymbol{x}_1' - \boldsymbol{x}_2'$ are the relative coordinates between the quark and antiquark. The quarkonium wavefunction $\Psi_\mathcal{Q}(\boldsymbol{r})$, which we take to be unit normalized, satisfies the Schrödinger equation

$$\left[-\frac{\boldsymbol{\nabla}}{m} + V(\boldsymbol{r},\boldsymbol{\nabla})\right]\Psi_\mathcal{Q}(\boldsymbol{r}) = E_\mathcal{Q}\Psi_\mathcal{Q}(\boldsymbol{r}), \quad (3.2)$$

where $\boldsymbol{\nabla} = \boldsymbol{\nabla}_r$. The potential $V(\boldsymbol{r},\boldsymbol{\nabla})$ is obtained by matching pNRQCD to NRQCD order by order in expansion in powers of $1/m$, and $E_\mathcal{Q}$ is the binding energy of the $\mathcal{Q}$ state. For the LDMEs in eq. (2.1), the $V_\mathcal{O}$ are given by [22, 24]

$$V_{\mathcal{O}(^{2S+1}P_J)} = N_c T_{SJ}^{ij}\nabla_{\boldsymbol{r}}^i\left[1 + \frac{2}{3}\frac{i\mathcal{E}_2}{m} + O(1/m^2)\right]\delta^{(3)}(\boldsymbol{r})\nabla_{\boldsymbol{r}}^j, \quad (3.3)$$

where T_{SJ}^{ij} are the spin projections in 3 spatial dimensions that are given by

$$T_{10}^{ij} = \frac{1}{3}\sigma^i \otimes \sigma^j, \quad (3.4\text{a})$$

$$T_{11}^{ij} = \frac{1}{2}\epsilon_{kim}\epsilon_{kjn}\sigma^m \otimes \sigma^n, \quad (3.4\text{b})$$

$$T_{12}^{ij} = \left(\frac{\delta_{im}\sigma^n + \sigma_{in}\sigma^m}{2} - \frac{\delta_{mn}}{3}\sigma^i\right) \otimes \left(\frac{\delta_{jm}\sigma^n + \sigma_{jn}\sigma^m}{2} - \frac{\delta_{mn}}{3}\sigma^j\right), \quad (3.4\text{c})$$

$$T_{01}^{ij} = \delta^{ij}1 \otimes 1, \quad (3.4\text{d})$$

and $i\mathcal{E}_2$ is a gluonic correlator defined by [22, 24]

$$i\mathcal{E}_2 = \frac{iT_F}{N_c}\int_0^\infty dt\, t^2\langle 0|g_s\boldsymbol{E}^{i,a}(t,\boldsymbol{0})\Phi_{ab}(t,0)g_s\boldsymbol{E}^{i,b}(0,\boldsymbol{0})|0\rangle, \quad (3.5)$$

where $T_F = 1/2$, $\boldsymbol{E}^{i,a}T^a = G^{i0}$ is the chromoelectric field, $G^{\mu\nu}$ is the gluon field-strength tensor, and $\Phi_{ab}(t,0)$ is an adjoint Wilson line in the temporal direction connecting the

points $(0, \mathbf{0})$ and $(t, \mathbf{0})$. The expressions for T_{SJ}^{ij} follow from the 3-dimensional definitions of the LDMEs in eqs. (2.1). The spin indices on the Pauli matrices in T_{SJ}^{ij} on the left and right of the $\otimes$ symbol contract with the implicit Q and $\bar{Q}$ spin indices on the wavefunctions $\Psi_{\mathcal{Q}}^*(\mathbf{r})$ and $\Psi_{\mathcal{Q}}(\mathbf{r})$, respectively. Since the gluonic correlator $i\mathcal{E}_2$ scales like Λ_{QCD}, the LDMEs computed from eq. (3.3) are accurate to relative order Λ_{QCD}/m, and the uncalculated order $1/m^2$ terms in the contact term give corrections to the LDMEs of at most order v^2. Hence, eq. (3.3) implies that

$$\langle \mathcal{Q}|\mathcal{O}(^{2S+1}P_J)|\mathcal{Q}\rangle = N_c \left[\left(\boldsymbol{\nabla}_{\mathbf{r}}^i \Psi_{\mathcal{Q}}^*(\mathbf{r})\right) T_{SJ}^{ij} \left(\boldsymbol{\nabla}_{\mathbf{r}}^j \Psi_{\mathcal{Q}}(\mathbf{r})\right)\right]_{\mathbf{r}=\mathbf{0}} \times \left[1 + \frac{2}{3}\frac{i\mathcal{E}_2}{m} + O(v^2)\right]. \quad (3.6)$$

The spin projections in eq. (3.6) can be simplified when the wavefunctions $\Psi_{\mathcal{Q}}(\mathbf{r})$ have definite $^{2S+1}P_J$ quantum numbers, so that the wavefunction at the origin $\boldsymbol{\nabla}\Psi_{\mathcal{Q}}(\mathbf{0}) \equiv \boldsymbol{\nabla}_{\mathbf{r}}\Psi_{\mathcal{Q}}(\mathbf{r} = \mathbf{0})$ is annihilated by all but one of the T_{SJ}^{ij}. In this case, from the completeness of spin projections we have $(\boldsymbol{\nabla}^i \Psi_{\mathcal{Q}}^*(\mathbf{0}))T_{SJ}^{ij}(\boldsymbol{\nabla}^j \Psi_{\mathcal{Q}}(\mathbf{0})) = 2|\boldsymbol{\nabla}\Psi_{\mathcal{Q}}(\mathbf{0})|^2$. Here, the factor 2 comes from the trace over the spin indices of $\sum_{S,J} T_{SJ}^{ij}$. It is useful to compute the average over the polarization of the $\mathcal{Q}$ state, because of rotational symmetry, the LDME for each polarization is the same as the average of the LDMEs over polarizations of the $\mathcal{Q}$ state. We write the average of $|\boldsymbol{\nabla}\Psi_{\mathcal{Q}}(\mathbf{0})|^2$ over polarizations as $\overline{|\boldsymbol{\nabla}\Psi_{\mathcal{Q}}(\mathbf{0})|^2}$. In this case, since there is no preferred direction, we obtain

$$\overline{|\boldsymbol{\nabla}\Psi_{\mathcal{Q}}(\mathbf{0})|^2} = \overline{|\hat{\mathbf{r}} \cdot \boldsymbol{\nabla}\Psi_{\mathcal{Q}}(\mathbf{0})|^2}, \quad (3.7)$$

where $\hat{\mathbf{r}} = \mathbf{r}/|\mathbf{r}|$.

For the limit $\mathbf{r} \to \mathbf{0}$ to be meaningful, $\boldsymbol{\nabla}_{\mathbf{r}}\Psi_{\mathcal{Q}}(\mathbf{r})$ must be regular at $\mathbf{r} = \mathbf{0}$. That is, the limit $\mathbf{r} \to \mathbf{0}$ cannot be taken if $\boldsymbol{\nabla}_{\mathbf{r}}\Psi_{\mathcal{Q}}(\mathbf{r})$ is divergent at $\mathbf{r} = \mathbf{0}$. Since $\mathcal{E}_2$ does not have logarithmic UV divergences, the anomalous dimension of the LDME $\langle \mathcal{Q}|\mathcal{O}(^{2S+1}P_J)|\mathcal{Q}\rangle$ must come from $\boldsymbol{\nabla}\Psi_{\mathcal{Q}}(\mathbf{0})$.[2] That is, the derivative of the wavefunction at the origin contains UV divergences, so that the limit $|\mathbf{r}| \to 0$ can only be taken after the divergences are subtracted through renormalization.

Since $\boldsymbol{\nabla}\Psi_{\mathcal{Q}}(\mathbf{0})$ is UV divergent, we need d-dimensional expressions of the LDMEs in terms of wavefunctions in order to compute the correct $\overline{\mathrm{MS}}$-renormalized LDMEs. Given our d-dimensional definitions of LDMEs, it is straightforward to find the d-dimensional versions of $V_{\mathcal{O}}$:

$$V_{\mathcal{O}(^{2S+1}P_J)}^{\mathrm{DR}} = N_c \bar{T}_{SJ}^{ij} \nabla_{\mathbf{r}}^i \left[1 + \frac{2}{3}\frac{i\mathcal{E}_2}{m} + O(1/m^2)\right] \delta^{(3)}(\mathbf{r})\nabla_{\mathbf{r}}^j, \quad (3.8)$$

where $\bar{T}_{SJ}^{ij}$ are the spin projections defined in $d-1$ spatial dimensions, given by

$$\bar{T}_{10}^{ij} = \frac{1}{d-1}\sigma^i \otimes \sigma^j, \quad (3.9\text{a})$$

$$\bar{T}_{11}^{ij} = \left(\frac{\delta_{im}\sigma^n - \delta_{in}\sigma^m}{2}\right) \otimes \left(\frac{\delta_{jm}\sigma^n - \delta_{jn}\sigma^m}{2}\right), \quad (3.9\text{b})$$

$$\bar{T}_{12}^{ij} = \left(\frac{\delta_{im}\sigma^n + \delta_{in}\sigma^m}{2} - \frac{\delta_{mn}}{d-1}\sigma^i\right) \otimes \left(\frac{\delta_{jm}\sigma^n + \delta_{jn}\sigma^m}{2} - \frac{\delta_{mn}}{d-1}\sigma^j\right), \quad (3.9\text{c})$$

$$\bar{T}_{01}^{ij} = \delta^{ij}\sigma_5 \otimes \sigma_5. \quad (3.9\text{d})$$

---

[2]This is consistent with the calculation of the anomalous dimensions in ref. [26], where the UV divergences in the NRQCD LDMEs are computed in terms of potential exchanges between Q and $\bar{Q}$.

It is easy to see that $\bar{T}_{SJ}^{ij}$ reduce to T_{SJ}^{ij} in 3 spatial dimensions. Strictly speaking, since the denominator factor 3 in the coefficient of $i\mathcal{E}_2/m$ in eq. (3.3) comes from the number of spatial dimensions, the term $\frac{2}{3}\frac{i\mathcal{E}_2}{m}$ in eq. (3.8) should instead read $\frac{2}{d-1}\frac{i\mathcal{E}_2}{m}$. However, since there are no poles in ϵ associated with $\mathcal{E}_2$, we can safely set $d = 4$ in this term. The dimensionally regulated NRQCD LDMEs are then given by

$$\langle \mathcal{Q}|\mathcal{O}(^{2S+1}P_J)|\mathcal{Q}\rangle^{\mathrm{DR}} = N_c \left[\left(\boldsymbol{\nabla}^i \Psi_{\mathcal{Q}}^*(\mathbf{0}) \right) \bar{T}_{SJ}^{ij} \left(\boldsymbol{\nabla}^j \Psi_{\mathcal{Q}}(\mathbf{0}) \right) \right] \times \left[1 + \frac{2}{3}\frac{i\mathcal{E}_2}{m} + O(v^2) \right]. \quad (3.10)$$

With these expressions at hand, we can write the $\overline{\mathrm{MS}}$-renormalization of the wavefunction at the origin at two-loop level as follows:

$$\left[\frac{\delta^{ij}\boldsymbol{\sigma} \cdot \boldsymbol{\nabla}}{d-1} \Psi_{\mathcal{Q}}(\mathbf{0}) \right]^{\overline{\mathrm{MS}}} = \left[1 - \frac{\alpha_s^2}{4\epsilon_{\mathrm{UV}}} \gamma_{^3P_0}^{(2)} + O(\alpha_s^3) \right] \left[\frac{\delta^{ij}\boldsymbol{\sigma} \cdot \boldsymbol{\nabla}}{d-1} \Psi_{\mathcal{Q}}(\mathbf{0}) \right]^{\mathrm{DR}}, \quad (3.11\mathrm{a})$$

$$\left[\sigma^{[i}\nabla^{j]} \Psi_{\mathcal{Q}}(\mathbf{0}) \right]^{\overline{\mathrm{MS}}} = \left[1 - \frac{\alpha_s^2}{4\epsilon_{\mathrm{UV}}} \gamma_{^3P_1}^{(2)} + O(\alpha_s^3) \right] \left[\sigma^{[i}\nabla^{j]} \Psi_{\mathcal{Q}}(\mathbf{0}) \right]^{\mathrm{DR}}, \quad (3.11\mathrm{b})$$

$$\left[\sigma^{(i}\nabla^{j)} \Psi_{\mathcal{Q}}(\mathbf{0}) \right]^{\overline{\mathrm{MS}}} = \left[1 - \frac{\alpha_s^2}{4\epsilon_{\mathrm{UV}}} \gamma_{^3P_2}^{(2)} + O(\alpha_s^3) \right] \left[\sigma^{(i}\nabla^{j)} \Psi_{\mathcal{Q}}(\mathbf{0}) \right]^{\mathrm{DR}}, \quad (3.11\mathrm{c})$$

$$\left[\sigma_5 \boldsymbol{\nabla} \Psi_{\mathcal{Q}}(\mathbf{0}) \right]^{\overline{\mathrm{MS}}} = \left[1 - \frac{\alpha_s^2}{4\epsilon_{\mathrm{UV}}} \gamma_{^1P_1}^{(2)} + O(\alpha_s^3) \right] \left[\sigma_5 \boldsymbol{\nabla} \Psi_{\mathcal{Q}}(\mathbf{0}) \right]^{\mathrm{DR}}, \quad (3.11\mathrm{d})$$

where the spin indices on $\boldsymbol{\sigma}$ and σ_5 contract with the implicit Q and $\bar{Q}$ spin indices on the wavefunctions. These expressions provide definitions of the spin projections onto states with definite $^{2S+1}P_J$ quantum numbers in $d-1$ spatial dimensions, and are consistent with the $\overline{\mathrm{MS}}$ renormalization of the NRQCD LDMEs. That is, when we compute the NRQCD LDMEs from the $\overline{\mathrm{MS}}$-renormalized wavefunctions at the origin in eq. (3.11), we automatically obtain the correct $\overline{\mathrm{MS}}$-renormalized LDMEs. Once the wavefunctions are renormalized, so that the UV divergences regulated by nonzero $d-4$ are removed, the spin projections can now be computed in 3 spatial dimensions. The $\overline{\mathrm{MS}}$-renormalized LDMEs are then given by

$$\langle \mathcal{Q}|\mathcal{O}(^{2S+1}P_J)|\mathcal{Q}\rangle^{\overline{\mathrm{MS}}} = 2N_c \overline{\left| [\hat{\boldsymbol{r}} \cdot \boldsymbol{\nabla} \Psi_{\mathcal{Q}}(\mathbf{0})]^{\overline{\mathrm{MS}}} \right|^2} \times \left[1 + \frac{2}{3}\frac{i\mathcal{E}_2}{m} + O(v^2) \right], \quad (3.12)$$

which is valid when the wavefunction $\Psi_{\mathcal{Q}}(\boldsymbol{r})$ has definite $^{2S+1}P_J$ quantum numbers.

In order to compute the $\overline{\mathrm{MS}}$-renormalized wavefunctions at the origin, we need to obtain the $\boldsymbol{\nabla}\Psi(\mathbf{0})$ in DR, where the UV divergences are given by poles in ϵ and organized in powers of α_s. In general, this is difficult because dimensionally regulated calculations are done in perturbation theory in momentum space, while nonperturbative calculations of the wavefunctions are best done in position space, as nonperturbative potentials are usually given as functions of $\boldsymbol{r}$. In position-space calculations of $\boldsymbol{\nabla}\Psi(\mathbf{0})$, the UV divergences can be regulated by introducing a position-space cutoff. The relation between the position-space regularized wavefunction at the origin and the dimensionally regulated one can be written as

$$\left[\boldsymbol{\nabla}^i \Psi(\mathbf{0}) \right]^{\mathrm{DR}} = \bar{Z}^{ij} \left[\boldsymbol{\nabla}^j \Psi(\mathbf{0}) \right]_{(r_0)}, \quad (3.13)$$

where the subscript (r_0) on $\boldsymbol{\nabla}\Psi(\mathbf{0})$ denotes that the UV divergences are regulated in position space, and $\bar{Z}^{ij}$ is the scheme conversion coefficient between position-space regularization and DR. The definition of the position-space regularization that we use in this paper will be given in the next section. The scheme conversion coefficient Z^{ij} between the position-space regularization and $\overline{\mathrm{MS}}$ can then be found from $\bar{Z}^{ij}$ by subtracting the UV poles according to eq. (3.11), which leads to the relation

$$\left[\hat{\boldsymbol{r}}\cdot\boldsymbol{\nabla}\Psi(\mathbf{0})\right]^{\overline{\mathrm{MS}}} = \hat{\boldsymbol{r}}^i Z^{ij}\left[\boldsymbol{\nabla}^j\Psi(\mathbf{0})\right]_{(r_0)}. \tag{3.14}$$

We discuss the calculation of the wavefunctions at the origin in position-space regularization and the scheme conversion coefficient in the following sections.

4 P-wave quarkonium wavefunctions in position space

In this section, we compute the P-wave quarkonium wavefunctions by solving the Schrödinger equation in position space. The potential in position space can be written generically as

$$V(\boldsymbol{r},\boldsymbol{\nabla}) = V^{(0)}(r) + \frac{1}{m}V^{(1)}(r) + \frac{1}{m^2}\Big[V_r^{(2)}(r) + \frac{1}{2}\{V_{p^2}^{(2)}(r), -\boldsymbol{\nabla}^2\} + V_{L^2}(r)\boldsymbol{L}^2$$
$$+ V_{S^2}^{(2)}(r)\boldsymbol{S}^2 + V_{S_{12}}^{(2)}(r)S_{12} + V_{so}^{(2)}(r)\boldsymbol{L}\cdot\boldsymbol{S}\Big] - \frac{\boldsymbol{\nabla}^4}{4m^3} + \cdots, \tag{4.1}$$

where $\boldsymbol{L} = -i\boldsymbol{r}\times\boldsymbol{\nabla}$, $\boldsymbol{S}$ is the $Q\bar{Q}$ spin, and $S_{12} = \sigma^i\otimes\sigma^i - 3\hat{\boldsymbol{r}}\cdot\boldsymbol{\sigma}\otimes\hat{\boldsymbol{r}}\cdot\boldsymbol{\sigma}$, where the Pauli matrices on the left and right of $\otimes$ apply to the antiquark and quark spin indices of the wavefunction.[3] The contribution at leading power in $1/m$ is the static potential, which has a nonperturbative expression in terms of a vacuum expectation value of a Wilson loop [20, 34–36]. At short distances ($r \ll 1/\Lambda_{\mathrm{QCD}}$), $V^{(0)}(r)$ can be expressed as series in α_s, which reads $V^{(0)}(r) = -\alpha_s C_F/r$ at leading order in α_s [37, 38]. The explicit expressions for the order $1/m$ and $1/m^2$ potentials at short distances are shown in appendix B. The potentials of orders $1/m$ and higher generally depend on the matching scheme, while the static potential $V^{(0)}(r)$ is scheme independent. In order to obtain results that are consistent with the short-distance coefficients appearing in NRQCD factorization formulae, the wavefunctions must be computed by using potentials from the on-shell matching scheme, because matching calculations in NRQCD are done by comparing on-shell $Q\bar{Q}$ amplitudes with QCD counterparts. On the other hand, the nonperturbative long-distance behaviors of the potentials are available in the Wilson loop matching scheme, which provides nonperturbative expressions of the potentials that allow lattice QCD determinations [33, 39]. The wavefunctions in the on-shell matching scheme can be obtained from the ones in the Wilson loop matching scheme by unitary transformations; explicit calculations of the unitary transformation will be done in section 5.4.

Our goal is to compute P-wave wavefunctions including the effect of the potential to leading nontrivial order in $1/m$. Because unitary transformations can reshuffle the $1/m$

---

[3]We note that the form of S_{12} that we use differs from ref. [33], because we use the particle-antiparticle basis for Q and $\bar{Q}$ spin indices instead of the particle-particle basis used in ref. [33].

and $1/m^2$ terms in the potential, it is necessary to include also the $1/m^2$ terms in order to determine the effect of the $1/m$ potential unambiguously. The last term in eq. (4.1), which comes from the relativistic correction to the kinetic energy, should be regarded as a order $1/m$ correction, because by using the Schrödinger equation, a power of $\boldsymbol{\nabla}^2$ can be traded with a power of $m(E_Q - V^{(0)}(r))$.

Since the $V^{(1)}(r)/m$ term in the potential comes from the spin-independent dimension-5 terms in the NRQCD Lagrangian, in the standard NRQCD power counting, the effects of the $1/m$ potential to wavefunctions are suppressed by v^2. Computation of the corrections from the $1/m$ and $1/m^2$ potentials correspond to computing the order v^2 corrections to the wavefunctions. We compute the effect from the higher order potentials by using the quantum-mechanical perturbation theory (QMPT) to first order, where corrections to the wavefunctions are computed by using the Rayleigh-Schrödinger perturbation theory.[4] We define the leading-order potential as the static potential, minus the loop corrections at short distances beyond leading order in α_s. That is, $V_{\rm LO}(r) = V^{(0)}(r) - \delta V_C(r)$, where $\delta V_C(r)$ corresponds to the corrections to the static potential at orders α_s^2 and beyond computed in perturbative QCD. Then, $\delta V(\boldsymbol{r}, \boldsymbol{\nabla}) \equiv V(\boldsymbol{r}, \boldsymbol{\nabla}) - V_{\rm LO}(r)$ is given by $\delta V_C(r)$ plus the potentials of higher orders in $1/m$.

The leading-order Hamiltonian reads

$$h_{\rm LO}(r, \boldsymbol{\nabla}) = -\frac{\boldsymbol{\nabla}^2}{m} + V_{\rm LO}(r). \tag{4.2}$$

The LO wavefunctions $\Psi_n^{\rm LO}$ are normalized bound-state solutions of the LO Schrödinger equation

$$h_{\rm LO}(r, \boldsymbol{\nabla})\Psi_n^{\rm LO}(\boldsymbol{r}) = E_n^{\rm LO}\Psi_n^{\rm LO}(\boldsymbol{r}), \tag{4.3}$$

with corresponding binding energies $E_n^{\rm LO}$. Before we move onto the calculation of the corrections, we first discuss some properties of the LO wavefunctions. Since the LO potential $V_{\rm LO}(r)$ diverges like $1/r$ at $r \to 0$, the wavefunctions are regular at $r = 0$. From the series solution method for solving Schrödinger equations in nonrelativistic quantum mechanics, we know that in this case, the P-wave LO wavefunctions vanish linearly as $r \to 0$, while the D- and F-wave LO wavefunctions vanish quadratically and cubically, respectively. That is, the first derivative of the P-wave LO wavefunction is finite at the origin, while $\boldsymbol{\nabla}\Psi_n^{\rm LO}(\boldsymbol{0})$ vanishes for states with higher orbital angular momentum. While S-wave wavefunctions are finite at the origin, its first derivative vanishes at the origin due to reflection symmetry. Hence, at leading order in the QMPT, only P-wave wavefunctions contribute to the LDMEs in eqs. (3.6). We also note that since spin and orbital angular momenta are

---

[4]It has been suggested in refs. [23, 33, 39] that in a more conservative power counting, $V^{(1)}(r)/m$ can be the same order as the static potential, and so, its effect must be included at leading order. However, it is possible that this power counting overestimates the effect of the $V^{(1)}(r)/m$ term to the wavefunctions, because wavefunctions depend only on the shape of the potential. In order to address this issue, in appendix E we compute numerically the bound-state wavefunctions from the potential $V^{(0)}(r) + V^{(1)}(r)/m$ without expanding the $1/m$ potential, and compare with the result from first order Rayleigh-Schrödinger perturbation theory. The calculation in appendix E shows that the bulk of the effects of the $V^{(1)}(r)/m$ term to the wavefunctions are well reproduced at first order in the Rayleigh-Schrödinger perturbation theory, and hence, the expansion of the $V^{(1)}(r)/m$ term in powers of $1/m$ is well justified.

conserved separately by $h_{\rm LO}$, we can write the LO wavefunctions as linear combinations of spherical harmonics times a function of $|\boldsymbol{r}| = r$:

$$R_{\rm LO}(r)Y_1^{\lambda_L}(\hat{\boldsymbol{r}})\Sigma_S, \qquad (4.4)$$

where $R_{\rm LO}(r)$ is the radial wavefunction, and $Y_1^{\lambda_L}(\hat{\boldsymbol{r}})$ is the spherical harmonics of orbital angular momentum 1 that encodes the dependence on the angles of $\boldsymbol{r}$, with $\lambda_L = -1$, 0, or 1. Because $V_{\rm LO}(r)$ is real, we can always choose the overall phase of the wavefunction $\Psi_n^{\rm LO}(\boldsymbol{r})$ so that $R_{\rm LO}(r)$ is real. The $Q\bar{Q}$ spin indices of the wavefunction are carried by a 2×2 matrix Σ_S, which we normalize as $\mathrm{tr}(\Sigma_S^\dagger \Sigma_S) = 1$. In this normalization, the radial wavefunction is normalized as $\int_0^\infty dr\, r^2 |R_{\rm LO}(r)|^2 = 1$. In 3 spatial dimensions, $\Sigma_{S=0}$ is proportional to the identity matrix $1_{2\times 2}$, while the $\Sigma_{S=1}$ are linear combinations of Pauli matrices. Wavefunctions with specific angular momentum quantum numbers $^{2S+1}P_J$ can be constructed from linear combinations of $R_{\rm LO}(r)Y_1^{\lambda_L}(\hat{\boldsymbol{r}})\Sigma_S$ by using Clebsch-Gordan coefficients. By using the orthonormality of Clebsch-Gordan coefficients, we find by direct computation

$$\left|\boldsymbol{\nabla}\Psi_n^{\rm LO}(\boldsymbol{0})\right|^2 = \frac{3}{4\pi}\left|R'_{\rm LO}(0)\right|^2 \qquad (4.5)$$

where $R'_{\rm LO}(0)$ is the first derivative of $R_{\rm LO}(r)$ at $r = 0$.

For analytical calculations, it is convenient to use a different basis for the $\hat{\boldsymbol{r}}$ dependence based on irreducible Cartesian tensors. In this basis, the wavefunctions with quantum numbers $^1P_1$, $^3P_0$, $^3P_1$, and $^3P_2$ are given by the tensors $1_{2\times 2}\hat{\boldsymbol{r}}^i$, $\frac{\delta^{ij}}{3}\hat{\boldsymbol{r}}\cdot\boldsymbol{\sigma}$, $\hat{\boldsymbol{r}}^{[i}\sigma^{j]}$, and $\hat{\boldsymbol{r}}^{(i}\sigma^{j)}$, respectively, multiplied by the radial wavefunction $R_{\rm LO}(r)$, up to a normalization. Here $1_{2\times 2}$ is an identity in the $Q\bar{Q}$ spin. In each case, spatial indices of the tensors represent polarizations of the $^{2S+1}P_J$ state. In particular, the tensors for the ^3P_J states are just the irreducible representations of $\hat{\boldsymbol{r}}^i\sigma^j$ for spin J, so that for all spin triplet cases, we can consider wavefunctions that are proportional to $\hat{\boldsymbol{r}}^i\sigma^j$ and project onto the spin-J components whenever necessary. The average over polarizations of the square of a wavefunction is given by summing over repeated indices of these tensors and taking the trace over the $Q\bar{Q}$ spin. In this case, we obtain $\overline{|\boldsymbol{\nabla}\Psi_n^{\rm LO}(\boldsymbol{0})|^2} = \overline{|\hat{\boldsymbol{r}}\cdot\boldsymbol{\nabla}\Psi_n^{\rm LO}(\boldsymbol{0})|^2} = \frac{3}{4\pi}|R'_{\rm LO}(0)|^2$. In the calculations in this paper, the Cartesian basis will be used in analytical calculations of the scheme conversion, while the spherical harmonics is more appropriate in organizing the numerical calculations of the Schrödinger equation.

While $\boldsymbol{\nabla}\Psi_n^{\rm LO}(\boldsymbol{r})$ is regular at $\boldsymbol{r} = \boldsymbol{0}$, the corrections from $\delta V(\boldsymbol{r}, \boldsymbol{\nabla})$ can produce divergences, because the $1/m$ and $1/m^2$ potentials contain terms that diverge faster than $1/r$ at $r = 0$. For example, the $1/m$ potential diverges like $1/r^2$ at $r = 0$, and so, the correction from $V^{(1)}(r)/m$ will make $\boldsymbol{\nabla}\Psi(\boldsymbol{0})$ diverge logarithmically. Similarly, the spin-dependent $1/m^2$ potentials diverge like $1/r^3$, which can make the wavefunctions diverge linearly at $r = 0$.

Now we discuss the calculation of the correction to the wavefunctions in the QMPT. To first order in the Rayleigh-Schrödinger perturbation theory, the wavefunction $\Psi_n(\boldsymbol{r})$ is given in terms of the LO wavefunction $\Psi_n^{\rm LO}(\boldsymbol{r})$ by

$$\Psi_n(\boldsymbol{r}') = \Psi_n^{\rm LO}(\boldsymbol{r}') + \delta\Psi_n(\boldsymbol{r}') = \Psi_n^{\rm LO}(\boldsymbol{r}') - \int d^3r\, \hat{G}_n(\boldsymbol{r}',\boldsymbol{r})\delta V(\boldsymbol{r},\boldsymbol{\nabla})\Psi_n^{\rm LO}(\boldsymbol{r}), \qquad (4.6)$$

where $\hat{G}_n(\boldsymbol{r}', \boldsymbol{r})$ is the reduced Green's function for the eigenstate n, defined by

$$\hat{G}_n(\boldsymbol{r}', \boldsymbol{r}) = \sum_{k \neq n} \frac{\Psi_k^{\mathrm{LO}}(\boldsymbol{r}')\Psi_k^{\mathrm{LO}*}(\boldsymbol{r})}{E_k^{\mathrm{LO}} - E_n^{\mathrm{LO}}}, \tag{4.7}$$

where the sum runs over all eigenstates of the LO Schrödinger equation except for the state n. The reduced Green's function can be defined in terms of the Green's function $G(\boldsymbol{r}', \boldsymbol{r}; E)$, defined for arbitrary complex E by

$$G(\boldsymbol{r}', \boldsymbol{r}; E) = \sum_k \frac{\Psi_k^{\mathrm{LO}}(\boldsymbol{r}')\Psi_k^{\mathrm{LO}*}(\boldsymbol{r})}{E_k^{\mathrm{LO}} - E}, \tag{4.8}$$

where the sum is over all eigenstates of h_{LO}. From this we have

$$\hat{G}_n(\boldsymbol{r}', \boldsymbol{r}) = \lim_{E \to E_n^{\mathrm{LO}}} \left[G(\boldsymbol{r}', \boldsymbol{r}; E) - \frac{\Psi_n^{\mathrm{LO}}(\boldsymbol{r}')\Psi_n^{\mathrm{LO}*}(\boldsymbol{r})}{E_n^{\mathrm{LO}} - E} \right], \tag{4.9}$$

and

$$\hat{G}_n(\boldsymbol{r}', \boldsymbol{r}) = \lim_{\eta \to 0} \frac{1}{2} \left[G(\boldsymbol{r}', \boldsymbol{r}; E_n^{\mathrm{LO}} + \eta) + G(\boldsymbol{r}', \boldsymbol{r}; E_n^{\mathrm{LO}} - \eta) \right]. \tag{4.10}$$

The correction to $\boldsymbol{\nabla}\Psi(\boldsymbol{0})$ at first order is given by $-\boldsymbol{\nabla}_{\boldsymbol{r}'} \int d^3r\, \hat{G}_n(\boldsymbol{r}', \boldsymbol{r})\delta V(\boldsymbol{r}, \boldsymbol{\nabla})\Psi_n^{\mathrm{LO}}(\boldsymbol{r})$ at $\boldsymbol{r}' = \boldsymbol{0}$. As argued previously, this integral contains divergences at $\boldsymbol{r}' = \boldsymbol{0}$ when $\delta V(\boldsymbol{r}, \boldsymbol{\nabla})$ contains terms that diverge faster than $1/r$ at $r = 0$. The contribution in $\delta V(\boldsymbol{r}, \boldsymbol{\nabla})$ that diverges like $1/r^2$ at $r = 0$ such as the $1/m$ potential produces a logarithmic divergence that is proportional to $\log r$ at first order in QMPT. Similarly, contributions that diverge like $1/r^3$ such as the spin-dependent terms in $\delta V(\boldsymbol{r}, \boldsymbol{\nabla})$ produce linear UV divergences. In the case of P-wave states, the delta functions $\delta^{(3)}(\boldsymbol{r})$ in $\delta V(\boldsymbol{r}, \boldsymbol{\nabla})$ do not contribute to $\delta\Psi_n(\boldsymbol{r}')$ to first order in the QMPT, because the P-wave wavefunctions $\Psi_n^{\mathrm{LO}}(\boldsymbol{r})$ vanish at $\boldsymbol{r} = \boldsymbol{0}$.

The $\delta V(\boldsymbol{r}, \boldsymbol{\nabla})$ contains differentiation that act on the wavefunctions $\Psi_n^{\mathrm{LO}}(\boldsymbol{r})$. They come from the $\boldsymbol{\nabla}^2$ in the velocity-dependent potential and the relativistic corrections to the kinetic energy, as well as the spin-dependent terms in the potential, which also depend on the angles of $\boldsymbol{r}$ and the $Q\bar{Q}$ spin. The $\boldsymbol{\nabla}^2$ can be reduced into functions of $|\boldsymbol{r}| = r$ by using the Schrödinger equation, similarly to what has been done in ref. [16] for the S-wave case. In the case of the spin-dependent contributions, the terms that depend on $\boldsymbol{r}$, $\boldsymbol{\nabla}$, and the $Q\bar{Q}$ spin can also be reduced into functions of r by diagonalizing their matrix elements on states with definite angular momentum quantum numbers. The spin-dependent contributions in $\delta V(\boldsymbol{r}, \boldsymbol{\nabla})$ that apply to P-wave wavefunctions come from $\boldsymbol{L} \cdot \boldsymbol{S}$ and S_{12}. As is known from nonrelativistic quantum mechanics, the operator $\boldsymbol{L} \cdot \boldsymbol{S}$ takes values 0, -2, -1, and 1 when applied to wavefunctions with angular momentum quantum numbers $^1P_1$, $^3P_0$, $^3P_1$, and $^3P_2$, respectively. The operator S_{12} is more involved, because it can change the orbital angular momentum by two units. Explicit calculations of the action of S_{12} on P-wave wavefunctions are done in appendix C. The operator S_{12} takes values 0, -4, and 2 when applied to wavefunctions with angular momentum quantum numbers $^1P_1$, $^3P_0$, and $^3P_1$, respectively, while when we apply S_{12} to a $^3P_2$ wavefunction, we obtain

$-\frac{2}{5}$ times the ${}^3P_2$ wavefunction plus a F-wave contribution. The exact form of the F-wave contribution in the Cartesian basis is shown in eq. (C.5). Because the tensor structure of the F-wave contribution is orthogonal to the tensor structures of P-wave wavefunctions, the F-wave contribution vanishes in $\overline{|\boldsymbol{\nabla}\Psi_n(\boldsymbol{0})|^2}$ to first order in the QMPT. Therefore, at the current level of accuracy, we can neglect the F-wave contribution, and consider only P-wave states when computing the LDMEs.[5] In this case, the operators $\boldsymbol{L} \cdot \boldsymbol{S}$ and S_{12} take definite values when applied to wavefunctions of definite ${}^{2S+1}P_J$ quantum numbers, so that the tensor structures of the P-wave wavefunctions in the Cartesian basis remain unchanged. Hence, the corrections from $\delta V(\boldsymbol{r}, \boldsymbol{\nabla})$ affect only the radial wavefunctions, which acquire dependence on S and J from first order in the QMPT. The same is true in terms of spherical harmonics.

While in position space in 3 spatial dimensions it is possible to reduce the action of $\delta V(\boldsymbol{r}, \boldsymbol{\nabla})$ to P-wave wavefunctions of definite ${}^{2S+1}P_J$ quantum numbers into functions of r, the reduction of spin-dependent potentials do not easily generalize to $d-1$ spatial dimensions. Later, we will need to obtain definite expressions in DR that match with the position-space expressions in order to identify the UV divergences in d dimensions, so that we can carry out renormalization in the $\overline{\text{MS}}$ scheme. Hence, we keep the spin-dependent operators in $\delta V(\boldsymbol{r}, \boldsymbol{\nabla})$ as is, while we can still reduce the $\boldsymbol{\nabla}^2$ in the velocity-dependent potential and the relativistic corrections to the kinetic energy. We obtain

$$
\begin{aligned}
\delta \Psi_n(\boldsymbol{r}') = &-\int d^3 r\, \hat{G}_n(\boldsymbol{r}', \boldsymbol{r}) \delta\mathcal{V}(\boldsymbol{r}, \boldsymbol{\nabla})\Psi_n^{\text{LO}}(\boldsymbol{r}) \\
&- \int d^3 r\, \hat{G}_n(\boldsymbol{r}', \boldsymbol{r}) \left\{ \delta V_C(r) + \frac{E_n^{\text{LO}}}{m} \left[V_{p^2}^{(2)}(r) + \frac{1}{2} V_{\text{LO}}(r) \right] \right\} \Psi_n^{\text{LO}}(\boldsymbol{r}) \\
&+ \frac{1}{2m} \Psi_n^{\text{LO}}(\boldsymbol{r}') \int d^3 r \left[V_{p^2}^{(2)}(r) + \frac{1}{2} V_{\text{LO}}(r) \right] \left| \Psi_n^{\text{LO}}(\boldsymbol{r}) \right|^2 \\
&- \frac{1}{2m} V_{p^2}^{(2)}(r') \Psi_n^{\text{LO}}(\boldsymbol{r}') - \frac{1}{4m} V_{\text{LO}}(r') \Psi_n^{\text{LO}}(\boldsymbol{r}'),
\end{aligned}
\tag{4.11}
$$

where $\delta V_C(r) = V^{(0)}(r) - V_{\text{LO}}(r)$, and

$$
\delta\mathcal{V}(\boldsymbol{r}, \boldsymbol{\nabla}) = \frac{V^{(1)}(r)}{m} - \frac{V_{p^2}^{(2)}(r) V_{\text{LO}}(r)}{m} - \frac{(V_{\text{LO}}(r))^2}{4m} + \frac{V^{(2)}(\boldsymbol{r}, \boldsymbol{\nabla})}{m^2}.
\tag{4.12}
$$

In eq. (4.11), the UV-divergent contributions to $\boldsymbol{\nabla}\delta\Psi_n(\boldsymbol{0})$ are contained in the first integral. The second integral gives a finite contribution to $\boldsymbol{\nabla}\delta\Psi_n(\boldsymbol{0})$, because the terms in the curly brackets diverge like $1/r$ at $r=0$. The third integral is also finite, because the terms in the square brackets diverge like $1/r$ at $r=0$, while $|\Psi_n^{\text{LO}}(\boldsymbol{r})|^2$ vanishes quadratically at $r=0$. The terms in the last line requires some investigation, because their contributions to $\boldsymbol{\nabla}\delta\Psi_n(\boldsymbol{0})$ involve $V_{p^2}^{(2)}(r)$ and $V_{\text{LO}}(r)$ and their derivatives at $r=0$. In the case of the LO

---

[5]If there are degeneracies in the LO Hamiltonian, corrections in the Rayleigh-Schrödinger perturbation theory must be computed in the basis that diagonalizes the higher order potentials. For example, in perturbative QCD where $V_{\text{LO}}(r) = -\alpha_s C_F/r$, radially excited P-wave states can have same LO binding energies as F-wave states. However, the degeneracies between P-wave and F-wave states disappear when we include the long-distance nonperturbative contributions to the static potential.

potential, since the static potential is perturbative at $r = 0$, so is $V_{\text{LO}}(r)$, and hence, both $V_{\text{LO}}(0)$ and $\boldsymbol{\nabla}V_{\text{LO}}(0)$ vanish in DR because they are scaleless [22, 36, 37]. On the other hand, while $\boldsymbol{\nabla}V_{p^2}^{(2)}(r)$ is perturbative at $r = 0$, $V_{p^2}^{(2)}(0)$ has a nonperturbative expression in Wilson-loop matching given by [33]

$$V_{p^2}^{(2)}(0)|^{\text{WL}} = 2i\hat{\boldsymbol{r}}^i\hat{\boldsymbol{r}}^j\frac{T_F}{N_c}\int_0^\infty dt\, t^2 \langle 0|g_s\boldsymbol{E}^{i,a}(t,\mathbf{0})\Phi_{ab}(t,0)g_s\boldsymbol{E}^{j,b}(0,\mathbf{0})|0\rangle = \frac{2i}{3}\mathcal{E}_2, \quad (4.13)$$

where the second equality follows from refs. [22, 24]. Interestingly, the correction from $V_{p^2}^{(2)}(0)$ to the P-wave wavefunction at the origin cancels the order-$1/m$ correction to $V_{\mathcal{O}}$, so that the NRQCD LDMEs are independent of $\mathcal{E}_2$, up to corrections of order v^2.

Now we compute $\boldsymbol{\nabla}\delta\Psi_n(\mathbf{0})$ from eq. (4.11). We first regulate the divergent integral in position space, by setting $|\boldsymbol{r}'| = r_0$ small but nonzero. This defines finite-r regularization, which is the position-space regularization that we use in this work. This is a straightforward generalization of the position-space regularization used in refs. [16, 17, 25] to P-wave states. We define the finite-r regularized wavefunction at the origin by the following expression

$$\boldsymbol{\nabla}\delta\Psi_n(\mathbf{0})|_{(r_0)} = -\int d^3r\, \boldsymbol{\nabla}_{\boldsymbol{r}'}\hat{G}_n(\boldsymbol{r}',\boldsymbol{r})\delta\mathcal{V}(\boldsymbol{r},\boldsymbol{\nabla})\Psi_n^{\text{LO}}(\boldsymbol{r})\Big|_{|\boldsymbol{r}'|=r_0} \quad (4.14)$$

$$-\int d^3r\, \boldsymbol{\nabla}_{\boldsymbol{r}'}\hat{G}_n(\boldsymbol{r}',\boldsymbol{r})\left\{\delta V_C(r) + \frac{E_n^{\text{LO}}}{m}\left[V_{p^2}^{(2)}(r) + \frac{1}{2}V_{\text{LO}}(r)\right]\right\}\Psi_n^{\text{LO}}(\boldsymbol{r})\Big|_{|\boldsymbol{r}'|=0}$$

$$+\frac{\left[\boldsymbol{\nabla}\Psi_n^{\text{LO}}(\mathbf{0})\right]}{2m}\left\{-V_{p^2}^{(2)}(0) + \int d^3r\left[V_{p^2}^{(2)}(r) + \frac{1}{2}V_{\text{LO}}(r)\right]\left|\Psi_n^{\text{LO}}(\boldsymbol{r})\right|^2\right\},$$

where we use the subscript (r_0) to denote that the UV divergences are regulated by using finite-r regularization. We keep the divergences and finite contributions in the limit $r_0 \to 0$, while we neglect any contributions that vanish as $r_0 \to 0$, such as positive powers of r_0. The UV divergences that are regulated by nonzero r_0 are isolated in the first integral. As a result, the difference in $\boldsymbol{\nabla}\Psi_n(\mathbf{0})$ between finite-r regularization and DR at first order in the QMPT is given by

$$\delta\bar{Z}^{ij}\left[\boldsymbol{\nabla}^j\Psi_n(\mathbf{0})\right]_{(r_0)} = \boldsymbol{\nabla}^i\Psi_n(\mathbf{0})|_{(r_0)} - \boldsymbol{\nabla}^i\Psi_n(\mathbf{0})|^{\text{DR}}$$

$$= \int d^3r\, \boldsymbol{\nabla}_{\boldsymbol{r}'}^i\hat{G}_n(\boldsymbol{r}',\boldsymbol{r})\delta\mathcal{V}(\boldsymbol{r},\boldsymbol{\nabla})\Psi_n^{\text{LO}}(\boldsymbol{r})\Big|_{|\boldsymbol{r}'|=0}^{\text{DR}}$$

$$-\int d^3r\, \boldsymbol{\nabla}_{\boldsymbol{r}'}^i\hat{G}_n(\boldsymbol{r}',\boldsymbol{r})\delta\mathcal{V}(\boldsymbol{r},\boldsymbol{\nabla})\Psi_n^{\text{LO}}(\boldsymbol{r})\Big|_{|\boldsymbol{r}'|=r_0}, \quad (4.15)$$

where $\delta\bar{Z}^{ij}$ is defined through the relation $\bar{Z}^{ij} = \delta^{ij} - \delta\bar{Z}^{ij}$, so that $\delta\bar{Z}^{ij}$ corresponds to the subtraction term that appears from first order in the QMPT. Because the right-hand side of eq. (4.15) is linear in $\delta\mathcal{V}$, eq. (4.15) is equal to $\delta\bar{Z}^{ij}\left[\boldsymbol{\nabla}^j\Psi_n^{\text{LO}}(\mathbf{0})\right]$ to first order in the QMPT. Hence, the wavefunction at the origin in DR is

$$\left[\boldsymbol{\nabla}^i\Psi_n(\mathbf{0})\right]_{\text{DR}} = \left[\boldsymbol{\nabla}^i\Psi_n(\mathbf{0})\right]_{(r_0)} - \delta\bar{Z}^{ij}\left[\boldsymbol{\nabla}^j\Psi_n^{\text{LO}}(\mathbf{0})\right]. \quad (4.16)$$

We compute $\delta\bar{Z}^{ij}$ in the next section by examining the UV diveregences in the integrands of eq. (4.15). We also define δZ^{ij} through the relation $Z^{ij} = \delta^{ij} - \delta Z^{ij}$, so that δZ^{ij} is

obtained from $\delta\bar{Z}^{ij}$ by subtracting the poles in ϵ. The $\overline{\text{MS}}$-renormalized wavefunctions at the origin are then given by

$$\left[\hat{\boldsymbol{r}} \cdot \boldsymbol{\nabla}\Psi_n(\boldsymbol{0})\right]^{\overline{\text{MS}}} = \hat{\boldsymbol{r}} \cdot \left[\boldsymbol{\nabla}\Psi_n(\boldsymbol{0})\right]_{(r_0)} - \hat{r}^i\delta Z^{ij}\left[\boldsymbol{\nabla}^j\Psi_n^{\text{LO}}(\boldsymbol{0})\right]. \tag{4.17}$$

As was discussed in the previous section, in order to compute the NRQCD LDMEs from eq. (4.17), the wavefunctions must carry definite $^{2S+1}P_J$ quantum numbers. While the spin projections on the finite-r regularized wavefunction at the origin $\left[\boldsymbol{\nabla}\Psi_n(\boldsymbol{0})\right]_{(r_0)}$ can be done in 3 spatial dimensions, the spin projections must be done for the subtraction term $\delta\bar{Z}^{ij}\left[\boldsymbol{\nabla}^j\Psi_n^{\text{LO}}(\boldsymbol{0})\right]$ in DR before renormalization in $\overline{\text{MS}}$, because from order ϵ the spin-dependent potentials can induce transitions between states with different $^{2S+1}P_J$ quantum numbers, which can affect the finite parts in δZ^{ij}. This can be done by diagonalizing $\delta\bar{Z}^{ij}$ to order ϵ^0 accuracy according to the spin projections of the wavefunctions in DR, by using the d-dimensional definitions in eq. (3.11). Explicit calculations of δZ^{ij} will be done in the next section.

We have argued that the corrections to the wavefunctions at the origin from the $1/m$ potential scales like v^2. We have found that the correction from the velocity-dependent potential at order $1/m^2$ involves a correction that scales like Λ_{QCD}/m. Since corrections of similar form may arise at second order in the QMPT, we assume that the wavefunctions at the origin that we compute in this section are accurate up to corrections of relative orders v^3 and $\Lambda_{\text{QCD}}^2/m^2$.

5 Scheme conversion

In this section we compute the scheme conversion coefficient $\delta Z_{ij} = Z_{ij} - \delta_{ij}$, which is obtained by subtracting the $1/\epsilon$ poles in $\delta\bar{Z}_{ij}$ according to the $\overline{\text{MS}}$ prescription. Equation (4.15) implies that $\delta\bar{Z}_{ij}$ is determined by the UV-divergent behavior of the integral

$$-\int d^3r\,\boldsymbol{\nabla}_{\boldsymbol{r}'}\hat{G}_n(\boldsymbol{r}',\boldsymbol{r})\delta\mathcal{V}(\boldsymbol{r},\boldsymbol{\nabla})\Psi_n^{\text{LO}}(\boldsymbol{r}) \tag{5.1}$$

at $\boldsymbol{r}' = \boldsymbol{0}$. If we split this integral into a UV-divergent part plus a UV-finite part, the UV-finite part vanishes in $\delta\bar{Z}^{ij}$, because the UV-finite part does not depend on the UV regulator. That is, for the purpose of computing $\delta\bar{Z}_{ij}$, it suffices to identify the UV-divergent part of the integral, whose integrand is same in both DR and finite-r regularization when the regularizations are lifted ($\epsilon \to 0$ and $r_0 \to 0$). Since $\hat{G}_n(\boldsymbol{r}',\boldsymbol{r})$ can be obtained from $G(\boldsymbol{r}',\boldsymbol{r};E)$ by using the relation in eq. (4.10), it suffices to compute the UV divergence of the integral

$$-\int d^3r\,\boldsymbol{\nabla}_{\boldsymbol{r}'}G(\boldsymbol{r}',\boldsymbol{r};E)\delta\mathcal{V}(\boldsymbol{r},\boldsymbol{\nabla})\Psi_n^{\text{LO}}(\boldsymbol{r}) \tag{5.2}$$

at $\boldsymbol{r}' = \boldsymbol{0}$. We first identify the divergence of this integral in position space, and then derive the equivalent expression in momentum space in d spacetime dimensions.

5.1 Position-space divergences in the wavefunctions at the origin

We investigate the UV divergence in the finite-r regularized integral

$$-\int d^3r\,\boldsymbol{\nabla}_{\boldsymbol{r}'}G(\boldsymbol{r}',\boldsymbol{r};E)\delta\mathcal{V}(\boldsymbol{r},\boldsymbol{\nabla})\Psi_n^{\text{LO}}(\boldsymbol{r})\Big|_{|\boldsymbol{r}'|=r_0} \tag{5.3}$$

at small $|\boldsymbol{r'}| = r_0$. To find a simplified expression of the UV divergence in this integral, we examine the small-r behavior of the integrand. We note that the contribution from $V^{(1)}(r)$ is logarithmically divergent, because $V^{(1)}(r)$ diverges like $1/r^2$ at $r = 0$. The same applies to contribution from $V_{p^2}^{(2)}(r)V_{\mathrm{LO}}(r)$ and $(V_{\mathrm{LO}}(r))^2$ terms in $\delta\mathcal{V}(\boldsymbol{r},\boldsymbol{\nabla})$. On the other hand, the contribution from $V^{(2)}(r,\boldsymbol{\nabla})$ is linearly divergent, because $V^{(2)}(r,\boldsymbol{\nabla})$ contains contributions that diverge like $1/r^3$ at $r = 0$. If we expand $\Psi_n^{\mathrm{LO}}(\boldsymbol{r})$ in powers of r in the integrand, the UV-divergent contributions are contained in the order r and r^2 terms of the expansion.[6] That is,

$$
\begin{aligned}
&-\int d^3r\,\boldsymbol{\nabla}_{\boldsymbol{r'}}G(\boldsymbol{r'},\boldsymbol{r};E)\delta\mathcal{V}(\boldsymbol{r},\boldsymbol{\nabla})\Psi_n^{\mathrm{LO}}(\boldsymbol{r})\\
&=-\int d^3r\,\boldsymbol{\nabla}_{\boldsymbol{r'}}G(\boldsymbol{r'},\boldsymbol{r};E)\delta\mathcal{V}(\boldsymbol{r},\boldsymbol{\nabla})\left\{r\left[\frac{\partial}{\partial r}\Psi_n^{\mathrm{LO}}(\boldsymbol{r})\right]_{r=0}+\frac{1}{2}r^2\left[\frac{\partial^2}{\partial r^2}\Psi_n^{\mathrm{LO}}(\boldsymbol{r})\right]_{r=0}\right\}\\
&\quad+\text{UV-finite contributions,}
\end{aligned}
\tag{5.4}
$$

where the UV-finite contributions are finite in the limit $|\boldsymbol{r'}|\to 0$. We now express the terms in the curly brackets in terms of $\boldsymbol{\nabla}\Psi_n^{\mathrm{LO}}(\boldsymbol{0})$. The first term in the curly brackets is given by

$$
r\left[\frac{\partial}{\partial r}\Psi_n^{\mathrm{LO}}(r)\right]_{r=0}=\boldsymbol{r}\cdot\left[\boldsymbol{\nabla}\Psi_n^{\mathrm{LO}}(\boldsymbol{0})\right],
\tag{5.5}
$$

where $r=|\boldsymbol{r}|$. For the second term, we use the relation

$$
\frac{\partial^2}{\partial r^2}=\boldsymbol{\nabla}^2-\frac{2}{r}\frac{\partial}{\partial r}+\frac{\boldsymbol{L}^2}{r^2},
\tag{5.6}
$$

which gives

$$
\frac{\partial^2}{\partial r^2}\Psi_n^{\mathrm{LO}}(\boldsymbol{r})=m[V_{\mathrm{LO}}(r)-E]\Psi_n^{\mathrm{LO}}(\boldsymbol{r})-2\frac{\partial}{\partial r}\left(\frac{1}{r}\Psi_n^{\mathrm{LO}}(\boldsymbol{r})\right),
\tag{5.7}
$$

where we used $\boldsymbol{L}^2\Psi_n^{\mathrm{LO}}(\boldsymbol{r})=2\Psi_n^{\mathrm{LO}}(\boldsymbol{r})$ for P-wave states. Since $\Psi_n^{\mathrm{LO}}(\boldsymbol{r})$ vanishes linearly as $r\to 0$, we can write the limit $r\to 0$ as

$$
\lim_{r\to 0}\frac{\partial^2}{\partial r^2}\Psi_n^{\mathrm{LO}}(\boldsymbol{r})=m[rV_{\mathrm{LO}}(r)]_{r=0}\left[\frac{\partial}{\partial r}\Psi_n^{\mathrm{LO}}(\boldsymbol{r})\right]_{r=0}-2\left[\frac{\partial}{\partial r}\left(\frac{1}{r}\Psi_n^{\mathrm{LO}}(\boldsymbol{r})\right)\right]_{r=0}.
\tag{5.8}
$$

On the other hand, by using the fact that $\Psi_n^{\mathrm{LO}}(\boldsymbol{r})$ is regular and vanishes linearly at $r=0$, we obtain from Taylor series expansion,

$$
\lim_{r\to 0}\frac{\partial^2}{\partial r^2}\Psi_n^{\mathrm{LO}}(\boldsymbol{r})=2\left[\frac{\partial}{\partial r}\left(\frac{1}{r}\Psi_n^{\mathrm{LO}}(\boldsymbol{r})\right)\right]_{r=0},
\tag{5.9}
$$

which implies

$$
\lim_{r\to 0}\frac{\partial^2}{\partial r^2}\Psi_n^{\mathrm{LO}}(\boldsymbol{r})=\frac{1}{2}m[rV_{\mathrm{LO}}(r)]_{r=0}\left[\frac{\partial}{\partial r}\Psi_n^{\mathrm{LO}}(\boldsymbol{r})\right]_{r=0}.
\tag{5.10}
$$

---

[6]In the calculation of S-wave wavefunctions in ref. [16], only the leading-power contribution was kept, because power divergent contributions to S-wave wavefunctions at the origin only arise from delta functions in the potential, so that any positive powers of r can be neglected.

We note that $[rV_{\mathrm{LO}}(r)]_{r=0}$ is nothing but the Coulomb strength of the LO potential at short distances, which is given by $-\alpha_s C_F$. Then, the second term in the curly brackets in eq. (5.4) can be written as

$$\frac{1}{2}r^2\left[\frac{\partial^2}{\partial r^2}\Psi_n^{\mathrm{LO}}(\boldsymbol{r})\right]_{r=0} = -\frac{\alpha_s C_F}{4}mr\boldsymbol{r}\cdot\left[\boldsymbol{\nabla}\Psi_n^{\mathrm{LO}}(\boldsymbol{0})\right], \tag{5.11}$$

so that

$$-\int d^3r\,\boldsymbol{\nabla}_{\boldsymbol{r}'}G(\boldsymbol{r}',\boldsymbol{r};E)\delta\mathcal{V}(\boldsymbol{r},\boldsymbol{\nabla})\Psi_n^{\mathrm{LO}}(\boldsymbol{r})$$

$$= -\int d^3r\,\boldsymbol{\nabla}_{\boldsymbol{r}'}G(\boldsymbol{r}',\boldsymbol{r};E)\delta\mathcal{V}(\boldsymbol{r},\boldsymbol{\nabla})\left(1-\frac{\alpha_s C_F}{4}mr\right)\boldsymbol{r}\cdot\left[\boldsymbol{\nabla}\Psi_n^{\mathrm{LO}}(\boldsymbol{0})\right]$$

$$+\,\mathrm{UV\text{-}finite\ contributions.} \tag{5.12}$$

In order to be able to compare with dimensionally regulated expressions of the UV divergence, it is useful to find the momentum-space expression of the UV-divergent part. In 3 spatial dimensions, the momentum-space Green's function $\tilde{G}(\boldsymbol{p}',\boldsymbol{p};E)$ is related to the position-space counterpart by

$$G(\boldsymbol{r}',\boldsymbol{r};E) = \int_{\boldsymbol{p}}\int_{\boldsymbol{p}'}e^{i\boldsymbol{p}'\cdot\boldsymbol{r}'}e^{-i\boldsymbol{p}\cdot\boldsymbol{r}}\tilde{G}(\boldsymbol{p}',\boldsymbol{p};E)\Big|_{d=4}, \tag{5.13}$$

where

$$\int_{\boldsymbol{p}} \equiv \int\frac{d^{d-1}\boldsymbol{p}}{(2\pi)^{d-1}}. \tag{5.14}$$

This lets us write the leading term as

$$-\int d^3r\,\boldsymbol{\nabla}_{\boldsymbol{r}'}^i G(\boldsymbol{r}',\boldsymbol{r};E)\delta\mathcal{V}(\boldsymbol{r},\boldsymbol{\nabla})r^j$$

$$= -\int_{\boldsymbol{p}'}\int_{\boldsymbol{p}}e^{i\boldsymbol{p}'\cdot\boldsymbol{r}'}p'^i\tilde{G}(\boldsymbol{p}',\boldsymbol{p};E)[\boldsymbol{\nabla}_{\boldsymbol{q}}^j\delta\tilde{\mathcal{V}}(\boldsymbol{p},\boldsymbol{q})]\Big|_{\boldsymbol{q}=\boldsymbol{0},\,d=4}. \tag{5.15}$$

Here $\delta\tilde{\mathcal{V}}(\boldsymbol{p},\boldsymbol{q})$ is related to the position-space counterpart in 3 spatial dimensions by

$$\delta\tilde{\mathcal{V}}(\boldsymbol{p},\boldsymbol{q})\Big|_{d=4} = \int d^3r\,e^{i\boldsymbol{p}\cdot\boldsymbol{r}}\delta\mathcal{V}(\boldsymbol{r},\boldsymbol{\nabla})e^{-i\boldsymbol{q}\cdot\boldsymbol{r}}. \tag{5.16}$$

The d-dimensional expression for $\delta\tilde{\mathcal{V}}(\boldsymbol{p},\boldsymbol{q})$ will be given later. For the subleading term, we need the Fourier transform of $-\frac{1}{4}\alpha_s C_F mr\boldsymbol{r}$. We first compute the Fourier transform of $-\frac{1}{4}\alpha_s C_F mr$ as

$$-\frac{\alpha_s C_F m}{4}\int d^3r\,e^{i\boldsymbol{k}\cdot\boldsymbol{r}}r = \frac{\alpha_s C_F m}{4}\boldsymbol{\nabla}_{\boldsymbol{k}}^2\int d^3r\frac{e^{i\boldsymbol{k}\cdot\boldsymbol{r}}}{r} = \frac{2\pi\alpha_s C_F m}{\boldsymbol{k}^4}, \tag{5.17}$$

which gives us

$$-\frac{\alpha_s C_F m}{4}\int d^3re^{i\boldsymbol{k}\cdot\boldsymbol{r}}r\boldsymbol{r} = i\boldsymbol{\nabla}_{\boldsymbol{q}}\frac{2\pi\alpha_s C_F m}{(\boldsymbol{k}-\boldsymbol{q})^4}\Big|_{\boldsymbol{q}=\boldsymbol{0}} = i\frac{1}{-\boldsymbol{k}^2/m}\boldsymbol{\nabla}_{\boldsymbol{q}}\frac{-4\pi\alpha_s C_F}{(\boldsymbol{k}-\boldsymbol{q})^2}\Big|_{\boldsymbol{q}=\boldsymbol{0}}. \tag{5.18}$$

From this we obtain

$$-\int d^3r \, \boldsymbol{\nabla}_{\boldsymbol{r}'}^i G(\boldsymbol{r}',\boldsymbol{r};E)\delta\mathcal{V}(\boldsymbol{r},\boldsymbol{\nabla})\Psi_n^{\mathrm{LO}}(\boldsymbol{r})$$

$$= [\boldsymbol{\nabla}^j\Psi_n^{\mathrm{LO}}(\boldsymbol{0})]\Big[-\int_{\boldsymbol{p}'}\int_{\boldsymbol{p}} e^{i\boldsymbol{p}'\cdot\boldsymbol{r}'}\boldsymbol{p}'^i\tilde{G}(\boldsymbol{p}',\boldsymbol{p};E)[\boldsymbol{\nabla}_{\boldsymbol{q}}^j\delta\tilde{\mathcal{V}}(\boldsymbol{p},\boldsymbol{q})]_{\boldsymbol{q}=\boldsymbol{0}}$$

$$-\int_{\boldsymbol{p}'}\int_{\boldsymbol{p}} e^{i\boldsymbol{p}'\cdot\boldsymbol{r}'}\boldsymbol{p}'^i\tilde{G}(\boldsymbol{p}',\boldsymbol{p};E)\int_{\boldsymbol{k}}\delta\tilde{\mathcal{V}}(\boldsymbol{p},\boldsymbol{k})\frac{1}{-\boldsymbol{k}^2/m}\left[\boldsymbol{\nabla}_{\boldsymbol{q}}^j\frac{-4\pi\alpha_s C_F}{(\boldsymbol{k}-\boldsymbol{q})^2}\right]_{\boldsymbol{q}=\boldsymbol{0}}\Big]_{d=4}$$

$$+ \text{UV-finite contributions.} \tag{5.19}$$

Since the last integral in the brackets is at most logarithmically divergent, we are free to make modifications to this integrand as long as we keep its large loop momentum behavior unchanged. If we make the replacements $1/(-\boldsymbol{k}^2/m) \to 1/(E-\boldsymbol{k}^2/m)$ and $\frac{-4\pi\alpha_s C_F}{(\boldsymbol{k}-\boldsymbol{q})^2} \to \tilde{V}_{\mathrm{LO}}(\boldsymbol{k}-\boldsymbol{q})$, we obtain

$$-\boldsymbol{\nabla}_{\boldsymbol{r}'}^i\int d^3r \, G(\boldsymbol{r}',\boldsymbol{r};E)\delta\mathcal{V}(\boldsymbol{r},\boldsymbol{\nabla})\Psi_n^{\mathrm{LO}}(\boldsymbol{r})$$

$$= [\boldsymbol{\nabla}^j\Psi_n^{\mathrm{LO}}(\boldsymbol{0})]\Big[-\int_{\boldsymbol{p}'}\int_{\boldsymbol{p}} e^{i\boldsymbol{p}'\cdot\boldsymbol{r}'}\boldsymbol{p}'^i\tilde{G}(\boldsymbol{p}',\boldsymbol{p};E)[\boldsymbol{\nabla}_{\boldsymbol{q}}^j\delta\tilde{\mathcal{V}}(\boldsymbol{p},\boldsymbol{q})]_{\boldsymbol{q}=\boldsymbol{0}}$$

$$-\int_{\boldsymbol{p}'}\int_{\boldsymbol{p}} e^{i\boldsymbol{p}'\cdot\boldsymbol{r}'}\boldsymbol{p}'^i\tilde{G}(\boldsymbol{p}',\boldsymbol{p};E)\int_{\boldsymbol{k}}\frac{\delta\tilde{\mathcal{V}}(\boldsymbol{p},\boldsymbol{k})[\boldsymbol{\nabla}_{\boldsymbol{q}}^j\tilde{V}_{\mathrm{LO}}(\boldsymbol{k}-\boldsymbol{q})]_{\boldsymbol{q}=\boldsymbol{0}}}{E-\boldsymbol{k}^2/m}\Big]_{d=4}$$

$$+ \text{UV-finite contributions.} \tag{5.20}$$

Finally, we use the following form of the momentum-space Green's function

$$\tilde{G}(\boldsymbol{p}',\boldsymbol{p};E) = -\frac{(2\pi)^{d-1}\delta^{(d-1)}(\boldsymbol{p}-\boldsymbol{p}')}{E-\boldsymbol{p}^2/m} - \frac{1}{E-\boldsymbol{p}'^2/m}\tilde{V}_{\mathrm{LO}}(\boldsymbol{p}'-\boldsymbol{p})\frac{1}{E-\boldsymbol{p}^2/m}$$

$$-\frac{1}{E-\boldsymbol{p}'^2/m}T(\boldsymbol{p}',\boldsymbol{p},E)\frac{1}{E-\boldsymbol{p}^2/m}, \tag{5.21}$$

where[7]

$$T(\boldsymbol{p}',\boldsymbol{p},E) = \sum_{n=1}^{\infty}\int_{\boldsymbol{k}_1}\int_{\boldsymbol{k}_2}\cdots\int_{\boldsymbol{k}_n}\tilde{V}_{\mathrm{LO}}(\boldsymbol{k}_1)\prod_{i=1}^{n}\frac{\tilde{V}_{\mathrm{LO}}(\boldsymbol{k}_{i+1}-\boldsymbol{k}_i)}{\left[E-\frac{(\boldsymbol{p}'+\boldsymbol{k}_i)^2}{m}\right]}, \tag{5.22}$$

with $\boldsymbol{k}_{n+1}=\boldsymbol{p}-\boldsymbol{p}'$. Equation (5.21) is the solution of the momentum-space Lippmann-Schwinger equation

$$\left(\frac{\boldsymbol{p}'^2}{m}-E\right)\tilde{G}(\boldsymbol{p}',\boldsymbol{p};E) + \int_{\boldsymbol{k}}\tilde{V}_{\mathrm{LO}}(\boldsymbol{k})\tilde{G}(\boldsymbol{p}'-\boldsymbol{k},\boldsymbol{p};E) = (2\pi)^{d-1}\delta^{(d-1)}(\boldsymbol{p}-\boldsymbol{p}'). \tag{5.23}$$

For later convenience, we write eq. (5.21) in a form that is valid in $d-1$ spatial dimensions. Equation (5.21) is organized in a way that the large $\boldsymbol{p}$ and $\boldsymbol{p}'$ behavior becomes less divergent as the number of the LO potential increases. Hence, in the first momentum integral in eq. (5.20), which is at most linearly divergent, it suffices to keep only the first two terms of eq. (5.21), while in the second momentum integral in eq. (5.20), which is at

---

[7]Here we correct a typo in ref. [16] where $E-(\boldsymbol{p}'+\boldsymbol{k}_i)^2/(2m)$ was used instead of $E-(\boldsymbol{p}'+\boldsymbol{k}_i)^2/m$ in the denominators of $T(\boldsymbol{p}',\boldsymbol{p},E)$.
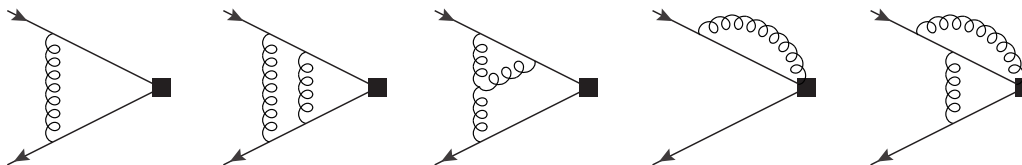
Figure 1. Some representative Feynman diagrams for one- and two-loop corrections to the NRQCD LDME $\langle 0|\chi^\dagger(-\frac{i}{2}\overleftrightarrow{\boldsymbol{D}})\psi|Q\bar{Q}\rangle$. Solid lines are heavy quarks and antiquarks, curly lines are gluons, and filled squares represent the operator $\chi^\dagger(-\frac{i}{2}\overleftrightarrow{\boldsymbol{D}})\psi$.

most logarithmically divergent, we keep only the first term of the iterative solution for the Green's function. From this we find our final form of the UV-divergent part of the finite-r regularized integral:

$$
-\boldsymbol{\nabla}^i_{\boldsymbol{r}'}\int d^3r\, G(\boldsymbol{r}',\boldsymbol{r};E)\delta\mathcal{V}(\boldsymbol{r},\boldsymbol{\nabla})\Psi^{\mathrm{LO}}_n(\boldsymbol{r})\Big|_{|\boldsymbol{r}'|=r_0}
$$
$$
=\Bigg[\int_{\boldsymbol{p}}e^{i\boldsymbol{p}\cdot\boldsymbol{r}'}\boldsymbol{p}^i\frac{\big[\boldsymbol{\nabla}^j_{\boldsymbol{q}}\delta\tilde{\mathcal{V}}(\boldsymbol{p},\boldsymbol{q})\big]_{\boldsymbol{q}=\boldsymbol{0}}}{E-\boldsymbol{p}^2/m}+\int_{\boldsymbol{p}'}\int_{\boldsymbol{p}}e^{i\boldsymbol{p}'\cdot\boldsymbol{r}'}\boldsymbol{p}'^i\frac{\tilde{V}_{\mathrm{LO}}(\boldsymbol{p}'-\boldsymbol{p})\big[\boldsymbol{\nabla}^j_{\boldsymbol{q}}\delta\tilde{\mathcal{V}}(\boldsymbol{p},\boldsymbol{q})\big]_{\boldsymbol{q}=\boldsymbol{0}}}{(E-\boldsymbol{p}'^2/m)(E-\boldsymbol{p}^2/m)}
$$
$$
+\int_{\boldsymbol{p}'}\int_{\boldsymbol{p}}e^{i\boldsymbol{p}'\cdot\boldsymbol{r}'}\boldsymbol{p}'^i\frac{\delta\tilde{\mathcal{V}}(\boldsymbol{p}',\boldsymbol{p})\big[\boldsymbol{\nabla}^j_{\boldsymbol{q}}\tilde{V}_{\mathrm{LO}}(\boldsymbol{p}-\boldsymbol{q})\big]_{\boldsymbol{q}=\boldsymbol{0}}}{(E-\boldsymbol{p}'^2/m)(E-\boldsymbol{p}^2/m)}\Bigg]_{|\boldsymbol{r}'|=r_0}[\boldsymbol{\nabla}^j\Psi^{\mathrm{LO}}_n(\boldsymbol{0})]
$$
$$
+\text{UV-finite contributions.} \tag{5.24}
$$

The UV divergences that are regulated by nonzero values of $|\boldsymbol{r}'|=r_0$ are now contained in the momentum integrals. Since we are only interested in the divergent contributions and finite terms in the limit $r_0\to 0$, we neglect any contributions that vanish as $r_0\to 0$ such as positive powers of r_0 in the UV-divergent integral in the square brackets.

We note that the UV-finite contributions can contain infrared divergences; in fact, the logarithmically divergent contribution in eq. (5.24) does contain IR divergences, because we obtained the momentum-space expression by computing the Fourier transformation of a position-space expression that does not vanish as $r\to\infty$. Since the IR divergence in the UV-divergent part cancels with the UV-finite part, it also cancels in the scheme conversion coefficient between the finite-r regularized integral and the dimensionally regulated one, as long as the IR divergences are regulated in the same way in both DR and finite-r regularization.

5.2 Divergences in the wavefunctions at the origin in DR

We now find the UV-divergent contribution of the dimensionally regulated integral. The correct dimensionally regulated expression must reproduce the loop corrections to the NRQCD LDMEs in the perturbative expansion in powers of α_s, because the renormalization of the LDMEs are carried out according to eq. (2.4).

We first examine the diagrams that contribute to the perturbative calculation of the NRQCD LDMEs at two-loop accuracy. We consider the perturbative matrix element $\langle 0|\chi^\dagger(-\frac{i}{2}\overleftrightarrow{\boldsymbol{D}})\psi|Q\bar{Q}\rangle$, where we keep the spin indices on χ and ψ unconstrained, while the color indices are contracted, and $|Q\bar{Q}\rangle$ is in a color-singlet state. The Q and $\bar{Q}$ are on shell, and have nonrelativistic spatial momenta $\boldsymbol{q}$ and $-\boldsymbol{q}$ in the rest frame of the $Q\bar{Q}$. Some

representative one- and two-loop diagrams are shown in figure 1. A general way to compute these diagrams in DR is to first integrate over the temporal components of the loop momenta, and then expand the resulting integrand in powers of the spatial components of momenta divided by the heavy quark mass, before integrating over the spatial components of the loop momenta.[8] The integration over the temporal components of loop momenta is carried out by using contour integration, where one picks up contributions from the poles coming from propagators of virtual lines. This enables us to separate the on-shell quark or antiquark contributions from on-shell gluon contributions. Note that, since in NRQCD the quark and antiquark propagator denominators are linear in the temporal components of the momenta they carry, contribution from a on-shell quark line cannot be defined unless there is an antiquark line that carries a momentum that contains the same loop momentum as the quark line. That is, if we have a virtual quark line whose propagator is $i/[k_0 - \boldsymbol{k}^2/(2m) + i\varepsilon]$, when integrating over k^0 we can neglect the contribution from its pole by closing the contour on the upper half plane. However, when there is also a virtual antiquark line that carries the momentum $k + \ell$, where ℓ is the relative momentum between the virtual quark and antiquark lines, the propagator of the antiquark line is given by $i/[-(k_0 + \ell_0) - (\boldsymbol{k} + \boldsymbol{\ell})^2/(2m) + i\varepsilon]$, and so, the contour integration over k^0 must enclose the pole from either the quark propagator or the antiquark propagator. Therefore, we define the contribution from on-shell quark or antiquark lines only when there are quark and antiquark lines that contain the same loop momentum.

In general, after integration over the temporal components of the loop momenta, we can define two subdiagrams of a generic loop diagram by the on-shell $Q\bar{Q}$ pair that is most adjacent to the NRQCD operator $\chi^\dagger(-\frac{i}{2}\overleftrightarrow{\boldsymbol{D}})\psi$ which, when removed, separates the diagram into two disconnected diagrams. Let us label the subdiagram that contains the NRQCD operator as S_O, and the subdiagram that contains the initial-state on-shell $Q\bar{Q}$ as S_V. We note that S_V depends on the relative spatial momenta of the initial and final $Q\bar{Q}$, while S_O depends on the relative spatial momenta of the on-shell Q and $\bar{Q}$ that connects S_O and S_V; the temporal components of these momenta are constrained by the on-shell condition. We include the on-shell $Q\bar{Q}$ lines between S_O and S_V in the subdiagram S_V. In this case, the sum of all Feynman diagrams is given by $\int_{\boldsymbol{p}} S_O(\boldsymbol{p}) S_V(\boldsymbol{p}, \boldsymbol{q})$. We note that the subdiagram S_V is given by scattering of on-shell Q and $\bar{Q}$ via gluon exchanges. This is nothing but the matching condition for the momentum-space potential in the on-shell matching scheme; that is, the potential in the on-shell matching scheme is the irreducible contribution in S_V that is obtained by amputating the external legs and removing on-shell heavy quark and antiquark lines [41]. The subdiagram S_V is then given to all orders in perturbation theory by

$$
S_V(\boldsymbol{p}, \boldsymbol{q}) = (2\pi)^{d-1}\delta^{(d-1)}(\boldsymbol{p} - \boldsymbol{q}) + \frac{1}{E_{\boldsymbol{q}} - \boldsymbol{p}^2/m}\left[\tilde{V}(\boldsymbol{p}, \boldsymbol{q}) + \int_{\boldsymbol{k}_1} \tilde{V}(\boldsymbol{p}, \boldsymbol{k}_1)\frac{\tilde{V}(\boldsymbol{k}_1, \boldsymbol{q})}{E_{\boldsymbol{q}} - \boldsymbol{k}_1^2/m}\right.
$$
$$
\left. + \int_{\boldsymbol{k}_1}\int_{\boldsymbol{k}_2} \tilde{V}(\boldsymbol{p}, \boldsymbol{k}_1)\frac{\tilde{V}(\boldsymbol{k}_1, \boldsymbol{k}_2)}{E_{\boldsymbol{q}} - \boldsymbol{k}_1^2/m}\frac{\tilde{V}(\boldsymbol{k}_2, \boldsymbol{q})}{E_{\boldsymbol{q}} - \boldsymbol{k}_2^2/m} + \cdots\right],
\tag{5.25}
$$

---

[8]An alternative way to compute these diagrams in DR is to use the method of regions [40], where the loop integrals are partitioned by regions of loop momenta, and expanded according to the power counting appropriate for each momentum region before integrating over the temporal and spatial components of loop momenta.

where $E_{\boldsymbol{q}} = \boldsymbol{q}^2/m - i\varepsilon$. Here, $\tilde{V}(\boldsymbol{p}, \boldsymbol{q})$ is the d-dimensional momentum-space potential in the on-shell matching scheme. Explicit expressions for the potential $\tilde{V}(\boldsymbol{p}, \boldsymbol{q})$ in $d-1$ spatial dimensions is shown in eq. (B.4). The first term in eq. (5.25) is the tree-level contribution that corresponds to the case where none of the virtual quark or antiquark lines are on shell. At tree level, the subdiagram S_O is just the tree-level NRQCD LDME. The contribution to the NRQCD LDME from S_O at tree level and S_V to all orders in α_s is given by

$$\int_{\boldsymbol{p}} S_O^{\text{tree}}(\boldsymbol{p}) S_V(\boldsymbol{p}, \boldsymbol{q}) = \boldsymbol{q} + \int_{\boldsymbol{p}} \frac{\boldsymbol{p}}{E_{\boldsymbol{q}} - \boldsymbol{p}^2/m} \left[\tilde{V}(\boldsymbol{p}, \boldsymbol{q}) + \int_{\boldsymbol{k}_1} \frac{\tilde{V}(\boldsymbol{p}, \boldsymbol{k}_1) \tilde{V}(\boldsymbol{k}_1, \boldsymbol{q})}{E_{\boldsymbol{q}} - \boldsymbol{k}_1^2/m} \right.$$
$$\left. + \int_{\boldsymbol{k}_1} \int_{\boldsymbol{k}_2} \frac{\tilde{V}(\boldsymbol{p}, \boldsymbol{k}_1) \tilde{V}(\boldsymbol{k}_1, \boldsymbol{k}_2) \tilde{V}(\boldsymbol{k}_2, \boldsymbol{q})}{(E_{\boldsymbol{q}} - \boldsymbol{k}_1^2/m)(E_{\boldsymbol{q}} - \boldsymbol{k}_2^2/m)} + \cdots \right]. \tag{5.26}$$

Here, we suppress the spin, color, and kinematical factors in S_O, so that the tree-level LDME is just $\boldsymbol{q}$. We note that $S_O^{\text{tree}}(\boldsymbol{p})$ has $Q\bar{Q}$ color indices that are proportional to the SU(3) identity matrix, and the $|Q\bar{Q}\rangle$ state is also in a color-singlet state. Hence, we only need to consider the color-singlet projection of the potential.

We can identify the contributions to eq. (5.26) from the Feynman diagrams in figure 1 as follows. The first diagram in figure 1 contributes to a single insertion of the tree-level potential when the virtual $Q\bar{Q}$ lines are on shell. The second diagram in figure 1 contributes to two insertions of the tree-level potential when all of the $Q\bar{Q}$ lines are on shell; if the $Q\bar{Q}$ lines between the gluon vertices are off shell, the diagram contributes to one insertion of the one-loop Abelian term of the potential. The third diagram contributes to one insertion of the one-loop non-Abelian term of the potential proportional to C_A when the virtual $Q\bar{Q}$ lines adjacent to the NRQCD operator $\chi^\dagger(-\frac{i}{2}\overleftrightarrow{\boldsymbol{D}})\psi$ are on shell (the virtual quark line between the two gluon vertices does not have a corresponding antiquark line, so that we can always neglect the contribution from the pole of its propagator). The remaining diagrams, as well as contributions from the first three diagrams in which the virtual $Q\bar{Q}$ lines adjacent to the NRQCD operator are off shell, involves loop corrections to S_O and are not included in eq. (5.26). Analyses of Feynman diagrams that are not shown in figure 1 can be carried out in the same way.

From scattering theory in nonrelativistic quantum mechanics, it is known that eq. (5.26) is the contribution from the wavefunction. We can rewrite eq. (5.26) as

$$\int_{\boldsymbol{p}} S_O^{\text{tree}}(\boldsymbol{p}) S_V(\boldsymbol{p}, \boldsymbol{q}) = \int_{\boldsymbol{p}} \boldsymbol{p} \lim_{E \to \boldsymbol{q}^2/m} \left[\tilde{G}_{\text{full}}(\boldsymbol{p}, \boldsymbol{q}; E)(\boldsymbol{q}^2/m - E) \right], \tag{5.27}$$

where $\tilde{G}_{\text{full}}(\boldsymbol{p}, \boldsymbol{q}; E)$ is the momentum-space Green's function that satisfies

$$\left(\frac{\boldsymbol{p}'^2}{m} - E \right) \tilde{G}_{\text{full}}(\boldsymbol{p}', \boldsymbol{p}; E) + \int_{\boldsymbol{k}} \tilde{V}(\boldsymbol{p}', \boldsymbol{k}) \tilde{G}_{\text{full}}(\boldsymbol{k}, \boldsymbol{p}; E) = (2\pi)^{d-1} \delta^{(d-1)}(\boldsymbol{p} - \boldsymbol{p}'). \tag{5.28}$$

The quantity in the square brackets in eq. (5.27) satisfies the momentum-space Schrödinger equation with respect to $\boldsymbol{p}$, with energy eigenvalue $E = \boldsymbol{q}^2/m$. Hence, eq. (5.27) represents $i\boldsymbol{\nabla}\Psi(\boldsymbol{0})$ in momentum space in $d-1$ spatial dimensions.

There are still contributions that come from loop corrections to the subdiagram S_O beyond tree level. For example, the last two Feynman diagrams in figure 1 correspond to

loop corrections to S_O. The first three Feynman diagrams in figure 1 can also contribute to S_O, when the quark lines are off shell. In general, loop corrections to S_O come from regions of loop momenta where the virtual quark lines are off shell. In the pNRQCD expression for the NRQCD LDMEs, the contribution from this momentum region corresponds to the corrections to the contact term $V_{\mathcal{O}}$, namely the term $\frac{2}{3}\frac{i\mathcal{E}_2}{m}$ and corrections of higher orders in $1/m$ that appear in eq. (3.8). Since we are only interested in the contributions that correspond to the wavefunctions, we do not need to consider S_O beyond tree level.

Having established that eq. (5.26) corresponds to the NRQCD LDME that comes from the wavefunction, we now use $\tilde{V}(\boldsymbol{p},\boldsymbol{q}) = \tilde{V}_{\text{LO}}(\boldsymbol{p}-\boldsymbol{q}) + \delta\tilde{V}(\boldsymbol{p},\boldsymbol{q})$ and expand in powers of $\delta\tilde{V}(\boldsymbol{p},\boldsymbol{q})$. This expansion corresponds to the Rayleigh-Schrödinger perturbation theory in momentum space, once the effect of $\delta\tilde{V}(\boldsymbol{p},\boldsymbol{q})$ to the energy eigenvalues are also taken into account. We can reduce the $\boldsymbol{p}^2$ and $\boldsymbol{q}^2$ terms in $\delta\tilde{V}(\boldsymbol{p},\boldsymbol{q})$ using the Schrödinger equation and the Lippmann-Schwinger equation in momentum space to obtain $\delta\tilde{\mathcal{V}}(\boldsymbol{p},\boldsymbol{q})$, which is the momentum-space version of $\delta\mathcal{V}(\boldsymbol{r},\boldsymbol{\nabla})$ in $d-1$ spatial dimensions. We display the explicit expression for $\delta\tilde{\mathcal{V}}(\boldsymbol{p},\boldsymbol{q})$ in eq. (B.6). Since we are only interested in the divergent contributions, we replace $\delta\tilde{V}(\boldsymbol{p},\boldsymbol{q})$ by $\delta\tilde{\mathcal{V}}(\boldsymbol{p},\boldsymbol{q})$ in the integrand. Then, the divergences in the loop corrections in eq. (5.26) at first order in the QMPT is given by

$$-\int_{\boldsymbol{p}} \lim_{E\to\boldsymbol{q}^2/m} \left[\int_{\boldsymbol{k}_1} \int_{\boldsymbol{k}_2} \tilde{G}(\boldsymbol{p},\boldsymbol{k}_1;E)\delta\tilde{\mathcal{V}}(\boldsymbol{k}_1,\boldsymbol{k}_2)\tilde{G}(\boldsymbol{k}_2,\boldsymbol{q};E)(\boldsymbol{q}^2/m - E) \right]. \tag{5.29}$$

In perturbative calculations of the LDMEs, we are interested in the UV divergences in this integral that is proportional to the tree-level LDME $\boldsymbol{q}$. By using the fact that this integral is at most linearly UV divergent, we can keep only the first two terms in the iterative solution in eq. (5.21), which gives

$$\int_{\boldsymbol{p}} S_O^{\text{tree}}(\boldsymbol{p})S_V(\boldsymbol{p},\boldsymbol{q})\Big|_{\text{UV}} = \int_{\boldsymbol{p}} \frac{\boldsymbol{p}\,\delta\tilde{\mathcal{V}}(\boldsymbol{p},\boldsymbol{q})}{E_{\boldsymbol{q}} - \boldsymbol{p}^2/m} + \int_{\boldsymbol{p}'}\int_{\boldsymbol{p}} \frac{\boldsymbol{p}'\tilde{V}_{\text{LO}}(\boldsymbol{p}'-\boldsymbol{p})\delta\tilde{\mathcal{V}}(\boldsymbol{p},\boldsymbol{q})}{(E_{\boldsymbol{q}} - \boldsymbol{p}'^2/m)(E_{\boldsymbol{q}} - \boldsymbol{p}^2/m)}$$
$$+ \int_{\boldsymbol{p}'}\int_{\boldsymbol{p}} \frac{\boldsymbol{p}'\delta\tilde{\mathcal{V}}(\boldsymbol{p}',\boldsymbol{p})\tilde{V}_{\text{LO}}(\boldsymbol{p}-\boldsymbol{q})}{(E_{\boldsymbol{q}} - \boldsymbol{p}'^2/m)(E_{\boldsymbol{q}} - \boldsymbol{p}^2/m)}. \tag{5.30}$$

Since in perturbation theory both $\tilde{V}_{\text{LO}}$ and $\delta\tilde{\mathcal{V}}$ are suppressed by at least α_s, this also corresponds to the expansion of eq. (5.29) to two-loop accuracy. Equation (5.30) will generally depend on $\boldsymbol{q}$, while we are only interested in the piece that is linear in $\boldsymbol{q}$, which is the contribution that is proportional to the tree-level LDME. We note that, due to rotational symmetry, eq. (5.30) vanishes when we set $\boldsymbol{q} = \boldsymbol{0}$ in $\delta\tilde{\mathcal{V}}(\boldsymbol{p},\boldsymbol{q})$ and $\tilde{V}_{\text{LO}}(\boldsymbol{p}-\boldsymbol{q})$. Hence, the nonvanishing contribution that is linear in $\boldsymbol{q}$ comes from the expansion of $\delta\tilde{\mathcal{V}}(\boldsymbol{p},\boldsymbol{q})$ and $\tilde{V}_{\text{LO}}(\boldsymbol{p}-\boldsymbol{q})$ to linear order in $\boldsymbol{q}$, which is given by

$$\int_{\boldsymbol{p}} S_O^{\text{tree}}(\boldsymbol{p})S_V(\boldsymbol{p},\boldsymbol{q})\Big|_{\text{UV}} = \left[\int_{\boldsymbol{p}} \frac{\boldsymbol{p}\left[\boldsymbol{\nabla}_{\boldsymbol{q}}^j \delta\tilde{\mathcal{V}}(\boldsymbol{p},\boldsymbol{q})\right]_{\boldsymbol{q}=\boldsymbol{0}}}{E - \boldsymbol{p}^2/m} + \int_{\boldsymbol{p}'}\int_{\boldsymbol{p}} \frac{\boldsymbol{p}'\tilde{V}_{\text{LO}}(\boldsymbol{p}'-\boldsymbol{p})\left[\boldsymbol{\nabla}_{\boldsymbol{q}}^j \delta\tilde{\mathcal{V}}(\boldsymbol{p},\boldsymbol{q})\right]_{\boldsymbol{q}=\boldsymbol{0}}}{(E - \boldsymbol{p}'^2/m)(E - \boldsymbol{p}^2/m)} \right.$$
$$\left. + \int_{\boldsymbol{p}'}\int_{\boldsymbol{p}} \frac{\boldsymbol{p}'\delta\tilde{\mathcal{V}}(\boldsymbol{p}',\boldsymbol{p})\left[\boldsymbol{\nabla}_{\boldsymbol{q}}^j \tilde{V}_{\text{LO}}(\boldsymbol{p}-\boldsymbol{q})\right]_{\boldsymbol{q}=\boldsymbol{0}}}{(E - \boldsymbol{p}'^2/m)(E - \boldsymbol{p}^2/m)} \right] \boldsymbol{q}^j. \tag{5.31}$$

This expression can also be regarded as the leading asymptotic behavior of the integrand of eq. (5.30) for large loop momenta. Because $\delta\tilde{\mathcal{V}}(\boldsymbol{p},\boldsymbol{q})$ is given as expansion in powers of

$1/m$, each coefficient of this expansion is a function of $\boldsymbol{p}$ and $\boldsymbol{q}$ and has a definite mass dimension. The same applies to $\tilde{V}_{\rm LO}(\boldsymbol{p}-\boldsymbol{q})$, which is a function of $|\boldsymbol{p}-\boldsymbol{q}|$ and also has a definite mass dimension. Hence, the large $\boldsymbol{p}$ behavior of the integrand is given by the expansions of $\tilde{V}_{\rm LO}(\boldsymbol{p}'-\boldsymbol{p})$ and $\delta\mathcal{V}(\boldsymbol{p},\boldsymbol{q})$ in powers of $\boldsymbol{q}$ at leading nonvanishing order. At this point, E in eq. (5.31) can be regarded as an arbitrary complex number, and we can take the limit $E \to E_n^{\rm LO}$ when necessary.

The quantity in the square brackets in eq. (5.31) is our expression for the UV-divergent part of the correction to the wavefunction in DR. Since we obtained eq. (5.31) from loop corrections to the NRQCD LDMEs in d spacetime dimensions, our result is valid in dimensionally regulated matching calculations in NRQCD. We also note that the loop integrands in eqs. (5.31) and (5.24) are same once the UV regulators are lifted ($\epsilon \to 0$ and $r_0 \to 0$). Hence, eq. (5.31) is the DR counterpart of eq. (5.24). We can now compute the $\delta\bar{Z}^{ij}$ from the difference in the divergent integrals in eqs. (5.24) and (5.31) between the two different regularizations. We define

$$\delta Z_E^{ij} = \mathcal{J}_{(r_0)}^{ij} - \mathcal{J}_{\rm DR}^{ij}, \tag{5.32}$$

where

$$\mathcal{J}_{(r_0)}^{ij} = \left[\int_{\boldsymbol{p}} \frac{e^{i\boldsymbol{p}\cdot\boldsymbol{r}}\boldsymbol{p}^i\big[\boldsymbol{\nabla}_{\boldsymbol{q}}^j\delta\mathcal{V}(\boldsymbol{p},\boldsymbol{q})\big]_{\boldsymbol{q}=\boldsymbol{0}}}{E-\boldsymbol{p}^2/m} + \int_{\boldsymbol{p}'}\int_{\boldsymbol{p}} \frac{e^{i\boldsymbol{p}'\cdot\boldsymbol{r}}\boldsymbol{p}'^i\tilde{V}_{\rm LO}(\boldsymbol{p}'-\boldsymbol{p})\big[\boldsymbol{\nabla}_{\boldsymbol{q}}^j\delta\mathcal{V}(\boldsymbol{p},\boldsymbol{q})\big]_{\boldsymbol{q}=\boldsymbol{0}}}{(E-\boldsymbol{p}'^2/m)(E-\boldsymbol{p}^2/m)} \right.$$
$$\left. + \int_{\boldsymbol{p}'}\int_{\boldsymbol{p}} \frac{e^{i\boldsymbol{p}'\cdot\boldsymbol{r}}\boldsymbol{p}'^i\delta\mathcal{V}(\boldsymbol{p}',\boldsymbol{p})\big[\boldsymbol{\nabla}_{\boldsymbol{q}}^j\tilde{V}_{\rm LO}(\boldsymbol{p}-\boldsymbol{q})\big]_{\boldsymbol{q}=\boldsymbol{0}}}{(E-\boldsymbol{p}'^2/m)(E-\boldsymbol{p}^2/m)} \right]_{|\boldsymbol{r}|=r_0}, \tag{5.33a}$$

$$\mathcal{J}_{\rm DR}^{ij} = \int_{\boldsymbol{p}} \frac{\boldsymbol{p}^i\big[\boldsymbol{\nabla}_{\boldsymbol{q}}^j\delta\mathcal{V}(\boldsymbol{p},\boldsymbol{q})\big]_{\boldsymbol{q}=\boldsymbol{0}}}{E-\boldsymbol{p}^2/m} + \int_{\boldsymbol{p}'}\int_{\boldsymbol{p}} \frac{\boldsymbol{p}'^i\tilde{V}_{\rm LO}(\boldsymbol{p}'-\boldsymbol{p})\big[\boldsymbol{\nabla}_{\boldsymbol{q}}^j\delta\mathcal{V}(\boldsymbol{p},\boldsymbol{q})\big]_{\boldsymbol{q}=\boldsymbol{0}}}{(E-\boldsymbol{p}'^2/m)(E-\boldsymbol{p}^2/m)}$$
$$+ \int_{\boldsymbol{p}'}\int_{\boldsymbol{p}} \frac{\boldsymbol{p}'^i\delta\mathcal{V}(\boldsymbol{p}',\boldsymbol{p})\big[\boldsymbol{\nabla}_{\boldsymbol{q}}^j\tilde{V}_{\rm LO}(\boldsymbol{p}-\boldsymbol{q})\big]_{\boldsymbol{q}=\boldsymbol{0}}}{(E-\boldsymbol{p}'^2/m)(E-\boldsymbol{p}^2/m)}. \tag{5.33b}$$

Here, the momentum integrals in $\mathcal{J}_{(r_0)}^{ij}$ are computed in finite-r regularization with $|\boldsymbol{r}|=r_0$, and the integrals in $\mathcal{J}_{\rm DR}^{ij}$ are computed in $d-1$ spatial dimensions. Note that we have now dropped the prime in $\boldsymbol{r}'$. We refer to the first terms in our definitions of $\mathcal{J}_{\rm DR}^{ij}$ and $\mathcal{J}_{(r_0)}^{ij}$ as the leading divergent contributions, and the remaining terms as the subleading divergent contributions, based on the analysis in the previous section. In case the integrals contain IR divergences, both $\mathcal{J}_{\rm DR}^{ij}$ and $\mathcal{J}_{(r_0)}^{ij}$ can be computed in $d-1$ spatial dimensions, so that the IR divergences in both integrals are regulated dimensionally, and cancel in δZ_E^{ij}. Once we obtain δZ_E^{ij}, $\delta\bar{Z}^{ij}$ is given by δZ_E^{ij} at values of E that coincide with the LO energy eigenvalues. Then, $\delta Z^{ij} = Z^{ij} - \delta^{ij}$ in the $\overline{\rm MS}$ scheme is found by subtracting the UV poles in $\delta\bar{Z}^{ij}$.

5.3 Calculation of the scheme conversion coefficient

In this section we compute the scheme conversion coefficient Z^{ij} by computing δZ_E^{ij} from the divergent integrals $\mathcal{J}_{\rm DR}^{ij}$ and $\mathcal{J}_{(r_0)}^{ij}$, which are regulated in DR and finite-r regularization, respectively. We note that since the NRQCD LDMEs are given in terms of $[\hat{\boldsymbol{r}}\cdot\boldsymbol{\nabla}\Psi(\boldsymbol{0})]^{\overline{\rm MS}}$,

we only need to obtain $\hat{\boldsymbol{r}}^i \delta Z^{ij}$. This, in turn, implies that we may contract $\hat{\boldsymbol{r}}^i$ with δZ_E^{ij} before renormalization is carried out, as long as doing so does not modify the finite parts. This is especially useful in calculations of the finite-r regularized integrals, because in this case, contracting $\hat{\boldsymbol{r}}^i$ in the integrand reduces the rank of the $\boldsymbol{r}$-dependent tensor integrals.

We first investigate the contribution to δZ_E^{ij} from the spin-independent terms in $\delta\tilde{\mathcal{V}}$. The leading divergent contribution to the dimensionally regulated integral $\mathcal{J}_{\text{DR}}^{ij}$ from the $1/m$ potential is given by

$$\frac{\pi^2 \alpha_s^2 C_F}{m}\left(\frac{C_F}{2}(1-2\epsilon) - C_A(1-\epsilon)\right) c_\epsilon \int_{\boldsymbol{p}} \frac{\boldsymbol{p}^i}{E-\boldsymbol{p}^2/m}\left[\boldsymbol{\nabla}_{\boldsymbol{q}}^j \frac{\Lambda^{2\epsilon}}{|\boldsymbol{p}-\boldsymbol{q}|^{1+2\epsilon}}\right]_{\boldsymbol{q}=0}, \qquad (5.34)$$

where c_ϵ is defined in eq. (B.5). The integral over $\boldsymbol{p}$ is computed as

$$\int_{\boldsymbol{p}} \frac{\boldsymbol{p}^i}{E-\boldsymbol{p}^2/m}\left[\boldsymbol{\nabla}_{\boldsymbol{q}}^j \frac{\Lambda^{2\epsilon}}{|\boldsymbol{p}-\boldsymbol{q}|^{1+2\epsilon}}\right]_{\boldsymbol{q}=0}$$
$$= \int_{\boldsymbol{p}} \frac{(1+2\epsilon)\hat{\boldsymbol{p}}^i \hat{\boldsymbol{p}}^j}{E-\boldsymbol{p}^2/m}\frac{\Lambda^{2\epsilon}}{|\boldsymbol{p}|^{1+2\epsilon}}$$
$$= -\frac{\delta^{ij}}{d-1}\frac{m(1+2\epsilon)}{8\pi^2}\left[\frac{1}{\epsilon_{\text{UV}}} + 2 + 2\log\left(-\frac{\Lambda^2}{2mE}\right) + O(\epsilon)\right]. \qquad (5.35)$$

Since this integral is logarithmically divergent, the contributions to the subleading terms in $\mathcal{J}_{\text{DR}}^{ij}$ from the $1/m$ potential are finite, so that we do not need to consider them. The leading divergent contribution to the finite-r regularized integral $\mathcal{J}_{(r_0)}^{ij}$ is given by

$$\frac{\pi^2 \alpha_s^2 C_F}{m}\left(\frac{C_F}{2} - C_A\right) \int_{\boldsymbol{p}} \frac{e^{i\boldsymbol{p}\cdot\boldsymbol{r}}\boldsymbol{p}^i}{E-\boldsymbol{p}^2/m}\left[\boldsymbol{\nabla}_{\boldsymbol{q}}^j \frac{\Lambda^{2\epsilon}}{|\boldsymbol{p}-\boldsymbol{q}|^{1+2\epsilon}}\right]_{\boldsymbol{q}=0}. \qquad (5.36)$$

The integral over $\boldsymbol{p}$, when contracted with $\hat{\boldsymbol{r}}^i$, is given by

$$\int_{\boldsymbol{p}} \frac{e^{i\boldsymbol{p}\cdot\boldsymbol{r}}\boldsymbol{p}\cdot\hat{\boldsymbol{r}}}{E-\boldsymbol{p}^2/m}\left[\boldsymbol{\nabla}_{\boldsymbol{q}}^j \frac{1}{|\boldsymbol{p}-\boldsymbol{q}|}\right]_{\boldsymbol{q}=0} = \int_{\boldsymbol{p}} \frac{e^{i\boldsymbol{p}\cdot\boldsymbol{r}}\hat{\boldsymbol{p}}\cdot\hat{\boldsymbol{r}}\hat{\boldsymbol{p}}^j}{E-\boldsymbol{p}^2/m}\frac{1}{|\boldsymbol{p}|} \qquad (5.37)$$
$$= -m\hat{\boldsymbol{r}}^j \frac{1}{24\pi^2}\left[\frac{4}{3} - 4\gamma_{\text{E}} - 2\log(-mEr_0^2)\right] + O(r_0),$$

where we set $|\boldsymbol{r}| = r_0$ in the last equality. From this we obtain the contribution from the $1/m$ potential to $\hat{\boldsymbol{r}}^i \delta Z_E^{ij}$ by subtracting eq. (5.34) from eq. (5.36), which gives

$$\hat{\boldsymbol{r}}^i \delta Z_E^{ij}\big|_{V^{(1)}} = \frac{\alpha_s C_F}{6}\hat{\boldsymbol{r}}^j\left[\frac{C_F}{6} - \frac{7C_A}{12} + \left(\frac{C_F}{2} - C_A\right)\left(\frac{1}{4\epsilon_{\text{UV}}} + \log(\Lambda r_0 e^{\gamma_{\text{E}}})\right)\right]. \qquad (5.38)$$

We see that the dependence on E has cancelled between the dimensionally regulated integral and the finite-r regularized integral. Hence, eq. (5.38) is valid for all P-wave eigenstates; that is, the contribution to $\delta\bar{Z}^{ij}$ from the $1/m$ potential is given by eq. (5.38) for all P-wave states. The scheme conversion coefficient $\hat{\boldsymbol{r}}^i \delta Z^{ij}$ is then given by subtracting the $1/\epsilon$ pole:

$$\hat{\boldsymbol{r}}^i \delta Z^{ij}\big|_{V^{(1)}} = \frac{\alpha_s^2 C_F}{6}\hat{\boldsymbol{r}}^j\left[\frac{C_F}{6} - \frac{7C_A}{12} + \left(\frac{C_F}{2} - C_A\right)\log(\Lambda r_0 e^{\gamma_{\text{E}}})\right]. \qquad (5.39)$$

The contributions from the velocity-dependent potential and the relativistic correction to the kinetic energy are computed in the same way, as they appear in $\delta\tilde{\mathcal{V}}(\boldsymbol{p},\boldsymbol{q})$ in the same form as the $1/m$ potential, and differ only in the ϵ-dependent coefficients. We obtain

$$\hat{\boldsymbol{r}}^i \delta Z^{ij}\big|_{V^{(2)}_{p^2}} = -\frac{\alpha_s^2 C_F^2}{3}\hat{\boldsymbol{r}}^j\left[\frac{5}{6}+\log(\Lambda r_0 e^{\gamma_{\rm E}})\right], \tag{5.40}$$

and

$$\hat{\boldsymbol{r}}^i \delta Z^{ij}\big|_{-\frac{\boldsymbol{\nabla}^4}{4m^3}} = -\frac{\alpha_s^2 C_F^2}{12}\hat{\boldsymbol{r}}^j\left[\frac{5}{6}+\log(\Lambda r_0 e^{\gamma_{\rm E}})\right]. \tag{5.41}$$

We note that the $\boldsymbol{p}$ and $\boldsymbol{p}'$-independent term in the momentum-space potential does not contribute to δZ_E. In position space, this term corresponds to the delta function potential, which vanishes on P-wave LO wavefunctions.

Now we move over to the spin-dependent contributions, which come from the hyperfine and the spin-orbit potentials. The leading divergent contribution to $\mathcal{J}_{\rm DR}^{ij}$ from the hyperfine potential is given by

$$\frac{\pi\alpha_s C_F}{4m^2}[\sigma_{i_0},\sigma_{i_1}]\otimes[\sigma_{i_0},\sigma_{i_2}]\int_{\boldsymbol{p}}\frac{\boldsymbol{p}^i}{E-\boldsymbol{p}^2/m}\left[\boldsymbol{\nabla}_{\boldsymbol{q}}^j\frac{(\boldsymbol{p}-\boldsymbol{q})^{i_1}(\boldsymbol{p}-\boldsymbol{q})^{i_2}}{(\boldsymbol{p}-\boldsymbol{q})^2}\right]_{\boldsymbol{q}=\boldsymbol{0}}$$

$$=\frac{\pi\alpha_s C_F}{4m^2}[\sigma_{i_0},\sigma_{i_1}]\otimes[\sigma_{i_0},\sigma_{i_2}]\left[2I_3^{ii_1i_2j}-\delta^{i_1j}I_1^{ii_2}-\delta^{i_2j}I_1^{ii_1}\right]_{\rm DR}, \tag{5.42}$$

and the leading divergent contribution from the spin-orbit potential to $\mathcal{J}_{\rm DR}^{ij}$ is given by

$$-\frac{3\pi\alpha_s C_F}{2m^2}\left([\sigma_{i_1},\sigma_{i_2}]\otimes 1-1\otimes[\sigma_{i_1},\sigma_{i_2}]\right)\int_{\boldsymbol{p}}\frac{\boldsymbol{p}^i}{E-\boldsymbol{p}^2/m}\left[\boldsymbol{\nabla}_{\boldsymbol{q}}^j\frac{(\boldsymbol{p}-\boldsymbol{q})^{i_1}\boldsymbol{q}^{i_2}}{(\boldsymbol{p}-\boldsymbol{q})^2}\right]_{\boldsymbol{q}=\boldsymbol{0}}$$

$$=-\frac{3\pi\alpha_s C_F}{2m^2}\left([\sigma_{i_1},\sigma_{i_2}]\otimes 1-1\otimes[\sigma_{i_1},\sigma_{i_2}]\right)\delta^{ii_2}I_1^{ii_1}\big|_{\rm DR}, \tag{5.43}$$

where the tensor integrals I_3 and I_1 are defined in DR by

$$I_3^{ijkl}\big|_{\rm DR} = \int_{\boldsymbol{p}}\frac{\boldsymbol{p}^i\boldsymbol{p}^j\boldsymbol{p}^k\boldsymbol{p}^l}{E-\boldsymbol{p}^2/m}\frac{1}{\boldsymbol{p}^4}, \tag{5.44a}$$

$$I_1^{ij}\big|_{\rm DR} = \delta^{kl}I_3^{ijkl}\big|_{\rm DR}. \tag{5.44b}$$

The corresponding contributions to $\mathcal{J}_{(r_0)}^{ij}$ are given by eqs. (5.42) and (5.43), with the tensor integrals computed in finite-r regularization:

$$I_3^{ijkl}\big|_{(r_0)} = \int_{\boldsymbol{p}}\frac{e^{i\boldsymbol{p}\cdot\boldsymbol{r}}\boldsymbol{p}^i\boldsymbol{p}^j\boldsymbol{p}^k\boldsymbol{p}^l}{E-\boldsymbol{p}^2/m}\frac{1}{\boldsymbol{p}^4}\bigg|_{|\boldsymbol{r}|=r_0}, \tag{5.45a}$$

$$I_1^{ij}\big|_{(r_0)} = \delta^{kl}I_3^{ijkl}\big|_{(r_0)}. \tag{5.45b}$$

The dimensionally regulated integrals are evaluated as

$$I_3^{ijkl}\big|_{\rm DR} = \frac{1}{d^2-1}(\delta^{ij}\delta^{kl}+\delta^{ik}\delta^{jl}+\delta^{il}\delta^{jk})\int_{\boldsymbol{p}}\frac{1}{E-\boldsymbol{p}^2/m}$$

$$=(\delta^{ij}\delta^{kl}+\delta^{ik}\delta^{jl}+\delta^{il}\delta^{jk})\frac{m^2}{60\pi^2}\sqrt{-\frac{E}{m}}+O(\epsilon), \tag{5.46a}$$

$$I_1^{ij}\big|_{\rm DR} = \delta^{ij}\frac{m^2}{12\pi}\sqrt{-\frac{E}{m}}+O(\epsilon), \tag{5.46b}$$

We note that both tensor integrals are power UV divergent. Since in DR, power UV divergences are subtracted automatically, they do not appear in the final results, especially after expansion in powers of ϵ. We note that neither tensor integrals contain logarithmic divergences. Now we compute the finite-r regularized integrals. As we have done in the case of the spin-independent contributions, we will compute the finite-r regularized integrals contracted with $\hat{\boldsymbol{r}}^i$ in the integrand, which reduces the rank of the tensor integral that we need to consider. They are computed as

$$
\begin{aligned}
\hat{\boldsymbol{r}}^i I_3^{ijkl}|_{(r_0)} &= \left(-i\frac{\partial}{\partial r}\right)\int_{\boldsymbol{p}} \frac{e^{i\boldsymbol{p}\cdot\boldsymbol{r}}}{E-\boldsymbol{p}^2/m}\frac{\boldsymbol{p}^j\boldsymbol{p}^k\boldsymbol{p}^l}{\boldsymbol{p}^4}\bigg|_{|\boldsymbol{r}|=r_0} \\
&= -im(\delta^{jk}\hat{\boldsymbol{r}}^l + \delta^{kl}\hat{\boldsymbol{r}}^j + \delta^{lm}\hat{\boldsymbol{r}}^k)\left(-i\frac{\partial}{\partial r_0}\right)\left[\frac{1}{32\pi} - \frac{\sqrt{-mE}r_0}{60\pi} + O(r_0^2)\right] \\
&\quad -i\hat{\boldsymbol{r}}^j\hat{\boldsymbol{r}}^k\hat{\boldsymbol{r}}^l\left(-i\frac{\partial}{\partial r_0}\right)\left[\frac{1}{32\pi} + O(r_0^2)\right] \\
&= \frac{m^2}{60\pi}(\delta^{jk}\hat{\boldsymbol{r}}^l + \delta^{kl}\hat{\boldsymbol{r}}^j + \delta^{lm}\hat{\boldsymbol{r}}^k)\sqrt{-\frac{E}{m}} + O(r_0), \quad (5.47\text{a})
\end{aligned}
$$

$$
\hat{\boldsymbol{r}}^i I_1^{ij}|_{(r_0)} = m^2\hat{\boldsymbol{r}}^j \frac{1}{12\pi}\sqrt{-\frac{E}{m}} + O(r_0). \quad (5.47\text{b})
$$

Here, we used $-i\frac{\partial}{\partial r}e^{i\boldsymbol{p}\cdot\boldsymbol{r}} = \boldsymbol{p}\cdot\hat{\boldsymbol{r}}e^{i\boldsymbol{p}\cdot\boldsymbol{r}}$. From the quantities in the square brackets, we see that power UV divergent corrections to the P-wave wavefunction can produce nonzero values of $\Psi_n(\boldsymbol{0})$, which vanish in $\boldsymbol{\nabla}\Psi_n(\boldsymbol{0})$. The difference in the tensor integrals between DR and finite-r regularization vanish:

$$
\hat{\boldsymbol{r}}^i I_3^{ijkl}|_{\text{DR}} - \hat{\boldsymbol{r}}^i I_3^{ijkl}|_{(r_0)} = 0 + O(\epsilon, r_0), \quad (5.48\text{a})
$$

$$
\hat{\boldsymbol{r}}^i I_1^{ij}|_{\text{DR}} - \hat{\boldsymbol{r}}^i I_1^{ij}|_{(r_0)} = 0 + O(\epsilon, r_0). \quad (5.48\text{b})
$$

Hence, the leading divergent contributions from the spin-dependent potentials cancel between $\hat{\boldsymbol{r}}^i \mathcal{J}_{\text{DR}}^{ij}$ and $\hat{\boldsymbol{r}}^i \mathcal{J}_{(r_0)}^{ij}$.

Because the leading divergent contributions from the spin-dependent potentials are power divergent, the subleading divergent contributions may contain logarithmic divergences, and must be included in the calculation of the scheme conversion coefficient. The subleading divergent contributions to $\mathcal{J}_{\text{DR}}^{ij}$ from the hyperfine and the spin-orbit potentials are given by

$$
\begin{aligned}
&\frac{\pi\alpha_s C_F}{4m^2}[\sigma_{i_0}, \sigma_{i_1}] \otimes [\sigma_{i_0}, \sigma_{i_2}] \\
&\times \Bigg\{ \int_{\boldsymbol{p}'}\int_{\boldsymbol{p}} \frac{\boldsymbol{p}'^i\tilde{V}_{\text{LO}}(\boldsymbol{p}'-\boldsymbol{p})}{(E-\boldsymbol{p}'^2/m)(E-\boldsymbol{p}^2/m)}\left[\boldsymbol{\nabla}_{\boldsymbol{q}}^j \frac{(\boldsymbol{p}-\boldsymbol{q})^{i_1}(\boldsymbol{p}-\boldsymbol{q})^{i_2}}{(\boldsymbol{p}-\boldsymbol{q})^2}\right]_{\boldsymbol{q}=0} \\
&\quad + \int_{\boldsymbol{p}'}\int_{\boldsymbol{p}} \frac{\boldsymbol{p}'^i(\boldsymbol{p}'-\boldsymbol{p})^{i_1}(\boldsymbol{p}'-\boldsymbol{p})^{i_2}}{(E-\boldsymbol{p}'^2/m)(\boldsymbol{p}'-\boldsymbol{p})^2(E-\boldsymbol{p}^2/m)}\left[\boldsymbol{\nabla}_{\boldsymbol{q}}^j \tilde{V}_{\text{LO}}(\boldsymbol{p}-\boldsymbol{q})\right]_{\boldsymbol{q}=0} \Bigg\} \\
&= -\frac{\pi^2\alpha_s^2 C_F^2}{m^2}[\sigma_{i_0}, \sigma_{i_1}] \otimes [\sigma_{i_0}, \sigma_{i_2}]\left[2J_{3a}^{ii_1i_2j} + 2J_{3b}^{ii_1i_2j} - \delta^{i_1j}J_1^{ii_2} - \delta^{i_2j}J_1^{ii_1}\right]_{\text{DR}}, \quad (5.49)
\end{aligned}
$$

and

$$
-\frac{3\pi\alpha_s C_F}{2m^2} \left([\sigma_{i_1}, \sigma_{i_2}] \otimes 1 - 1 \otimes [\sigma_{i_1}, \sigma_{i_2}]\right)
$$

$$
\times \Bigg\{ \int_{\boldsymbol{p}'} \int_{\boldsymbol{p}} \frac{\boldsymbol{p}'^i \tilde{V}_{\mathrm{LO}}(\boldsymbol{p}' - \boldsymbol{p})}{(E - \boldsymbol{p}'^2/m)(E - \boldsymbol{p}^2/m)} \left[\boldsymbol{\nabla}_{\boldsymbol{q}}^j \frac{(\boldsymbol{p} - \boldsymbol{q})^{i_1} \boldsymbol{q}^{i_2}}{(\boldsymbol{p} - \boldsymbol{q})^2} \right]_{\boldsymbol{q}=\boldsymbol{0}}
$$

$$
+ \int_{\boldsymbol{p}'} \int_{\boldsymbol{p}} \frac{\boldsymbol{p}'^i (\boldsymbol{p}' - \boldsymbol{p})^{i_1} \boldsymbol{p}^{i_2}}{(E - \boldsymbol{p}'^2/m)(\boldsymbol{p}' - \boldsymbol{p})^2 (E - \boldsymbol{p}^2/m)} \left[\boldsymbol{\nabla}_{\boldsymbol{q}}^j \tilde{V}_{\mathrm{LO}}(\boldsymbol{p} - \boldsymbol{q}) \right]_{\boldsymbol{q}=\boldsymbol{0}} \Bigg\}
$$

$$
= \frac{6\pi^2 \alpha_s^2 C_F^2}{m^2} \left([\sigma_{i_1}, \sigma_{i_2}] \otimes 1 - 1 \otimes [\sigma_{i_1}, \sigma_{i_2}]\right) \left[2 J_{3c}^{i i_1 i_2 j} + \delta^{i_2 j} J_1^{i i_1} \right]_{\mathrm{DR}}, \tag{5.50}
$$

respectively, where J_{3a}, J_{3b}, J_{3c}, and J_1 are logarithmically UV divergent tensor integrals defined in DR by

$$
J_{3a}^{ijkl}|_{\mathrm{DR}} = \int_{\boldsymbol{p}'} \int_{\boldsymbol{p}} \frac{\boldsymbol{p}'^i}{(E - \boldsymbol{p}'^2/m)(\boldsymbol{p}' - \boldsymbol{p})^2 (E - \boldsymbol{p}^2/m)} \frac{\boldsymbol{p}^j \boldsymbol{p}^k \boldsymbol{p}^l}{\boldsymbol{p}^4}, \tag{5.51a}
$$

$$
J_{3b}^{ijkl}|_{\mathrm{DR}} = \int_{\boldsymbol{p}'} \int_{\boldsymbol{p}} \frac{\boldsymbol{p}'^i (\boldsymbol{p}' - \boldsymbol{p})^j (\boldsymbol{p}' - \boldsymbol{p})^k}{(E - \boldsymbol{p}'^2/m)(\boldsymbol{p}' - \boldsymbol{p})^2 (E - \boldsymbol{p}^2/m)} \frac{\boldsymbol{p}^l}{\boldsymbol{p}^4}, \tag{5.51b}
$$

$$
J_{3c}^{ijkl}|_{\mathrm{DR}} = \int_{\boldsymbol{p}'} \int_{\boldsymbol{p}} \frac{\boldsymbol{p}'^i (\boldsymbol{p}' - \boldsymbol{p})^j \boldsymbol{p}^k}{(E - \boldsymbol{p}'^2/m)(\boldsymbol{p}' - \boldsymbol{p})^2 (E - \boldsymbol{p}^2/m)} \frac{\boldsymbol{p}^l}{\boldsymbol{p}^4}, \tag{5.51c}
$$

$$
J_1^{ij}|_{\mathrm{DR}} = \delta^{kl} J_{3a}^{ijkl}|_{\mathrm{DR}}. \tag{5.51d}
$$

The subleading divergent contributions to $\mathcal{J}_{(r_0)}^{ij}$ are also given by eqs. (5.49) and (5.50), with the UV-divergent tensor integrals regulated in finite-r regularization:

$$
J_{3a}^{ijkl}|_{(r_0)} = \int_{\boldsymbol{p}'} \int_{\boldsymbol{p}} \frac{e^{i\boldsymbol{p}'\cdot\boldsymbol{r}} \boldsymbol{p}'^i}{(E - \boldsymbol{p}'^2/m)(\boldsymbol{p}' - \boldsymbol{p})^2 (E - \boldsymbol{p}^2/m)} \frac{\boldsymbol{p}^j \boldsymbol{p}^k \boldsymbol{p}^l}{\boldsymbol{p}^4}\Big|_{|\boldsymbol{r}|=r_0}, \tag{5.52a}
$$

$$
J_{3b}^{ijkl}|_{(r_0)} = \int_{\boldsymbol{p}'} \int_{\boldsymbol{p}} \frac{e^{i\boldsymbol{p}'\cdot\boldsymbol{r}} \boldsymbol{p}'^i (\boldsymbol{p}' - \boldsymbol{p})^j (\boldsymbol{p}' - \boldsymbol{p})^k}{(E - \boldsymbol{p}'^2/m)(\boldsymbol{p}' - \boldsymbol{p})^2 (E - \boldsymbol{p}^2/m)} \frac{\boldsymbol{p}^l}{\boldsymbol{p}^4}\Big|_{|\boldsymbol{r}|=r_0}, \tag{5.52b}
$$

$$
J_{3c}^{ijkl}|_{(r_0)} = \int_{\boldsymbol{p}'} \int_{\boldsymbol{p}} \frac{e^{i\boldsymbol{p}'\cdot\boldsymbol{r}} \boldsymbol{p}'^i (\boldsymbol{p}' - \boldsymbol{p})^j \boldsymbol{p}^k}{(E - \boldsymbol{p}'^2/m)(\boldsymbol{p}' - \boldsymbol{p})^2 (E - \boldsymbol{p}^2/m)} \frac{\boldsymbol{p}^l}{\boldsymbol{p}^4}\Big|_{|\boldsymbol{r}|=r_0}, \tag{5.52c}
$$

$$
J_1^{ij}|_{(r_0)} = \delta^{kl} J_{3a}^{ijkl}|_{(r_0)}. \tag{5.52d}
$$

As the leading divergent contributions from the spin-dependent potentials cancel in δZ_E^{ij}, the spin-dependent contributions are determined by the logarithmically UV divergent tensor integrals in eqs. (5.51) and (5.52). We compute the differences in the tensor integrals between finite-r regularization and DR in appendix D. We write the results in terms of the spin and angular momentum basis given in eqs. (3.11). This requires computation of the $d - 1$-dimensional Pauli matrix combinations of the form $a \otimes b$ that appear in the spin-dependent potentials in momentum space. We do this by applying the projections onto spin triplet and spin singlet to the $a \otimes b$ as is done in eqs. (3.11). That is, we contract the Q and $\bar{Q}$ indices of $a \otimes b$ with $\boldsymbol{\sigma}$ for spin triplet and σ_5 for spin singlet, which give $a\boldsymbol{\sigma}b$ and $a\sigma_5 b$, respectively. The reduction of Pauli matrices in $d - 1$ spatial dimensions is done by repeated application of the identity $\{\sigma^i, \sigma^j\} = 2\delta^{ij}$, keeping in mind that σ_5

commutes with Pauli matrices with 3-dimensional indices, while it anticommutes with ones carrying $d-4$-dimensional indices. The Pauli matrix algebra in $d-1$ spatial dimensions can be done easily by using the MATHEMATICA package FEYNCALC with the FEYNONIUM addon [42–45]. In the spin triplet case, we apply the decomposition of the rank-2 tensor carrying indices i and j from $\sigma^i \hat{r}^k \delta Z_E^{kj}$ into the trace, antisymmetric, and symmetric traceless parts, following eqs. (3.11). We have, for spin triplet,

$$
\begin{aligned}
\sigma^i \hat{\boldsymbol{r}}^k \delta Z_E^{kj}\big|_{V_{HF}^{(2)}} &= \alpha_s^2 C_F^2 \frac{\delta^{ij}}{d-1}\boldsymbol{\sigma}\cdot\hat{\boldsymbol{r}}\left(-\frac{1}{48\epsilon_{\mathrm{UV}}}-\frac{1}{12}\log(\Lambda r_0 e^{\gamma_{\mathrm{E}}})-\frac{13}{144}\right) \\
&\quad + \alpha_s^2 C_F^2 \sigma^{[i}\hat{\boldsymbol{r}}^{j]}\left(\frac{1}{96\epsilon_{\mathrm{UV}}}+\frac{1}{24}\log(\Lambda r_0 e^{\gamma_{\mathrm{E}}})+\frac{1}{18}\right) \\
&\quad + \alpha_s^2 C_F^2 \sigma^{(i}\hat{\boldsymbol{r}}^{j)}\left(-\frac{1}{480\epsilon_{\mathrm{UV}}}-\frac{1}{120}\log(\Lambda r_0 e^{\gamma_{\mathrm{E}}})-\frac{7}{900}\right) \\
&\quad + \frac{\alpha_s^2 C_F^2}{200}f^{ij}(\hat{\boldsymbol{r}},\boldsymbol{\sigma}) + O(\epsilon, r_0), \quad\quad\quad\quad (5.53a)\\
\sigma^i \hat{\boldsymbol{r}}^k \delta Z_E^{kj}\big|_{V_{SO}^{(2)}} &= \alpha_s^2 C_F^2 \frac{\delta^{ij}}{d-1}\boldsymbol{\sigma}\cdot\hat{\boldsymbol{r}}\left(-\frac{1}{16\epsilon_{\mathrm{UV}}}-\frac{1}{4}\log(\Lambda r_0 e^{\gamma_{\mathrm{E}}})-\frac{19}{48}\right) \\
&\quad + \alpha_s^2 C_F^2 \sigma^{[i}\hat{\boldsymbol{r}}^{j]}\left(-\frac{1}{32\epsilon_{\mathrm{UV}}}-\frac{1}{8}\log(\Lambda r_0 e^{\gamma_{\mathrm{E}}})-\frac{11}{48}\right) \\
&\quad + \alpha_s^2 C_F^2 \sigma^{(i}\hat{\boldsymbol{r}}^{j)}\left(\frac{1}{32\epsilon_{\mathrm{UV}}}+\frac{1}{8}\log(\Lambda r_0 e^{\gamma_{\mathrm{E}}})+\frac{11}{48}\right) + O(\epsilon, r_0), \quad (5.53b)
\end{aligned}
$$

where $f^{ij}(\hat{\boldsymbol{r}},\boldsymbol{\sigma})$ is the F-wave contribution defined in 3 spatial dimensions in eq. (C.5). As we have argued in section 4, this contribution vanishes in the LDMEs to first order in QMPT, and so, we can neglect the F-wave contribution from the scheme conversion coefficient. For the spin singlet case, we obtain

$$
\sigma_5 \hat{\boldsymbol{r}}^i \delta Z_E^{ij}\big|_{V_{HF}^{(2)}} = -\frac{\alpha_s^2 C_F^2}{40}\sigma_5 \hat{\boldsymbol{r}}^j + O(\epsilon, r_0), \quad\quad\quad (5.54a)
$$

$$
\sigma_5 \hat{\boldsymbol{r}}^i \delta Z_E^{ij}\big|_{V_{SO}^{(2)}} = 0 + O(\epsilon, r_0). \quad\quad\quad\quad\quad (5.54b)
$$

To obtain these results, we need to compute the following Pauli matrix combinations containing σ_5 in $d-1$ spatial dimensions

$$
[\sigma^{i_0}, \sigma^i]\sigma_5[\sigma^{i_0}, \sigma^j] + [\sigma^{i_0}, \sigma^j]\sigma_5[\sigma^{i_0}, \sigma^i] = -16(1+\epsilon)\sigma_5 \delta^{ij}, \quad\quad (5.55a)
$$

$$
[\sigma^{i_0}, \sigma^{i_1}]\sigma_5[\sigma^{i_0}, \sigma^{i_1}] = -8(3+7\epsilon+2\epsilon^2)\sigma_5, \quad\quad (5.55b)
$$

$$
[\sigma^i, \sigma^j]\sigma_5 - \sigma_5[\sigma^i, \sigma^j] = 0, \quad\quad (5.55c)
$$

$$
[\sigma^{i_0}, \sigma^{i_1}]\sigma_5[\sigma^{i_0}, \sigma^{i_2}]\hat{\boldsymbol{r}}^{i_1}\hat{\boldsymbol{r}}^{i_2} = -8\sigma_5 + O(\epsilon), \quad\quad (5.55d)
$$

where i and j are 3-dimensional indices. We note that the second relation cannot be obtained from the first one, because dummy indices must be summed over in $d-1$ spatial dimensions. We compute the last relation in 3 spatial dimensions, because there are no poles in ϵ associated with this term. We note that if we were to use a scheme for spin singlet where σ_5 commutes with all Pauli matrices, similarly to what is done in naïve dimensional regularization, the spin-dependent contributions to δZ_E^{ij} for the $^1P_1$ state vanish to order ϵ^0.

We note that our results for the spin-dependent contributions in δZ_E^{ij} in eqs. (5.53) and (5.54) are independent of E, and therefore, they are the spin-dependent contributions to $\delta \bar{Z}^{ij}$ for all P-wave states. The decomposition into irreducible tensors in eqs. (5.53) diagonalizes $\delta \bar{Z}^{ij}$ in terms of wavefunctions of definite $^{2S+1}P_J$ quantum numbers in DR, because they are exactly in the form of the spin projections in DR defined in eqs. (3.11). That is, the coefficients of the tensors $\delta^{ij} \boldsymbol{\sigma} \cdot \hat{\boldsymbol{r}}/(d-1)$, $\sigma^{[i}\hat{\boldsymbol{r}}^{j]}$, $\sigma^{(i}\hat{\boldsymbol{r}}^{j)}$, and $\sigma_5 \hat{\boldsymbol{r}}^j$ apply individually to wavefunctions with quantum numbers $^3P_0$, $^3P_1$, $^3P_2$, and $^1P_1$, respectively, in the subtraction term $\hat{\boldsymbol{r}}^i \delta Z^{ij} \left[\boldsymbol{\nabla}^j \Psi_n^{\mathrm{LO}}(\mathbf{0}) \right]$. Hence, renormalization in the $\overline{\mathrm{MS}}$ scheme is carried out simply by subtracting the $1/\epsilon$ poles in the coefficients of these tensors. We combine the spin-dependent and spin-independent contributions to obtain $\hat{\boldsymbol{r}}^i \delta Z^{ij}$, which is given by

$$\sigma^i \hat{\boldsymbol{r}}^k \delta Z^{kj} = \frac{\delta^{ij}}{d-1} \boldsymbol{\sigma} \cdot \hat{\boldsymbol{r}} \delta Z_{^3P_0} + \sigma^{[i}\hat{\boldsymbol{r}}^{j]}\delta Z_{^3P_1} + \sigma^{(i}\hat{\boldsymbol{r}}^{j)}\delta Z_{^3P_2}, \tag{5.56a}$$

$$\sigma_5 \hat{\boldsymbol{r}}^k \delta Z^{kj} = \sigma_5 \hat{\boldsymbol{r}}^j \delta Z_{^1P_1}, \tag{5.56b}$$

where

$$\delta Z_{^3P_0} = -\alpha_s^2 \left[\left(\frac{2C_F^2}{3} + \frac{C_F C_A}{6} \right) \log(\Lambda r_0 e^{\gamma_{\mathrm{E}}}) + \frac{7C_F C_A}{72} + \frac{29C_F^2}{36} \right], \tag{5.57a}$$

$$\delta Z_{^3P_1} = -\alpha_s^2 \left[\left(\frac{5C_F^2}{12} + \frac{C_F C_A}{6} \right) \log(\Lambda r_0 e^{\gamma_{\mathrm{E}}}) + \frac{7C_F C_A}{72} + \frac{71C_F^2}{144} \right], \tag{5.57b}$$

$$\delta Z_{^3P_2} = -\alpha_s^2 \left[\left(\frac{13C_F^2}{60} + \frac{C_F C_A}{6} \right) \log(\Lambda r_0 e^{\gamma_{\mathrm{E}}}) + \frac{7C_F C_A}{72} + \frac{353C_F^2}{3600} \right], \tag{5.57c}$$

$$\delta Z_{^1P_1} = -\alpha_s^2 \left[\left(\frac{C_F^2}{3} + \frac{C_F C_A}{6} \right) \log(\Lambda r_0 e^{\gamma_{\mathrm{E}}}) + \frac{7C_F C_A}{72} + \frac{31C_F^2}{90} \right]. \tag{5.57d}$$

Equations (5.56) and (5.57) are our final results for the scheme conversion coefficient. The $\delta Z_{^{2S+1}P_J}$ are the diagonal elements of δZ^{ij} in terms of the $^{2S+1}P_J$ quantum numbers, so that $\hat{\boldsymbol{r}}^i \delta Z^{ij}[\boldsymbol{\nabla}^j \Psi_{n(^{2S+1}P_J)}^{\mathrm{LO}}(\mathbf{0})] = \delta Z_{^{2S+1}P_J} \hat{\boldsymbol{r}} \cdot [\boldsymbol{\nabla}\Psi_{n(^{2S+1}P_J)}^{\mathrm{LO}}(\mathbf{0})]$. This result allows us to compute the $\overline{\mathrm{MS}}$-renormalized wavefunctions at the origin by using eq. (4.17).

Similarly to the S-wave calculation in ref. [16], our calculation of the scheme-conversion coefficient is unaffected by the nonperturbative long-distance behaviors of the potential, because δZ only depends on the short-distance behaviors that determine the UV divergences of the integrals $\mathcal{J}_{\mathrm{DR}}^{ij}$ and $\mathcal{J}_{(r_0)}^{ij}$.

Equation (4.17) implies that the Λ dependence of the $\overline{\mathrm{MS}}$-renormalized P-wave wavefunction is determined by δZ. From this we obtain the following evolution equations

$$\frac{d\log\left[\hat{\boldsymbol{r}} \cdot \boldsymbol{\nabla}\Psi_{n(^3P_0)}(\mathbf{0}) \right]^{\overline{\mathrm{MS}}}}{d\log\Lambda} = -\frac{d\delta Z_{^3P_0}}{d\log\Lambda} = \alpha_s^2 \left(\frac{2}{3}C_F^2 + \frac{1}{6}C_F C_A \right), \tag{5.58a}$$

$$\frac{d\log\left[\hat{\boldsymbol{r}} \cdot \boldsymbol{\nabla}\Psi_{n(^3P_1)}(\mathbf{0}) \right]^{\overline{\mathrm{MS}}}}{d\log\Lambda} = -\frac{d\delta Z_{^3P_1}}{d\log\Lambda} = \alpha_s^2 \left(\frac{5}{12}C_F^2 + \frac{1}{6}C_F C_A \right), \tag{5.58b}$$

$$\frac{d \log \left[\hat{\boldsymbol{r}} \cdot \boldsymbol{\nabla} \Psi_{n(^3P_2)}(\mathbf{0}) \right]^{\overline{\text{MS}}}}{d \log \Lambda} = -\frac{d \delta Z_{^3P_2}}{d \log \Lambda} = \alpha_s^2 \left(\frac{13}{60} C_F^2 + \frac{1}{6} C_F C_A \right), \qquad (5.58\text{c})$$

$$\frac{d \log \left[\hat{\boldsymbol{r}} \cdot \boldsymbol{\nabla} \Psi_{n(^1P_1)}(\mathbf{0}) \right]^{\overline{\text{MS}}}}{d \log \Lambda} = -\frac{d \delta Z_{^1P_1}}{d \log \Lambda} = \alpha_s^2 \left(\frac{1}{3} C_F^2 + \frac{1}{6} C_F C_A \right), \qquad (5.58\text{d})$$

which reproduce the anomalous dimensions in eqs. (2.3).

5.4 Unitary transformation

As previously described, our calculation of the scheme-conversion coefficient δZ is valid when we compute the finite-r regularized wavefunctions at the origin by using the potentials in the on-shell matching scheme. However, long-distance nonperturbative behaviors of the potentials are given in position space in the Wilson loop matching scheme. The short-distance behaviors of the potentials differ in the two schemes, as shown in appendix B. The two matching schemes are related by a unitary transformation. If $\Psi_n^{\text{OS}}(\boldsymbol{r})$ is a solution of the Schrödinger equation with the potentials from on-shell matching, the wavefunction $\Psi_n^{\text{WL}}(\boldsymbol{r})$ that satisfies the Schrödinger equation with the potentials from Wilson loop matching is given by

$$\Psi_n^{\text{WL}}(\boldsymbol{r}) = U^{-1}(r) \Psi_n^{\text{OS}}(\boldsymbol{r}), \qquad (5.59)$$

where the unitary transformation $U(r)$ is given at short distances by [16, 39, 46]

$$U(r) = 1 + \frac{\alpha_s C_F}{4m} \left(\frac{1}{r} + \frac{\partial}{\partial r} \right) + O(1/m^2). \qquad (5.60)$$

Here we have expanded $U(r)$ in powers of $1/m$, consistently with our calculation of the wavefunctions in the QMPT. Since for P-wave states, $\boldsymbol{\nabla} \Psi_n^{\text{WL}}(\mathbf{0})|_{(r_0)}$ and $\boldsymbol{\nabla} \Psi_n^{\text{OS}}(\mathbf{0})|_{(r_0)}$ have same logarithmic divergences at $r_0 \to 0$, and power divergences disappear in $\boldsymbol{\nabla} \Psi_n(\mathbf{0})$, we expect the difference between $\boldsymbol{\nabla} \Psi_n^{\text{WL}}(\mathbf{0})$ and $\boldsymbol{\nabla} \Psi_n^{\text{OS}}(\mathbf{0})$ to be suppressed by at least $1/m$. We compute the leading nonvanishing contribution to $\boldsymbol{\nabla} \Psi_n^{\text{OS}}(\mathbf{0}) - \boldsymbol{\nabla} \Psi_n^{\text{WL}}(\mathbf{0})$ by

$$
\begin{aligned}
\hat{\boldsymbol{r}} \cdot \boldsymbol{\nabla} \Psi_n^{\text{OS}}(\mathbf{0})\big|_{(r_0)} &= \hat{\boldsymbol{r}} \cdot \boldsymbol{\nabla} U(r) \Psi_n^{\text{WL}}(\mathbf{0})\big|_{(r_0)} \\
&= \hat{\boldsymbol{r}} \cdot \boldsymbol{\nabla} \delta \Psi_n^{\text{WL}}(\mathbf{0})\big|_{(r_0)} + \hat{\boldsymbol{r}} \cdot \boldsymbol{\nabla} U(r) \Psi_n^{\text{LO}}(\mathbf{0}) + O(1/m^2) \\
&= \hat{\boldsymbol{r}} \cdot \boldsymbol{\nabla} \Psi_n^{\text{WL}}(\mathbf{0})\big|_{(r_0)} - \frac{3 \alpha_s C_F}{8m} \frac{\partial^2}{\partial r^2} \Psi_n^{\text{LO}}(\mathbf{0}) + O(1/m^2), \qquad (5.61)
\end{aligned}
$$

where in the second and third lines we used $\Psi_n^{\text{WL}}(\boldsymbol{r}) = \Psi_n^{\text{LO}}(\boldsymbol{r}) + \delta \Psi_n^{\text{WL}}(\boldsymbol{r})$. If we use eq. (5.10) to compute the second derivative of $\Psi_n^{\text{LO}}(\boldsymbol{r})$ at $r = 0$, we obtain

$$\hat{\boldsymbol{r}} \cdot \boldsymbol{\nabla} \Psi_n^{\text{OS}}(\mathbf{0})\big|_{(r_0)} = \hat{\boldsymbol{r}} \cdot \boldsymbol{\nabla} \Psi_n^{\text{WL}}(\mathbf{0})\big|_{(r_0)} - \frac{3 \alpha_s^2 C_F^2}{16} \hat{\boldsymbol{r}} \cdot \boldsymbol{\nabla} \Psi_n^{\text{LO}}(\mathbf{0}), \qquad (5.62)$$

which lets us compute $\hat{\boldsymbol{r}} \cdot \boldsymbol{\nabla} \Psi_n(\mathbf{0})$ in the on-shell matching scheme from the result in the Wilson-loop matching scheme. Similarly to the S-wave case, since the difference in the wavefunctions at the origin between the two schemes depend only on the behaviors of the

potentials at short distances, we can write the following approximate relation for P-wave states:

$$-\hat{\boldsymbol{r}} \cdot \boldsymbol{\nabla}_{\boldsymbol{r}'} \int d^3 r\, \hat{G}_n(\boldsymbol{r}', \boldsymbol{r}) \left(\frac{\alpha_s C_F \boldsymbol{L}^2}{2m^2 r^3} - \frac{\alpha_s^2 C_F^2}{4mr^2} \right) \Psi_n^{\rm LO}(\boldsymbol{r}) \Big|_{|\boldsymbol{r}'|=0} = \frac{3\alpha_s^2 C_F^2}{16} \hat{\boldsymbol{r}} \cdot \boldsymbol{\nabla} \Psi_n^{\rm LO}(\boldsymbol{0}), \ (5.63)$$

which is accurate up to corrections from second order in the QMPT. The terms in the parenthesis come from the difference in the potential in on-shell matching and Wilson-loop matching schemes at short distances. We have neglected the delta function term, because it does not contribute to P-wave states in position space. If this approximate relation holds, we may compute P-wave wavefunctions in position space in the on-shell matching scheme by using the following prescription for the potential

$$\delta V(\boldsymbol{r}, \boldsymbol{\nabla})|^{\rm OS} = \delta V(\boldsymbol{r}, \boldsymbol{\nabla})|^{\rm WL} + \frac{\alpha_s^2 C_F^2}{4mr^2} - \frac{\alpha_s C_F}{2m^2 r^3} \boldsymbol{L}^2, \tag{5.64}$$

so that while the potential in the on-shell scheme at short distance is given by the expressions in eqs. (B.2), long-distance nonperturbative behavior of the potential is given by Wilson loop matching.

6 Numerical results

We now compute electromagnetic decay rates, exclusive production cross sections, and decay constants of P-wave quarkonia, based on NRQCD factorization formulae with short-distance coefficients at two-loop accuracy and our calculation of the wavefunctions at the origin. We consider electromagnetic decay rates of χ_{Q0} and χ_{Q2} into $\gamma\gamma$, where $Q = c$ or b. We also consider exclusive production cross sections $\sigma(e^+ e^- \to \chi_{cJ} + \gamma)$ at $\sqrt{s} = 10.58\,{\rm GeV}$, which was first computed in ref. [5]. Finally, we compute scalar and axialvector decay constants $f_{\chi_{Q0}}$ and $f_{\chi_{Q1}}$, which we define in QCD by

$$\langle 0 | \bar{Q} Q | \chi_{Q0} \rangle = -m_{\chi_{Q0}} f_{\chi_{Q0}}, \tag{6.1a}$$

$$\langle 0 | \bar{Q} \gamma \gamma_5 Q | \chi_{Q1} \rangle = i f_{\chi_{Q1}} m_{\chi_{Q1}} \boldsymbol{\epsilon}_{\chi_{Q1}}, \tag{6.1b}$$

where Q is the quark field in QCD, and $\boldsymbol{\epsilon}_{\chi_{Q1}}$ is the polarization vector of χ_{Q1}. In the QCD definitions of the decay constants, the quarkonium states are relativistically normalized, while the states in the NRQCD LDMEs are normalized nonrelativistically. Although these decay constants cannot be measured directly in experiments, the axialvector decay constant appears in hard exclusive production rates of χ_{Q1} [47–50], and the scalar decay constant could be measured in lattice QCD. The NRQCD factorization formulae for these quantities at leading order in v, and corresponding short-distance coefficients at two-loop accuracies are summarized in appendix A.

6.1 Numerical inputs

We first describe the numerical inputs that we use for obtaining our results. We work consistently with the S-wave calculation in ref. [16], except that we extend the calculation of the wavefunctions and the reduced Green's functions to nonzero orbital angular momentum.

6.1.1 Heavy quark mass and strong coupling

We compute α_s in the $\overline{\text{MS}}$ scheme by using RunDec [51, 52] at 4-loop accuracy at a fixed QCD renormalization scale μ_R, which facilitates exact order by order cancellation of the logarithm of the NRQCD factorization scale between the wavefunctions at the origin and the short-distance coefficients. We set the active number of flavors n_f to be $n_f = 3$ for calculations involving charmonia, and $n_f = 4$ for bottomonia, counting only the light quark flavors. The value of μ_R that we use are $\mu_R = 2.5^{+1.5}_{-1.0}\,\text{GeV}$ for charmonium and $\mu_R = 5^{+3}_{-3}\,\text{GeV}$ for bottomonium; these ranges are obtained in ref. [53] from theoretical descriptions of masses of lowest-lying quarkonium states that have mild dependences on the scale, and have also been used for calculations of S-wave quarkonium wavefunctions in ref. [16]. As will be discussed in the next section, we also compute α_s at different scales when considering resummation of logarithms that appear in loop corrections to the potentials.

The mass m that appears in the pNRQCD expressions of the LDMEs, as well as the Schrödinger equation, is the heavy quark pole mass. As is well known, the pole mass contains a renormalon ambiguity, which makes it impossible to assign a precise numerical value to m. In order to circumvent this issue, we use the modified renormalon subtracted (RS′) mass [54], which is related to the pole mass m by

$$m = m_{\text{RS}'}(\nu_f) + \delta m_{\text{RS}'}(\nu_f), \tag{6.2}$$

where $\delta m_{\text{RS}'}(\nu_f)$ is the renormalon subtraction term that has a perturbative expansion in powers of α_s, and ν_f is the scale associated with the subtraction. The subtraction term $\delta m_{\text{RS}'}$ contains the same renormalon ambiguity as the pole mass at leading power in $1/m$, so that unlike the pole mass, $m_{\text{RS}'}(\nu_f)$ has a well-defined value. We use eq. (6.2) to replace m in the Schrödinger equation by $m_{\text{RS}'} + \delta m_{\text{RS}'}$ and expand in powers of $\delta m_{\text{RS}'}$, and then compute corrections from $\delta m_{\text{RS}'}$ by using the Rayleigh-Schrödinger perturbation theory. The expression for $\delta m_{\text{RS}'}$ can be found in refs. [53, 54]. The scale ν_f can be different from μ_R, but a value of ν_f that is too different from μ_R can produce large logarithms of ν_f/μ_R in the perturbative expansion of the renormalon subtraction term; on the other hand, a large ν_f would result in a large value of $\delta m_{\text{RS}'}$, which could negatively impact the convergence of the perturbation series. We choose $\nu_f = 2\,\text{GeV}$, and expand $\delta m_{\text{RS}'}$ in powers of $\alpha_s(\mu_R)$. At $\nu_f = 2\,\text{GeV}$, the RS′ quark masses are given by $m_{c,\text{RS}'} = 1316(41)\,\text{MeV}$ for charm, and $m_{b,\text{RS}'} = 4743(41)\,\text{MeV}$ for bottom [53]. Because $\delta m_{\text{RS}'}$ begins at order α_s^2, we only need to consider the correction to the wavefunction that comes from the kinetic energy term in the Schrödinger equation.

Equation (6.2) can also be used in the NRQCD factorization formulae, where inverse powers of the heavy quark pole mass appear. In this case, replacing m by $m_{\text{RS}'} + \delta m_{\text{RS}'}$ and expanding in powers of $\delta m_{\text{RS}'}$ produces corrections to the short-distance coefficients at relative order α_s^2.

6.1.2 Potentials at long distances

For the static potential and the $1/m$ potential, we adopt the approach in ref. [16] to combine the perturbative expressions that are valid at short distances and lattice determinations at

long distances. The potentials can be written as

$$V^{(0)}(r) = V^{(0)}(r)|_{\text{pert}} + V^{(0)}(r)|_{\text{long}}, \tag{6.3a}$$

$$V^{(1)}(r)|^{\text{WL}} = V^{(1)}(r)|_{\text{pert}}^{\text{WL}} + V^{(1)}(r)|_{\text{long}}^{\text{WL}}, \tag{6.3b}$$

where the superscript WL denotes that the $1/m$ potential is computed in the Wilson loop matching scheme. The $V^{(0)}(r)|_{\text{long}}$ and $V^{(1)}(r)|_{\text{long}}^{\text{WL}}$ are smooth functions of r that vanish at short distances, which are chosen so that the expressions in eqs. (6.3) reproduce the lattice QCD determinations in refs. [55, 56] at long distances. We use the explicit expressions for the potentials in ref. [16], where perturbative corrections are included up to order α_s^3 (relative order α_s^2) in $V^{(0)}(r)|_{\text{pert}}$ [57, 58], and $V^{(1)}(r)|_{\text{pert}}^{\text{WL}}$ is computed at leading order in α_s (order α_s^2) [39]. In computing the $V^{(0)}(r)|_{\text{pert}}$ and $V^{(1)}(r)|_{\text{pert}}^{\text{WL}}$, we choose the renormalization scale as $\mu_r = (r^{-2} + \mu_R^2)^{1/2}$, so that $\mu_r \approx 1/r$ at short distances; this resums the logarithms in r that appear in the loop corrections to the static potential. This resummation makes the effects of higher order perturbative corrections to $V^{(0)}(r)|_{\text{pert}}$ beyond what we include our calculations numerically insignificant [16].

We use the expressions in eqs. (6.3) to define the LO potential and the $1/m$ potential that we use for computing the wavefunctions in the on-shell matching scheme. We define the LO potential by

$$V_{\text{LO}}(r) = -\frac{\alpha_s(\mu_R)C_F}{r} + V^{(0)}(r)|_{\text{long}}, \tag{6.4}$$

where in the first term, we compute α_s at a fixed renormalization scale μ_R. In this case, the Coulombic correction term $\delta V_C(r)$ is given by

$$\delta V_C(r) = V^{(0)}(r) - V_{\text{LO}}(r) = V^{(0)}(r)|_{\text{pert}} + \frac{\alpha_s(\mu_R)C_F}{r}. \tag{6.5}$$

Here, the last term combined with the leading-order (order-α_s) term in the perturbative expression for the static potential $V^{(0)}(r)|_{\text{pert}}$ gives $[\alpha_s(\mu_R) - \alpha_s(\mu_r)]C_F/r$, which cancels the μ_R dependence of the LO potential. Hence, corrections from $\delta V_C(r)$ cancel the μ_R dependences of the LO wavefunctions. Since this term and the order-α_s^2 term in $V^{(0)}(r)|_{\text{pert}}$ correspond to the change of the Coulomb strength of the LO potential of relative order α_s, we consider the correction from $\delta V_C(r)$ to the wavefunction as a correction of relative order α_s.

Following the prescription in eq. (5.64), we write the $1/m$ potential in the on-shell scheme by

$$V^{(1)}(r)|^{\text{OS}} = \frac{\alpha_s^2(\mu_R)C_F(\frac{1}{2}C_F - C_A)}{2r^2} + V^{(1)}(r)|_{\text{long}}^{\text{WL}}, \tag{6.6}$$

where in the first term, we compute α_s at a fixed scale μ_R. This allows us to compute the wavefunctions in the on-shell matching scheme directly without computing the unitary transformation of the wavefunction in the Wilson loop matching scheme, provided that the approximate relation in eq. (5.63) is satisfied.

6.1.3 Reduced Green's function

We now describe the method that we use to compute the reduced Green's function $\hat{G}_n(\boldsymbol{r}', \boldsymbol{r})$. We use two different methods for numerical computation depending on the

region of $|\boldsymbol{r}|$ and $|\boldsymbol{r}'|$. In the first method, which is valid for small $|\boldsymbol{r}|$ or $|\boldsymbol{r}'|$, we obtain the reduced Green's function from the relation in eq. (4.10) by computing numerically the Green's function $G(\boldsymbol{r}, \boldsymbol{r}'; E)$ for different values of E. Since we only need P-wave contributions, we first decompose the Green's function into specific orbital angular momentum contributions as

$$G(\boldsymbol{r}', \boldsymbol{r}; E) = \sum_{L=0}^{\infty} \sum_{M=-L}^{+L} G^L(r', r; E) Y_L^M(\hat{\boldsymbol{r}}') Y_L^{M*}(\hat{\boldsymbol{r}}), \qquad (6.7)$$

where $r = |\boldsymbol{r}|$ and $r' = |\boldsymbol{r}'|$. For each L, $G^L(r', r; E)$ satisfies the differential equation

$$\left[-\frac{1}{m} \left(\frac{\partial^2}{\partial r^2} + \frac{2}{r} \frac{\partial}{\partial r} \right) + V_{\mathrm{LO}}(r) + \frac{L(L+1)}{mr^2} - E \right] G^L(r', r; E) = \frac{1}{r^2} \delta(r - r'). \qquad (6.8)$$

To obtain solutions of eq. (6.8), we extend the method used in refs. [16, 25, 59] for S-wave states to arbitrary orbital angular momentum. The solution of eq. (6.8) can be written in the form

$$G^L(r', r; E) = m \frac{u_>(r_>)}{r_>} \frac{u_<(r_<)}{r_<}, \qquad (6.9)$$

where $r_> = \max(r, r')$, $r_< = \min(r, r')$, and $u_>$, $u_<$ are two linearly independent solutions of the homogeneous equation

$$\left[\frac{d^2}{dr^2} + m(E - V_{\mathrm{LO}}(r)) - \frac{L(L+1)}{r^2} \right] u(r) = 0, \qquad (6.10)$$

with the boundary conditions

$$W(u_>, u_<)(r) = u_>(r) u_<'(r) - u_>'(r) u_<(r) = 1, \qquad (6.11)$$

for any r. We note that the Wrońskian $W(u_>, u_<)(r)$ of the two solutions is independent of r, since eq. (6.10) does not contain $du(r)/dr$. The conditions that uniquely determine $u_>(r)$ and $u_<(r)$ read

$$\lim_{r \to 0} r^{-L} u_<(r) = 0, \qquad\qquad \lim_{r \to 0} \frac{d}{dr} \left(r^{-L} u_<(r) \right) = 1, \qquad (6.12a)$$

$$\lim_{r \to \infty} u_>(r) = 0, \qquad\qquad \lim_{r \to 0} r^L u_>(r) = \frac{1}{2L+1}. \qquad (6.12b)$$

The conditions on the regular solution $u_<(r)$ are obtained from the fact that a solution of eq. (6.10) that is regular at $r = 0$ must vanish like r^{L+1} as $r \to 0$. The condition that $u_>(r)$ is square integrable unambiguously fixes $u_>(r)$, because in general the second solution is a linear combination of $u_>(r)$ and $u_<(r)$. We obtain $u_<(r)$ and $u_>(r)$ by solving eq. (6.10) numerically in MATHEMATICA, from which we determine $G^L(r', r; E)$ for a given E. Then, by using the relation in eq. (4.10), we obtain the reduced Green's function for small $r_<$. Since when $E = E_n^{\mathrm{LO}}$, $u_<(r)$ is a bound-state solution of eq. (6.10), the square-integrable solution $u_>(r)$ does not exist if E coincides with the eigenenergies of the Schrödinger equation. Hence, when using eq. (4.10), we cannot take E to be too close to E_n^{LO}. In our numerical calculations, we use $\eta = 10^{-2}\,\mathrm{GeV}$.

Since in the first method, $u_<(r)$ is determined by initial conditions at $r = 0$, and E cannot take values that are too close to the eigenenergies of the Schrödinger equation, the calculation of the Green's function becomes unstable when r and r' are both large. Hence, for large r and r', we use the formal expression in eq. (4.7) to compute the reduced Green's function by truncating the series by including a limited number of lowest eigenstates. In our numerical calculations, we include 9 lowest P-wave eigenstates in the truncated series. Similarly to the S-wave case, we expect this method to become unreliable for small r or r', because there the series may not converge well. Hence, we combine the reduced Green's functions computed from the two different methods by using

$$\hat{G}_n(\boldsymbol{r}', \boldsymbol{r}) = b(r_<) \times \hat{G}_n(\boldsymbol{r}', \boldsymbol{r})|_{\text{short}} + [1 - b(r_<)] \times \hat{G}_n(\boldsymbol{r}', \boldsymbol{r})|_{\text{long}}, \tag{6.13}$$

where $\hat{G}_n(\boldsymbol{r}', \boldsymbol{r})|_{\text{short}}$ is computed from eqs. (6.9) and (4.10), while $\hat{G}_n(\boldsymbol{r}', \boldsymbol{r})|_{\text{long}}$ is obtained by truncating the series in eq. (4.7). Here, $b(r)$ is a smooth function with $b(0) = 1$ and $b(\infty) = 0$, so that eq. (6.13) is reliable for all r and r'. The explicit form of $b(r)$ that we use is

$$b(r) = \frac{1}{\pi} \left[\tan^{-1}(4m(r_b - r)) - \tan^{-1}(4mr_b) \right] + 1, \tag{6.14}$$

with $r_b = 1 \, \text{GeV}^{-1}$. We note that although the above form of $b(r)$ has a nonzero $b(\infty)$, it is still adequate for our numerical calculations, because in practice we work in a finite range of r, and $b(r)$ is much smaller than 1 at large r for both charm and bottom masses. The validity of the reduced Green's function that we obtain can be tested numerically by checking the relations

$$\left(E_k^{\text{LO}} - E_n^{\text{LO}} \right) \int d^3r \, \hat{G}_n(\boldsymbol{r}', \boldsymbol{r}) \Psi_k^{\text{LO}}(\boldsymbol{r}) = \Psi_k^{\text{LO}}(\boldsymbol{r}'), \tag{6.15a}$$

$$\int d^3r \, \hat{G}_n(\boldsymbol{r}', \boldsymbol{r}) \Psi_n^{\text{LO}}(\boldsymbol{r}) = 0, \tag{6.15b}$$

for $k \neq n$. We note that $b(r)$ has negligible effects in calculations of the corrections $\delta \boldsymbol{\nabla} \Psi_n(\boldsymbol{0})|_{(r_0)}$, because the position-space integrals in eq. (4.14) are dominated by contributions at small r. On the other hand, the second term in eq. (6.13) becomes necessary for computing $\delta \Psi_n(\boldsymbol{r})$ at large r, or for reproducing the relations in eq. (6.15) numerically at large r'.

We compute the eigenenergies and wavefunctions of the LO Schrödinger equation by finding values of E that makes $u_<(r)$ square integrable; in this case, E is a LO eigenenergy and the corresponding radial wavefunction is given by $u_<(r)/r$ times a normalization coefficient. An alternative way for finding $\Psi_n^{\text{LO}}(\boldsymbol{r})$ and E_n^{LO} is to use the Crank-Nicolson method [60]. The advantage of this method is that it does not depend on an initial condition, so that this method is free of accumulating numerical errors for large r. We use the Crank-Nicolson method to test the validity of the numerical results for E_n^{LO} and $\Psi_n^{\text{LO}}(\boldsymbol{r})$ that we obtain. We use the modified Crank-Nicolson method developed in ref. [61], which has the advantage that it does not require the Gram-Schmidt process when computing eigenenergies and wavefunctions for excited states.

We also use the Crank-Nicolson method to test the convergence of the corrections to the wavefunctions that we compute. By using the Crank-Nicolson method, we can compute

corrections to the wavefunctions to all orders in the Rayleigh-Schrödinger perturbation theory by finding bound-state solutions of the Schrödinger equation including the correction terms to the potential, as long as the correction terms are smooth functions of r; this is possible because the Crank-Nicolson method remains reliable even when the potential diverges faster than $1/r$. This result can be compared with the wavefunction computed to first order in the Rayleigh-Schrödinger perturbation theory to estimate the size of higher order corrections. We present the numerical test of convergence of the corrections from the $1/m$ potential in Rayleigh-Schrödinger perturbation theory in appendix E. On the other hand, the all-orders calculation using the Crank-Nicolson method does not allow an order-by-order calculation that is necessary in establishing exact two-loop level cancellations of the divergent small r behavior between the finite-r regularized wavefunctions at the origin and the scheme conversion coefficient δZ. Therefore, the all-orders calculation will only be used to complement the order-by-order calculation in the Rayleigh-Schrödinger perturbation theory.

6.2 Numerical results for P-wave charmonia

We now present our numerical results for P-wave charmonia. We list the central values of $|R'_{\text{LO}}(0)|$ for the two lowest P-wave states in table 1. For brevity, we refer to $|R'_{\text{LO}}(0)|$ as the wavefunction at the origin in discussions of P-wave quarkonia. The LO binding energies for the $1P$ and $2P$ states are $E_{1P}^{\text{LO}} = 0.568\,\text{GeV}$ and $E_{2P}^{\text{LO}} = 1.03\,\text{GeV}$, respectively. We note that the LO binding energy for the $1P$ state is consistent with the χ_{cJ} and h_c masses, when compared with the LO binding energies of the S-wave states $E_{1S}^{\text{LO}} = 0.233\,\text{GeV}$ and $E_{2S}^{\text{LO}} = 0.769\,\text{GeV}$ in ref. [16]. The $1P$ charmonium mass $m_{1P} = 3.47\,\text{GeV}$ computed from $m_{1P} = 2m_{\text{RS}'} + 2\delta m_{\text{RS}'} + E_{1P}^{\text{LO}}$ is in good agreement with the PDG values of χ_{cJ} and h_c masses within $0.1\,\text{GeV}$ [62]. Because we find good agreement in the $1P$ charmonium masses with measurement, we use the measured charmonium masses from ref. [62] when computing decay rates and decay constants, because the experimental values have uncertainties that are negligible compared to the theoretical uncertainties. We identify the $1P$ states with angular momentum quantum numbers ^3P_J and $^1P_1$ as χ_{cJ} and h_c, respectively. While the binding energy for the $2P$ state is also consistent with the mass of the $X(3872)$, we do not identify the $2P$ states with the $X(3872)$ or other states of similar masses, because those states have masses that are heavier than the open flavor threshold, and are unlikely to be pure quarkonium states.[9]

Unsurprisingly, our results for $|R'_{\text{LO}}(0)|$ for charmonium states are much larger than what we obtain in perturbative QCD, where the long-distance nonperturbative effects in the potentials are neglected. For the $1P$ state, a perturbative QCD calculation at same values of α_s and m gives a value of $|R'_{\text{LO}}(0)|$ that is only a few percent of our result in table 1. The discrepancy is even stronger for the $2P$ state, because in perturbative QCD,

---

[9]This is also supported by the fact that the radial size of the LO wavefunction for the $2P$ state is not small compared to the distance $r_c \approx 5.8\,\text{GeV}^{-1}$ at which the static potential is expected to suffer from color screening [55]. For example, in the case of the $2P$ wavefunction, the contributions to the normalization $\int d^3r\, |\Psi^{\text{LO}}(\boldsymbol{r})|^2 = 1$ from the regions $r < r_c$ and $r > r_c$ are comparable in size, while the normalization of the $1P$ wavefunction is dominated by $r < r_c$.

State	$\|R'_{\mathrm{LO}}(0)\|$ (GeV$^{5/2}$)	$\delta_\Psi^{\mathrm{NC}}\|_{^3P_0}$	$\delta_\Psi^{\mathrm{NC}}\|_{^3P_1}$	$\delta_\Psi^{\mathrm{NC}}\|_{^3P_2}$	$\delta_\Psi^{\mathrm{NC}}\|_{^1P_1}$	δ_Ψ^{C}	$\delta_\Psi^{\mathrm{RS'}}$
$1P$	0.184	0.453	0.493	0.505	0.500	0.266	0.103
$2P$	0.243	0.513	0.547	0.569	0.558	0.201	0.102

Table 1. LO wavefunctions at the origin $|R'(0)|$ and relative corrections to the wavefunctions at the origin in the $\overline{\mathrm{MS}}$ scheme at scale $\Lambda = m$ for $1P$ and $2P$ charmonium states. $\delta_\Psi^{\mathrm{NC}}$ is the correction from the $1/m$ and $1/m^2$ potentials, δ_Ψ^{C} is the Coulombic correction, and $\delta_\Psi^{\mathrm{RS'}}$ is the correction from the RS$'$ subtraction term. The $\delta_\Psi^{\mathrm{NC}}$, δ_Ψ^{C}, and $\delta_\Psi^{\mathrm{RS'}}$ are dimensionless.

$|R'_{\mathrm{LO}}(0)|$ decreases with increasing radial excitation, which is opposite to what we find when we include the long-distance nonperturbative effects in the static potential.

We list the corrections to the wavefunctions at the origin relative to the leading-order wavefunction at the origin in table 1. The corrections are classified as the non-Coulombic correction $\delta_\Psi^{\mathrm{NC}}$ coming from the $1/m$ and $1/m^2$ potentials, the Coulombic correction δ_Ψ^{C} that comes from $\delta V_C(r)$, and the correction $\delta_\Psi^{\mathrm{RS'}}$ from the RS$'$ subtraction term. Explicit expressions for $\delta_\Psi^{\mathrm{NC}}$, δ_Ψ^{C}, and $\delta_\Psi^{\mathrm{RS'}}$ are given by

$$\delta_\Psi^{\mathrm{NC}} = -\delta Z_{^{2S+1}P_J} - \frac{1}{\hat{\boldsymbol{r}} \cdot \boldsymbol{\nabla}\Psi_n^{\mathrm{LO}}(\boldsymbol{0})}$$
$$\times \left[\hat{\boldsymbol{r}}' \cdot \boldsymbol{\nabla}_{\boldsymbol{r}'} \int d^3r\, \hat{G}_n(\boldsymbol{r}',\boldsymbol{r})\delta\mathcal{V}(\boldsymbol{r},\boldsymbol{\nabla})\Psi_n^{\mathrm{LO}}(\boldsymbol{r})\Big|_{|\boldsymbol{r}'|=r_0} \right.$$
$$\left. + \frac{E_n^{\mathrm{LO}}}{m}\hat{\boldsymbol{r}}' \cdot \boldsymbol{\nabla}_{\boldsymbol{r}'} \int d^3r\, \hat{G}_n(\boldsymbol{r}',\boldsymbol{r})\left(V_{p^2}^{(2)}(r) + \frac{1}{2}V_{\mathrm{LO}}(r)\right)\Psi_n^{\mathrm{LO}}(\boldsymbol{r})\Big|_{|\boldsymbol{r}'|=0} \right]$$
$$+ \frac{1}{2m}\left[-V_{p^2}^{(2)}(0) + \int d^3r\, \left(V_{p^2}^{(2)}(r) + \frac{1}{2}V_{\mathrm{LO}}(r)\right)\left|\Psi_n^{\mathrm{LO}}(\boldsymbol{r})\right|^2 \right], \tag{6.16a}$$

$$\delta_\Psi^{\mathrm{C}} = -\frac{1}{\hat{\boldsymbol{r}} \cdot \boldsymbol{\nabla}\Psi_n^{\mathrm{LO}}(\boldsymbol{0})}\hat{\boldsymbol{r}}' \cdot \boldsymbol{\nabla}_{\boldsymbol{r}'} \int d^3r\, \hat{G}_n(\boldsymbol{r}',\boldsymbol{r})\delta V_C(r)\Psi_n^{\mathrm{LO}}(\boldsymbol{r})\Big|_{|\boldsymbol{r}'|=0}, \tag{6.16b}$$

$$\delta_\Psi^{\mathrm{RS'}} = -\frac{1}{\hat{\boldsymbol{r}} \cdot \boldsymbol{\nabla}\Psi_n^{\mathrm{LO}}(\boldsymbol{0})}\frac{\delta m_{\mathrm{RS'}}}{m_{\mathrm{RS'}}}\hat{\boldsymbol{r}}' \cdot \boldsymbol{\nabla}_{\boldsymbol{r}'} \int d^3r\, \hat{G}_n(\boldsymbol{r}',\boldsymbol{r})V_{\mathrm{LO}}(r)\Psi_n^{\mathrm{LO}}(\boldsymbol{r})\Big|_{|\boldsymbol{r}'|=0}, \tag{6.16c}$$

so that the $\overline{\mathrm{MS}}$-renormalized wavefunctions at the origin are given by

$$\hat{\boldsymbol{r}} \cdot \boldsymbol{\nabla}\Psi_n(\boldsymbol{0})|_{\overline{\mathrm{MS}}} = \hat{\boldsymbol{r}} \cdot \boldsymbol{\nabla}\Psi_n^{\mathrm{LO}}(\boldsymbol{0}) \times \left(1 + \delta_\Psi^{\mathrm{NC}} + \delta_\Psi^{\mathrm{C}} + \delta_\Psi^{\mathrm{RS'}} + O(\Lambda_{\mathrm{QCD}}^2/m^2, v^3) \right). \tag{6.17}$$

We compute $\delta_\Psi^{\mathrm{NC}}$ at the $\overline{\mathrm{MS}}$ scale $\Lambda = m$. We neglect the term $-\frac{1}{2m}V_{p^2}^{(2)}(0)$ in $\delta_\Psi^{\mathrm{NC}}$, because it cancels the $i\mathcal{E}_2/m$ term in the pNRQCD expressions for the LDMEs, and does not contribute to decay or production rates.

In computing $\delta_\Psi^{\mathrm{NC}}$, the finite-$r$ regulator r_0 must be taken to be as small as possible to suppress terms of positive powers of r_0, as long as the numerical calculation is stable. Because in the P-wave case, there are no power divergences in the finite-r regularized wavefunction at the origin, we can take r_0 to be much smaller than the S-wave calculation in ref. [16], as long as the approximate relation in eq. (5.63) is well reproduced. We find that eq. (5.63) remains valid for both $1P$ and $2P$ states with errors of about 1.5% even at very small values of r_0 of about $0.001\,\mathrm{GeV}^{-1}$. The numerical results for $\delta_\Psi^{\mathrm{NC}}$ are almost
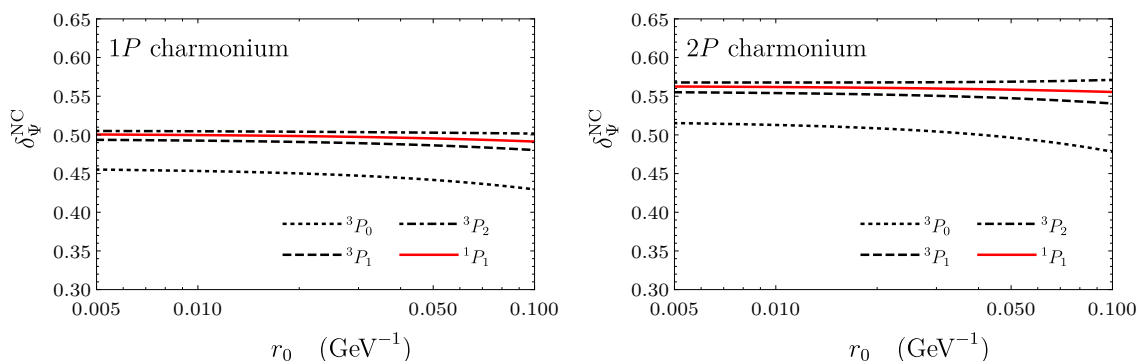
Figure 2. Non-Coulombic corrections $\delta_\Psi^{\rm NC}$ at finite r_0 for the charmonium $1P$ (left panel) and $2P$ (right panel) states, for angular momentum quantum numbers $^3P_0$ (dotted lines), $^3P_1$ (dashed lines), $^3P_2$ (dot-dashed lines), and $^1P_1$ (red solid lines). The r_0 dependences are mild for the range $r_0 < 0.02\,{\rm GeV}^{-1}$ that we consider.

insensitive to r_0 for values of r_0 less than about $0.02\,{\rm GeV}^{-1}$. We show the r_0 dependence of non-Coulombic corrections for $1P$ and $2P$ states in figure 2. We fix $r_0 = 0.01\,{\rm GeV}^{-1}$ for computing the central values of $\delta_\Psi^{\rm NC}$ and neglect the uncertainty in the numerical calculation of finite-r regularized wavefunctions at the origin compared to other uncertainties.

We note that the non-Coulombic corrections $\delta_\Psi^{\rm NC}$ are positive and sizable for all $^{2S+1}P_J$ states. This is in contrast with the negative order-α_s^2 corrections to the short-distance coefficients, as can be seen from the NRQCD factorization formulae appendix A. Hence, similarly to the S-wave case in ref. [16], we expect sizable cancellations in the Λ-independent finite parts between the order-α_s^2 short-distance coefficients and $\delta_\Psi^{\rm NC}$, and reductions in the size of the corrections to the decay and production rates beyond tree level.

The differences in $\delta_\Psi^{\rm NC}$ between different angular momentum states are small at the $\overline{\rm MS}$ scale $\Lambda = m$. The largest deviation occurs for the $^3P_0$ state, for which the non-Coulombic correction is smaller by about 5% compared to other angular momentum states. This shows that heavy quark spin symmetry is conserved approximately between P-wave quarkonium wavefunctions at the origin. The contributions from the long-distance part of the $1/m$ potential are tiny, and amount to less than 1% for both $1P$ and $2P$ states. It is worth noting that, as can be seen from the results in appendix F, the results for $\delta_\Psi^{\rm NC}$ obtained from perturbative QCD calculations are comparable in order of magnitude to the results in table 1 for a similar value of α_s [$\alpha_s(\mu_R = 2.5\ {\rm GeV}) \approx 0.27$], even though the specific values, especially the dependence on angular momentum quantum numbers, are quite different. This, and the fact that $\delta_\Psi^{\rm NC}$ contain finite parts of order α_s^2 that remain after subtracting the $1/\epsilon_{\rm UV}$ poles, suggest that the bulk of $\delta_\Psi^{\rm NC}$ may come from corrections to the wavefunctions at short distances.

In ref. [14], the authors argued that $|R'(0)|$ is larger for the $^3P_2$ state compared to the $^3P_0$ state, based on the fact that the spin-dependent potential is attractive for the $^3P_2$ state, while the sign is opposite for the $^3P_0$ state. This is opposite to what we find in the calculation of $\delta_\Psi^{\rm NC}$. However, the analysis in ref. [14] does not take into account the fact that the corrections from the spin-dependent potential are UV divergent, and so,

conclusions on the sizes or even the signs of the corrections can only be obtained after the divergences are subtracted through renormalization, as we have done in this work in the $\overline{\mathrm{MS}}$ scheme.

Since δ_Ψ^{C} is of relative order α_s, the Coulombic correction at second order in the Rayleigh-Schrödinger perturbation theory is of relative order α_s^2, and so, it may be important to include this correction. Explicit numerical calculations of the second order correction show that this correction is negligibly small. We also confirm this from the calculation of Coulombic corrections to all orders by using the modified Crank-Nicolson method [61], which also shows that the Coulombic corrections converge rapidly. Hence, we neglect the Coulombic corrections beyond first order in the QMPT. The corrections from the RS$'$ subtraction term are small for both $1P$ and $2P$ states.

Before we compute decay and production rates of P-wave charmonia at two-loop level, let us compare our results at leading order in $1/m$ with potential model calculations that are often used in phenomenological studies of P-wave charmonium production and decay.[10] Our first-principles calculation gives the value $|R'_{\mathrm{LO}}(0)|^2 = 0.034^{+0.03}_{-0.00}\,\mathrm{GeV}^5$ for the $1P$ state. Here, the uncertainties come mainly from the variation of μ_R. If we include the Coulombic correction δ_Ψ^{C}, which would be appropriate for calculations at one-loop level, we obtain $|R'_{\mathrm{LO}}(0)|^2(1+\delta_\Psi^{\mathrm{C}})^2 = 0.054^{+0.01}_{-0.00}\,\mathrm{GeV}^5$. This is close to the values obtained phenomenologically in refs. [5, 8] from two-photon decay rates of χ_{c0} and χ_{c2} at one-loop level, and also to the value obtained from inclusive hadroproduction rates of χ_{c1} and χ_{c2} in ref. [63]. On the other hand, potential-model calculations usually give larger values of the wavefunction at the origin; the results for $|R'(0)|^2$ for the $1P$ state from several widely used potential models in refs. [64–67] range from $0.068\,\mathrm{GeV}^5$ to $0.131\,\mathrm{GeV}^5$. We note that, however, potential models have charm quark masses whose numerical values differ wildly from the RS$'$ mass that we use. The model-dependent charm quark mass also affects NRQCD factorization formulae through their dependences on the heavy quark pole mass. As can be seen from the factorization formulae in appendix A, the heavy quark pole mass appears in electromagnetic decay rates and exclusive electromagnetic production rates at leading orders in v in the form $\langle Q|\mathcal{O}(^{2S+1}P_J)|Q\rangle/m^3$. Hence, for the purpose of comparing with phenomenological models, it makes more sense to consider the combination $|R'(0)|^2/m^3$. Our result including the Coulombic correction gives $|R'_{\mathrm{LO}}(0)|^2(1+\delta_\Psi^{\mathrm{C}})^2/m^3_{\mathrm{RS}'} = 0.024^{+0.01}_{-0.00}\,\mathrm{GeV}^2$, while potential-model calculations in refs. [64–67] give values of $|R'(0)|^2/m^3$ that are between $0.021\,\mathrm{GeV}^2$ and $0.023\,\mathrm{GeV}^2$. Considering that these values are only valid up to corrections of relative order v^2, we conclude that at one-loop level, the potential-model results agree well with our first-principles calculation of the wavefunctions at the origin for $1P$ charmonia, as long as the heavy quark mass is chosen appropriately in model calculations of decay and production rates, similarly to what has been done in the model-dependent analysis in ref. [24].

---

[10]While potential-model calculations may attempt to capture the effect of long-distance behavior of higher order potentials, this requires an arbitrary separation between short and long-distance contributions which is model dependent and can become uncontrollable. Moreover, it is likely that the long-distance behaviors of higher order potentials have insignificant effects to $|R'(0)|$ compared to uncertainties and model dependences of potential-model results, because the slope of the potential at long distances do not change appreciably by inclusion of the higher order potentials.

In the case of inclusive production processes, large p_T cross sections of P-wave quarkonia depend on the dimensionless combination of the leading-order LDMEs and the heavy quark mass given by $|R'(0)|^2/m^5$, which can be seen from the calculation of single-parton fragmentation functions into P-wave quarkonium [68]. Our first-principles calculation gives $|R'_{\rm LO}(0)|^2(1 + \delta_\Psi^{\rm C})^2/m^5_{\rm RS'} = 0.014$, while the potential-model calculations based on refs. [64–67] give values of $|R'(0)|^2/m^5$ that range from 0.006 to 0.011. Especially, the Buchmüller-Tye potential model in ref. [64] that is often adopted in phenomenological studies of P-wave charmonium hadroproduction (see, for example, refs. [69, 70]) gives the value $|R'(0)|^2/m^5 = 0.011$. While this model calculation is smaller than our first-principles calculation by about 23%, it is fair to say that they are consistent, considering the current level of accuracy of inclusive charmonium production phenomenology.

Even though our first-principles calculations of the P-wave wavefunctions at the origin are consistent with model-dependent calculations at one-loop level and at leading order in v, both radiative and relativistic corrections can be sizable in processes involving P-wave charmonia. Our calculations of the corrections to the P-wave wavefunctions at the origin from $1/m$ and $1/m^2$ potentials allow us to include consistently the radiative corrections to relative order α_s^2 in decay and production rates of P-wave quarkonia, where the dependence on the NRQCD factorization scale cancels exactly at two-loop level between the short-distance coefficients and the corrections to the wavefunctions at the origin. On the other hand, because our pNRQCD expressions for the leading-order LDMEs are valid up to corrections of relative order v^2, due to uncalculated corrections of order $1/m^2$ in the matching coefficients $V_\mathcal{O}$, it is not possible to fully incorporate the effects of relativistic corrections through relative order v^2. Hence, in computing the absolute decay and production rates, we work at leading order in v, neglecting the contributions from LDMEs of dimensions 6 and above in the NRQCD factorization formulae. On the other hand, we expect the uncalculated order-v^2 corrections coming from the matching coefficients $V_\mathcal{O}$ to cancel in ratios of LDMEs for different angular momentum quantum numbers, and the heavy-quark spin symmetry breaking effects in the matching coefficient $V_\mathcal{O}$ to be suppressed by $\Lambda_{\rm QCD}^2/m^2$. Hence, when considering ratios of decay rates, we include the order-v^2 corrections coming from higher dimensional LDMEs.

We begin by considering the two-photon decay rates of χ_{c0} and χ_{c2}. By using the NRQCD factorization formula in eq. (A.1) and the pNRQCD formula for the leading-order LDME, we obtain the following expression for $\Gamma(\chi_{c0} \to \gamma\gamma)$:

$$
\begin{aligned}
\Gamma(\chi_{c0} \to \gamma\gamma) &= \frac{12\pi e_c^4 \alpha^2}{m_{\chi_{c0}}} \frac{3N_c}{2\pi} \frac{|R'_{\rm LO}(0)|^2}{m_{\rm RS'}^3} \left(1 - \frac{3\delta m_{\rm RS'}}{m_{\rm RS'}}\right) \left(1 + \delta_\Psi^{\rm C} + \delta_\Psi^{\rm NC}|_{^3P_0} + \delta_\Psi^{\rm RS'}\right)^2 \\
&\quad \times \left|1 + \alpha_s c_{\gamma\gamma(00)}^{(1)} + \alpha_s^2 c_{\gamma\gamma(00)}^{(2)}\right|^2 + O(\alpha_s^3, v^2) \\
&= \frac{12\pi e_c^4 \alpha^2}{m_{\chi_{c0}}} \frac{3N_c}{2\pi} \frac{|R'_{\rm LO}(0)|^2}{m_{\rm RS'}^3} \Big[1 + 2\alpha_s c_{\gamma\gamma(00)}^{(1)} + 2\delta_\Psi^{\rm C} + \left(\alpha_s c_{\gamma\gamma(00)}^{(1)}\right)^2 \\
&\quad + \left(\delta_\Psi^{\rm C}\right)^2 + 4\alpha_s c_{\gamma\gamma(00)}^{(1)} \delta_\Psi^{\rm C} + 2\alpha_s^2 {\rm Re}(c_{\gamma\gamma(00)}^{(2)}) + 2\delta_\Psi^{\rm NC}|_{^3P_0} \\
&\quad + 2\delta_\Psi^{\rm RS'} - \frac{3\delta m_{\rm RS'}}{m_{\rm RS'}}\Big] + O(\alpha_s^3, v^2).
\end{aligned}
\tag{6.18}
$$

Here, $\alpha = 1/137.0$ is the electromagnetic coupling constant. The factor $(1 - 3\delta m_{\text{RS}'}/m_{\text{RS}'})$ comes from replacing $1/m^3$ in the NRQCD factorization formula by $1/(m_{\text{RS}'} + \delta m_{\text{RS}'})^3$ and expanding in powers of $\delta m_{\text{RS}'}$ to relative order α_s^2. In the last equality, we have expanded the factors in the parentheses to relative order α_s^2; the terms in the square brackets then correspond to the correction factors coming from radiative corrections to the short-distance coefficients and the corrections to the wavefunctions at the origin.

Similarly, we obtain the following expression for $\Gamma(\chi_{c2} \to \gamma\gamma)$:

$$
\begin{aligned}
\Gamma(\chi_{c2} \to \gamma\gamma) &= \frac{16\pi e_c^4 \alpha^2}{5 m_{\chi_{c2}}} \frac{3N_c}{2\pi} \frac{|R'_{\text{LO}}(0)|^2}{m_{\text{RS}'}^3} \left(1 - \frac{3\delta m_{\text{RS}'}}{m_{\text{RS}'}} \right) \left(1 + \delta_\Psi^{\text{C}} + \delta_\Psi^{\text{NC}}|_{^3P_2} + \delta_\Psi^{\text{RS}'} \right)^2 \\
&\quad \times \left(\left| 1 + \alpha_s c_{\gamma\gamma(22)}^{(1)} + \alpha_s^2 c_{\gamma\gamma(22)}^{(2)} \right|^2 + \left| \alpha_s c_{\gamma\gamma(20)}^{(1)} \right|^2 \right) + O(\alpha_s^3, v^2) \\
&= \frac{16\pi e_c^4 \alpha^2}{5 m_{\chi_{c2}}} \frac{3N_c}{2\pi} \frac{|R'_{\text{LO}}(0)|^2}{m_{\text{RS}'}^3} \left[1 + 2\alpha_s c_{\gamma\gamma(22)}^{(1)} + 2\delta_\Psi^{\text{C}} + \left(\alpha_s c_{\gamma\gamma(22)}^{(1)} \right)^2 \right. \\
&\quad + \left(\alpha_s c_{\gamma\gamma(20)}^{(1)} \right)^2 + 4\alpha_s c_{\gamma\gamma(22)}^{(1)} \delta_\Psi^{\text{C}} + \left(\delta_\Psi^{\text{C}} \right)^2 + 2\alpha_s^2 \text{Re}(c_{\gamma\gamma(22)}^{(2)}) \\
&\quad \left. + 2\delta_\Psi^{\text{NC}}|_{^3P_2} + 2\delta_\Psi^{\text{RS}'} - \frac{3\delta m_{\text{RS}'}}{m_{\text{RS}'}} \right] + O(\alpha_s^3, v^2).
\end{aligned}
\tag{6.19}
$$

Again, we obtain the last equality by expanding the correction factors to relative order α_s^2.

Based on the expressions in eqs. (6.18) and (6.19), we obtain the numerical results for the two-photon decay rates given by

$$\Gamma(\chi_{c0} \to \gamma\gamma) = 5.07^{+0.46}_{-0.00} \pm 1.52 \text{ keV} = 5.07^{+1.59}_{-1.52} \text{ keV}, \tag{6.20a}$$

$$\Gamma(\chi_{c2} \to \gamma\gamma) = 0.95^{+0.04}_{-0.01} \pm 0.29 \text{ keV} = 0.95 \pm 0.29 \text{ keV}, \tag{6.20b}$$

where the first uncertainties come from varying μ_R between $1.5\,\text{GeV}$ and $4\,\text{GeV}$, which represent the uncertainties from uncalculated corrections of higher orders in α_s, and the second uncertainties come from uncalculated corrections of order v^2, which we take to be 0.3 times the central values, based on the typical size of $v^2 \approx 0.3$ for charmonium states. In the last equalities, we add the uncertainties in quadrature. We note that the logarithms of the NRQCD factorization scale Λ cancel exactly at two-loop level between δ_Ψ^{NC} and the two-loop corrections to the short-distance coefficients, so that there is no uncertainty due to the dependence on Λ in our numerical results.

We first discuss the convergence of the corrections that we include in our calculation. In the case of the decay amplitude for $\chi_{c0} \to \gamma\gamma$, the one-loop correction to the short-distance coefficients coming from $\alpha_s c_{\gamma\gamma(00)}^{(1)}$ is about 0.008, while the two-loop correction coming from $\alpha_s^2 c_{\gamma\gamma(00)}^{(2)}$ is about -0.18. When combined with the corrections to the wavefunctions at the origin and the RS' subtraction term, at order α_s, the corrections coming from $\alpha_s c_{\gamma\gamma(00)}^{(1)}$ and δ_Ψ^{C} add up to 0.27, and the corrections coming from $\alpha_s^2 c_{\gamma\gamma(00)}^{(2)}$, δ_Ψ^{NC}, $\delta_\Psi^{\text{RS}'}$, and $\delta m_{\text{RS}'}$ are about 0.21. Although the corrections of order α_s^2 and v^2 are less in size than the order-α_s correction, the signs of the corrections are same. The correction factor at the squared amplitude level, given by the terms in the square brackets in eq. (6.18), is about 2.1. Hence,

in the case of the two-photon decay rate of χ_{c0}, the convergence of the corrections is not improved by inclusion of the corrections to the wavefunctions at the origin.

On the other hand, in the decay amplitudes for $\chi_{c2} \to \gamma\gamma$, the one-loop correction from $\alpha_s c^{(1)}_{\gamma\gamma(22)}$ is about -0.23, while the two-loop correction from $\alpha_s^2 c^{(2)}_{\gamma\gamma(22)}$ is about -0.29. When combined with the corrections to the wavefunctions at the origin and the RS$'$ subtraction term, the order-α_s corrections coming from $\alpha_s c^{(1)}_{\gamma\gamma(22)}$ and $\delta_\Psi^{\rm C}$ add up to 0.03, and the corrections from $\alpha_s^2 c^{(2)}_{\gamma\gamma(22)}$, $\delta_\Psi^{\rm NC}$, $\delta_\Psi^{\rm RS'}$, and $\delta m_{\rm RS'}$ add to about 0.15. The correction factor at the squared amplitude level, given by the terms in the square brackets in the last equality of eq. (6.19), is about 1.2.

If we compute the decay rates by expanding the corrections at the amplitude level instead of working at the squared amplitude level, which can be done by expanding the square roots of the terms in the square brackets in the last equalities in eqs. (6.18) and (6.19), the central value of $\Gamma(\chi_{c0} \to \gamma\gamma)$ increases to $5.48\,{\rm keV}$, and the central value of $\Gamma(\chi_{c2} \to \gamma\gamma)$ decreases to $0.80\,{\rm keV}$. These values are within the uncertainties of our numerical results.

We note that our numerical results have central values that are larger than the measured two-photon decay rates from BESIII [71], which are given by $\Gamma(\chi_{c0} \to \gamma\gamma) = 2.33 \pm 0.20 \pm 0.22\,{\rm keV}$ and $\Gamma(\chi_{c2} \to \gamma\gamma) = 0.63 \pm 0.04 \pm 0.06\,{\rm keV}$. While the measured two-photon decay rate of the χ_{c2} is compatible with our numerical result within uncertainties, our result overestimates the χ_{c0} two-photon rate by about 1.8 times the theoretical uncertainty.

It would be interesting if the relativistic corrections of relative order v^2 reduces the discrepancy between the measured decay rates and the theoretical values. Even though the order-v^2 corrections to the leading-order LDMEs are currently unknown, we expect the spin-dependent corrections to be suppressed by $\Lambda_{\rm QCD}^2/m^2$, so that the order-v^2 corrections to the ratio $\mathcal{R}_{\chi_c} = \Gamma(\chi_{c2} \to \gamma\gamma)/\Gamma(\chi_{c0} \to \gamma\gamma)$ comes solely from higher dimensional LDMEs. By using the results for the tree-level short-distance coefficients associated with the higher dimensional LDMEs [18], and the pNRQCD calculations of the LDMEs at leading nonvanishing orders in $1/m$ [24], we obtain the following expression for $\mathcal{R}_{\chi_c}$ that is valid through order α_s^2 and v^2:

$$
\begin{aligned}
\mathcal{R}_{\chi_c} = \frac{4}{15}\Bigg\{ &1 + 2\alpha_s \left(c^{(1)}_{\gamma\gamma(22)} - c^{(1)}_{\gamma\gamma(00)} \right) + \alpha_s^2 \Bigg[3\left(c^{(1)}_{\gamma\gamma(00)} \right)^2 + \left(c^{(1)}_{\gamma\gamma(20)} \right)^2 \\
&+ \left(c^{(1)}_{\gamma\gamma(22)} \right)^2 - 4 c^{(1)}_{\gamma\gamma(00)} c^{(1)}_{\gamma\gamma(22)} + 2\,{\rm Re}\big(c^{(2)}_{\gamma\gamma(22)} - c^{(2)}_{\gamma\gamma(00)} \big) \Bigg] \\
&+ 2\left(\delta_\Psi^{\rm NC}|_{^3P_2} - \delta_\Psi^{\rm NC}|_{^3P_0} \right) + \frac{E^{\rm LO}}{3 m_{\rm RS'}} \Bigg\} + O(\alpha_s^3, \Lambda_{\rm QCD}^2/m^2). \quad (6.21)
\end{aligned}
$$

The last term in the curly brackets comes from the contributions of LDMEs of dimensions 6 and 7 to the NRQCD factorization formulae [18, 24]. The logarithm of Λ in $c^{(2)}_{\gamma\gamma(22)} - c^{(2)}_{\gamma\gamma(00)}$ is cancelled exactly by $\delta_\Psi^{\rm NC}|_{^3P_2} - \delta_\Psi^{\rm NC}|_{^3P_0}$ through order α_s^2. By using our numerical results for $\delta_\Psi^{\rm NC}$, we obtain

$$
\mathcal{R}_{\chi_c} = 0.16^{+0.02}_{-0.04} \pm 0.02 = 0.16^{+0.03}_{-0.04}, \quad (6.22)
$$

where the first uncertainty comes from varying μ_R between $1.5\,\mathrm{GeV}$ and $4\,\mathrm{GeV}$, and the second uncertainty comes from uncalculated corrections of order $\Lambda_{\mathrm{QCD}}^2/m^2$, which we estimate to be $(500\,\mathrm{MeV}/m)^2 \approx 0.14$ times the central value. In the last equality, we add the uncertainties in quadrature.

The quantity in the curly brackets in eq. (6.21) contains the corrections of order α_s, α_s^2, and v^2. The order-α_s contribution coming from the one-loop corrections to the short-distance coefficients is about -0.48. The two-loop corrections to the short-distance coefficients amount to about -0.16, while the corrections to the wavefunctions at the origin is about 0.10 at $\Lambda = m$. Finally, the order-v^2 correction is about 0.14. While the corrections to the wavefunctions and the order-v^2 correction from higher dimensional LDMEs are moderate in size, they do help counter the effect of the large negative corrections from the short-distance coefficients: if we keep only the loop corrections to the short-distance coefficients, the correction factor given by the quantity in the curly brackets in eq. (6.21) is about 0.35. Inclusion of the corrections to the wavefunctions at the origin and the order-v^2 corrections from higher dimensional LDMEs increase this correction factor to about 0.60. Nevertheless, our numerical result is still smaller than the measured value $\mathcal{R}_{\chi_c} = 0.27 \pm 0.04$ from BESIII [71], even though the discrepancy is reduced by inclusion of the corrections to the wavefunctions at the origin and the order-v^2 corrections considered in this work.

Next, we consider the cross sections $\sigma(e^+e^- \to \chi_{cJ} + \gamma)$ ($J = 0$, 1, and 2) at $\sqrt{s} = 10.58\,\mathrm{GeV}$. By using the NRQCD factorization formula in appendix A, we obtain the following expression

$$
\begin{aligned}
\sigma(e^+e^- \to \chi_{cJ} + \gamma) = {} & \frac{3N_c}{2\pi} |R'_{\mathrm{LO}}(0)|^2 \, \sigma_{cJ}^{(0)}(s, m_{\mathrm{RS}'}) \\
& \times \Big[1 + \alpha_s \hat{\sigma}_{cJ}^{(1)}(r) + \alpha_s^2 \hat{\sigma}_{cJ}^{(2)}(r) + 2\delta_\Psi^{\mathrm{C}} + 2\alpha_s \delta_\Psi^{\mathrm{C}} \hat{\sigma}_{cJ}^{(1)}(r) + \left(\delta_\Psi^{\mathrm{C}}\right)^2 \\
& + 2\delta_\Psi^{\mathrm{NC}}|_{^3P_J} + 2\delta_\Psi^{\mathrm{RS}'} + c_m^J \frac{\delta m_{\mathrm{RS}'}}{m_{\mathrm{RS}'}} \Big] + O(\alpha_s^3, v^2), \quad (6.23)
\end{aligned}
$$

where $r = 4m^2/s$ and $c_m^J = m\frac{\partial}{\partial m} \log \sigma_{cJ}^{(0)}(s, m)|_{m=m_{\mathrm{RS}'}}$. The last term in the square brackets comes from replacing the heavy quark pole mass in $\hat{\sigma}_{cJ}^{(0)}$ by $m_{\mathrm{RS}'} + \delta m_{\mathrm{RS}'}$ and expanding in powers of $\delta m_{\mathrm{RS}'}$ to relative order α_s^2. Note that in the limit $s \to \infty$, $\lim_{m^2/s \to 0} c_m^J = -3$. The two-loop short-distance coefficients $\hat{\sigma}_{cJ}^{(2)}(r)$ contain logarithms in Λ, which cancel exactly with the Λ dependence in $\delta_\Psi^{\mathrm{NC}}$ through order α_s^2.

Our numerical results for the cross sections are

$$\sigma(e^+e^- \to \chi_{c0} + \gamma) = 3.11^{+0.47}_{-0.09} \pm 0.93 \text{ fb} = 3.11^{+1.05}_{-0.94} \text{ fb}, \quad (6.24\mathrm{a})$$

$$\sigma(e^+e^- \to \chi_{c1} + \gamma) = 23.3^{+3.8}_{-0.4} \pm 7.0 \text{ fb} = 23.3^{+7.9}_{-7.0} \text{ fb}, \quad (6.24\mathrm{b})$$

$$\sigma(e^+e^- \to \chi_{c2} + \gamma) = 4.93^{+0.59}_{-0.00} \pm 1.48 \text{ fb} = 4.93^{+1.59}_{-1.48} \text{ fb}, \quad (6.24\mathrm{c})$$

where the uncertainties are as in eq. (6.20). Again, since the Λ dependences cancel exactly through order α_s^2, there is no uncertainty from dependence on the NRQCD factorization scale. In the case of χ_{c0}, the one-loop correction to the short-distance coefficients is positive, while the two-loop correction is negative; the radiative corrections are small in size. On

the other hand, for χ_{c1} and χ_{c2}, the loop corrections are negative at both order α_s and α_s^2, and are sizable, especially for χ_{c2}. The corrections to the wavefunctions at the origin and the correction coming from the use of the RS′ mass are positive, which counteract the negative corrections from the short-distance coefficients. The correction factor, given by the quantity in the square brackets in eq. (6.23), is about 2.5, 1.9, and 1.1 for χ_{c0}, χ_{c1}, and χ_{c2}, respectively. Our result for the $\chi_{c1} + \gamma$ production rate is consistent with the Belle measurement $\sigma(e^+e^- \to \chi_{c1} + \gamma) = 17.3^{+4.2}_{-3.9} \pm 1.7$ fb [72] within uncertainties, while our result for the $\chi_{c2} + \gamma$ cross section is lower than, but close to the upper limit $\sigma(e^+e^- \to \chi_{c2} + \gamma) < 5.7$ fb from Belle [72].

Finally, we compute the scalar decay constant $f_{\chi_{c0}}$ and the axialvector decay constant $f_{\chi_{c1}}$, which are defined in eqs. (6.1). By using the NRQCD factorization formulae in appendix A, we obtain

$$
\begin{aligned}
m f_{\chi_{c0}}^{\mathrm{OS}} &= m_{\overline{\mathrm{MS}}}(\mu) f_{\chi_{c0}}^{\overline{\mathrm{MS}}}(\mu) \\
&= \sqrt{\frac{6 N_c}{\pi m_{\chi_{c0}}}} |R'_{\mathrm{LO}}(0)| \Big(1 + \alpha_s c_s^{(1)} + \alpha_s^2 c_s^{(2)} + \delta_\Psi^{\mathrm{C}} + \alpha_s c_s^{(1)} \delta_\Psi^{\mathrm{C}} \\
&\qquad\qquad + \delta_\Psi^{\mathrm{NC}}|_{^3P_0} + \delta_\Psi^{\mathrm{RS'}} \Big) + O(\alpha_s^3, v^2),
\end{aligned}
\tag{6.25a}
$$

$$
\begin{aligned}
f_{\chi_{c1}} &= \sqrt{\frac{9 N_c}{\pi m_{\chi_{c1}}}} \frac{|R'_{\mathrm{LO}}(0)|}{m_{\mathrm{RS'}}} \Big(1 + \alpha_s c_a^{(1)} + \alpha_s^2 c_a^{(2)} + \delta_\Psi^{\mathrm{C}} + \alpha_s c_a^{(1)} \delta_\Psi^{\mathrm{C}} \\
&\qquad\qquad + \delta_\Psi^{\mathrm{NC}}|_{^3P_1} + \delta_\Psi^{\mathrm{RS'}} - \frac{\delta m_{\mathrm{RS'}}}{m_{\mathrm{RS'}}} \Big) + O(\alpha_s^3, v^2),
\end{aligned}
\tag{6.25b}
$$

where $m_{\overline{\mathrm{MS}}}(\mu)$ is the charm quark mass in the $\overline{\mathrm{MS}}$ scheme at scale μ, and the superscripts OS and $\overline{\mathrm{MS}}$ on $f_{\chi_{c0}}$ denote the scheme in which the scalar decay constants are renormalized. Since the scalar decay constant is renormalized in the same way as the quark mass term in the QCD Lagrangian, the combination $m f_{\chi_{c0}}^{\mathrm{OS}} = \bar{m}(\mu) f_{\chi_{c0}}^{\overline{\mathrm{MS}}}(\mu)$ is scheme and scale independent. The axialvector decay constant is renormalization scheme and scale independent, although the short-distance coefficients do depend on the scheme in which γ_5 is defined in DR. We work with naïve dimensional regularization, because the two-loop short-distance coefficient $c_a^{(2)}$ is only available in this scheme. The one-loop coefficient $c_a^{(1)}$ has also been computed in the t'Hooft-Veltman scheme in ref. [50], where the authors find $c_a^{(1)}|_{\mathrm{HV}} = 0$.

The QCD matrix elements that define the decay constants can have imaginary parts coming from diagrams that contain on-shell intermediate states. The short-distance coefficients explicitly contain the imaginary parts from relative order α_s^2, which affect the size of the decay constants from relative order α_s^4. In practice, we are only interested in the size of the decay constants, because we can always absorb the phase into the quarkonium state; hence, we neglect the imaginary parts of the short-distance coefficients at the current level of accuracy.

Our numerical results for the decay constants are

$$
m f_{\chi_{c0}}^{\mathrm{OS}} = 0.439^{+0.042}_{-0.006} \pm 0.132 \text{ GeV}^2 = 0.439^{+0.138}_{-0.132} \text{ GeV}^2,
\tag{6.26a}
$$

$$
f_{\chi_{c1}} = 0.236^{+0.011}_{-0.000} \pm 0.071 \text{ GeV} = 0.236 \pm 0.071 \text{ GeV},
\tag{6.26b}
$$

where the uncertainties are as in eq. (6.20). By dividing $m f_{\chi_{c0}}^{\rm OS} = m_{\overline{\rm MS}}(\mu) f_{\chi_{c0}}^{\overline{\rm MS}}(\mu)$ by the $\overline{\rm MS}$ charm quark mass $\overline{m} = m_{\overline{\rm MS}}(\overline{m}) = 1.27 \pm 0.02\,{\rm GeV}$ [62], we obtain the $\overline{\rm MS}$-renormalized scalar decay constant at scale $\mu = \overline{m}$:

$$f_{\chi_{c0}}^{\overline{\rm MS}}(\mu = \overline{m}) = 0.346^{+0.109}_{-0.104}\,{\rm GeV}. \tag{6.27}$$

The correction factor given by the terms in the parenthesis in eq. (6.25a) is about 1.5. The order-α_s correction from $c_s^{(1)}$ and $\delta_\Psi^{\rm C}$ amounts to about 0.2, while the two-loop correction $c_s^{(2)}$ and the corrections to the wavefunctions at the origin add up to about 0.3. In the case of the axialvector decay constant, the order-α_s correction from $c_a^{(1)}$ and $\delta_\Psi^{\rm C}$ is about 0.15, and the two-loop correction from $c_a^{(2)}$, combined with the corrections to the wavefunctions at the origin and the $-\delta m_{\rm RS'}/m$ term, amount to about 0.17. As a result, the correction factor given by the terms in the parenthesis in eq. (6.25b) is about 1.32, which is a bit milder than that of the scalar decay constant. Since the $c_a^{(1)}$ and $c_a^{(2)}$ have been computed by using naïve dimensional regularization for γ_5, the numerical results will be different in the t'Hooft-Veltman scheme. For example, $c_a^{(1)} = 0$ in the t'Hooft-Veltman scheme, and in this case, the order-α_s correction increases to about 0.27.

Our numerical results have been computed with the RS' charm quark mass $m_{\rm RS'}$ at the scale $\nu_f = 2\,{\rm GeV}$. While this removes the ambiguity in the pole mass, the RS' mass itself depends on the scale ν_f. For example, setting the scale $\nu_f = 1\,{\rm GeV}$ increases $m_{\rm RS'}$ to 1.496(41) GeV. In decay and production rates, as well as decay constants, the change in $m_{\rm RS'}$ is compensated by the correction from $\delta m_{\rm RS'}$, which also affects the correction $\delta_\Psi^{\rm RS'}$ to the wavefunctions at the origin. We find that if we use $\nu_f = 1\,{\rm GeV}$, the $\chi_{c1} + \gamma$ and $\chi_{c2} + \gamma$ production cross sections, the two-photon rates of χ_{c0} and χ_{c2}, as well as the ratio $\mathcal{R}_{\chi_c}$, reduces by less than 10%, while the decay constants increase by less than 10%. While the $\chi_{c0} + \gamma$ production rate decreases by more than 15%, all of these changes are well within the estimated uncertainties of our results. Hence, it is fair to say that, by using the RS' mass, the heavy quark mass dependences in our numerical results are well under control.

6.3 Numerical results for P-wave bottomonia

We now present our numerical results for P-wave bottomonia. We list the central values of the radial wavefunctions at the origin $R'(0)$ for the three lowest P-wave states in table 2. The LO binding energies for the $1P$, $2P$, and $3P$ states are $E_{1P}^{\rm LO} = 0.298\,{\rm GeV}$, $E_{2P}^{\rm LO} = 0.614\,{\rm GeV}$, and $E_{3P}^{\rm LO} = 0.888\,{\rm GeV}$, respectively. Compared to the LO binding energies for $2S$ and $3S$ bottomonia in ref. [16], given by $E_{2S}^{\rm LO} = 0.417\,{\rm GeV}$ and $E_{3S}^{\rm LO} = 0.723\,{\rm GeV}$, respectively, the P-wave binding energies are consistent with the measured masses of the $\chi_{cJ}(nP)$ states. The nP bottomonium masses $m_{1P} = 9.94\,{\rm GeV}$, $m_{2P} = 10.26\,{\rm GeV}$, and $m_{3P} = 10.53\,{\rm GeV}$, computed from $m_{nP} = 2m_{\rm RS'} + 2\delta m_{\rm RS'} + E_{nP}^{\rm LO}$ ($n = 1$, 2, and 3) are in good agreement with the PDG values within 0.1 GeV [62]. In computing decay rates and decay constants, we use the PDG values of the bottomonium masses in ref. [62], because the measured values have uncertainties that are negligible compared to the theoretical uncertainties. We identify the bottomonium nP states with angular momentum quantum numbers ^3P_J and $^1P_1$ by $\chi_{bJ}(nP)$ and $h_b(nP)$, respectively.

State	$\lvert R'_{\mathrm{LO}}(0)\rvert$ (GeV$^{5/2}$)	$\delta_\Psi^{\mathrm{NC}}\rvert_{^3P_0}$	$\delta_\Psi^{\mathrm{NC}}\rvert_{^3P_1}$	$\delta_\Psi^{\mathrm{NC}}\rvert_{^3P_2}$	$\delta_\Psi^{\mathrm{NC}}\rvert_{^1P_1}$	δ_Ψ^{C}	$\delta_\Psi^{\mathrm{RS}'}$
$1P$	0.698	0.281	0.268	0.246	0.260	0.369	0.019
$2P$	0.880	0.285	0.275	0.256	0.268	0.280	0.018
$3P$	1.00	0.291	0.284	0.267	0.279	0.228	0.017

Table 2. LO wavefunctions at the origin $\lvert R'(0)\rvert$ and relative corrections to the wavefunctions at the origin in the $\overline{\mathrm{MS}}$ scheme at scale $\Lambda = m$ for $1P$, $2P$, and $3P$ bottomonium states. $\delta_\Psi^{\mathrm{NC}}$ is the correction from the $1/m$ and $1/m^2$ potentials, δ_Ψ^{C} is the Coulombic correction, and $\delta_\Psi^{\mathrm{RS}'}$ is the correction from the RS$'$ subtraction term. The $\delta_\Psi^{\mathrm{NC}}$, δ_Ψ^{C}, and $\delta_\Psi^{\mathrm{RS}'}$ are dimensionless.

The LO radial wavefunctions at the origin in table 2 are much larger than what we would get if we neglect the long-distance nonperturbative behavior of the static potential. Even for the $1P$ state, our result for $\lvert R'_{\mathrm{LO}}(0)\rvert$ is almost 10 times larger than what we obtain in perturbative QCD calculations of the wavefunctions at same values of α_s and m. Hence, even for the lowest-lying P-wave bottomonium states, the long-distance nonperturbative behavior of the potentials cannot be neglected.

In the case of bottomonia, the approximate relation in eq. (5.63) is well reproduced for all $1P$, $2P$, and $3P$ states by much better than 1%. The numerical results for $\delta_\Psi^{\mathrm{NC}}$ are almost insensitive to r_0 for values of r_0 less than about $0.02\,\mathrm{GeV}^{-1}$. We show the r_0 dependence of non-Coulombic corrections for $1P$, $2P$, and $3P$ states in figure 3. We fix $r_0 = 0.01\,\mathrm{GeV}^{-1}$ for computing the central values of $\delta_\Psi^{\mathrm{NC}}$ and neglect the uncertainty in the numerical calculation of finite-r regularized wavefunctions at the origin.

We list the corrections to $\lvert R'_{\mathrm{LO}}(0)\rvert$ from the $1/m$ and $1/m^2$ potentials at $\Lambda = m$ in the $\overline{\mathrm{MS}}$ scheme ($\delta_\Psi^{\mathrm{NC}}$), the Coulombic correction (δ_Ψ^{C}), and the correction from the RS$'$ subtraction term ($\delta_\Psi^{\mathrm{RS}'}$) in table 2. The non-Coulombic corrections are smaller compared to the charmonium case, but are nevertheless significant. Similarly to the charmonium case, the values of $\delta_\Psi^{\mathrm{NC}}$ that we obtain are similar in order of magnitude to what we obtain from perturbative QCD calculations in appendix F for similar values of α_s [$\alpha_s(\mu_R = 5\,\mathrm{GeV}) \approx 0.22$]. The Coulombic corrections are also sizable, especially for the $1P$ state. The corrections from the RS$'$ subtraction term are small. All of the corrections are positive.

Since the Coulombic corrections are large, especially for the $1P$ state, it is worth investigating its convergence at higher orders in the Rayleigh-Schrödinger perturbation theory. Compared to the all-orders calculation of the Coulombic corrections using the modified Crank-Nicolson method, our result for δ_Ψ^{C} for the $1P$ state differs from the all-orders result only by 3%. For $2P$ and $3P$ states, the agreement is even better at about 1%. We conclude that the Coulombic corrections converge rapidly, and at the current level of accuracy, it is sufficient to consider only the δ_Ψ^{C} from first order in the Rayleigh-Schrödinger perturbation theory.

Also in the bottomonium case it is worth comparing with potential models that are widely used for bottomonium phenomenology. At one-loop level, we have $\lvert R'_{\mathrm{LO}}(0)\rvert^2(1 + \delta_\Psi^{\mathrm{C}})^2 = 0.91\,\mathrm{GeV}^5$, $1.27\,\mathrm{GeV}^5$, and $1.51\,\mathrm{GeV}^5$ for the $1P$, $2P$, and $3P$ states, respectively. Potential model results from refs. [64, 65, 67, 73] have values of $\lvert R'_{1P}(0)\rvert^2$ that range
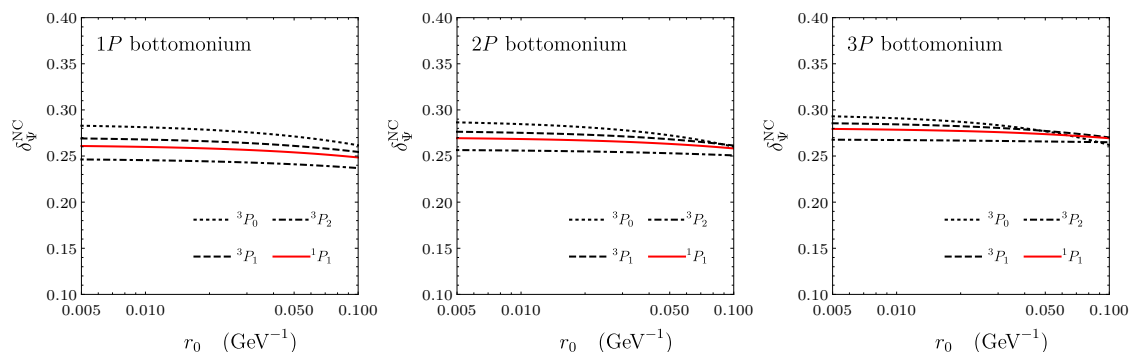
Figure 3. Non-Coulombic corrections $\delta_\Psi^{\rm NC}$ at finite r_0 for the bottomonium $1P$ (left panel), $2P$ (middle panel), and $3P$ (right panel) states, for angular momentum quantum numbers $^3P_0$ (dotted lines), $^3P_1$ (dashed lines), $^3P_2$ (dot-dashed lines), and $^1P_1$ (red solid lines). The r_0 dependences are mild for the range $r_0 < 0.02\,{\rm GeV}^{-1}$ that we consider.

from $0.93\,{\rm GeV}^5$ to $2.07\,{\rm GeV}^5$, $|R'_{2P}(0)|^2$ range from $1.15\,{\rm GeV}^5$ to $2.44\,{\rm GeV}^5$, and $|R'_{3P}(0)|^2$ range from $1.30\,{\rm GeV}^5$ to $2.70\,{\rm GeV}^5$. The model dependence of the values of $|R'(0)|^2$ is as strong as the charmonium case, with the largest values being more than twice the smallest values. Similarly to the charmonium case, the potential models have different bottom quark masses, and so, it makes more sense to compare the combination $|R'_{nP}(0)|^2/m^3$ that appears in decay and exclusive electromagnetic production rates. Our first-principles calculations at one-loop level give $|R'_{\rm LO}(0)|^2(1+\delta_\Psi^{\rm C})^2/m_{\rm RS'}^3 = 0.86 \times 10^{-2}\,{\rm GeV}^2$, $1.19 \times 10^{-2}\,{\rm GeV}^2$, and $1.41 \times 10^{-2}\,{\rm GeV}^2$ for the $1P$, $2P$, and $3P$ states, respectively. Potential-model calculations give values of $|R'_{nP}(0)|^2/m^3$ that are 10–70% larger than our results. In the case of inclusive production, our first-principles calculations at one-loop level give $|R'_{\rm LO}(0)|^2(1+\delta_\Psi^{\rm C})^2/m_{\rm RS'}^5 = 3.81\times 10^{-4}$, 5.28×10^{-4}, and 6.29×10^{-4} for the $1P$, $2P$, and $3P$ states, respectively, while potential-model calculations range about 85–145% of our results, except for the model in ref. [73], which gives results that are more than twice our first-principles calculation. Considering the current level of precision of inclusive quarkonium production phenomenology, the strong dependence of these values on potential models may not be catastrophic; nevertheless, it is difficult to obtain precise predictions from potential-models values of the wavefunctions at the origin.

We first compute the two-photon decay rates of $\chi_{b0}(nP)$ and $\chi_{b2}(nP)$. By using the formulas in eqs. (6.18) and (6.19), we obtain

$$\Gamma(\chi_{b0}(1P) \to \gamma\gamma) = 37.4^{+9.5}_{-1.5} \pm 3.7 \text{ eV} = 37.4^{+10.2}_{-4.0} \text{ eV}, \qquad (6.28a)$$

$$\Gamma(\chi_{b2}(1P) \to \gamma\gamma) = 7.5^{+0.5}_{-0.1} \pm 0.8 \text{ eV} = 7.5^{+0.9}_{-0.8} \text{ eV}, \qquad (6.28b)$$

$$\Gamma(\chi_{b0}(2P) \to \gamma\gamma) = 51.3^{+10.7}_{-2.0} \pm 5.1 \text{ eV} = 51.3^{+11.9}_{-5.5} \text{ eV}, \qquad (6.28c)$$

$$\Gamma(\chi_{b2}(2P) \to \gamma\gamma) = 10.0^{+0.4}_{-0.11} \pm 1.0 \text{ eV} = 10.0^{+1.1}_{-1.0} \text{ eV}, \qquad (6.28d)$$

$$\Gamma(\chi_{b0}(3P) \to \gamma\gamma) = 60.8^{+11.1}_{-2.4} \pm 6.1 \text{ eV} = 60.8^{+12.6}_{-6.5} \text{ eV}, \qquad (6.28e)$$

$$\Gamma(\chi_{b2}(3P) \to \gamma\gamma) = 11.7^{+0.2}_{-0.1} \pm 1.2 \text{ eV} = 11.7 \pm 1.2 \text{ eV}, \qquad (6.28f)$$

where the first uncertainties come form varying μ_R between $2\,{\rm GeV}$ and $8\,{\rm GeV}$, and the

second uncertainties come from uncalculated corrections of order v^2, which we estimate to be 10% of the central values; this is based on the typical size of $v^2 \approx 0.1$ for bottomonium states. We add the uncertainties in quadrature. We note that these results are more precise than the model-dependent calculations in ref. [24], because the results in ref. [24] have large uncertainties from dependence on potential models. In the case of bottomonia, we see better convergence of the corrections compared to the charmonium case. In the $\chi_{b0} \to \gamma\gamma$ decay rates, the order-α_s correction coming from the one-loop short-distance coefficient and the Coulombic correction δ_Ψ^C is about 80% of the leading-order value, and the higher order corrections from the two-loop short-distance coefficient, non-Coulombic corrections to the wavefunctions at the origin, and the corrections from the RS′ subtraction term add up to about 0.5 times the leading-order value. In the case of the $\chi_{b2} \to \gamma\gamma$ decay rates, the sizes of the corrections are smaller; the corrections at one loop and higher orders are both about 0.4 times the leading order values, respectively. Because the corrections have same signs at one-loop level and at higher orders, they are numerically significant.

We then compute the ratio $\mathcal{R}_{\chi_b(nP)} = \Gamma(\chi_{b2}(nP) \to \gamma\gamma)/\Gamma(\chi_{b0}(nP) \to \gamma\gamma)$ by using eq. (6.21). We obtain

$$\mathcal{R}_{\chi_b(1P)} = 0.126^{+0.013}_{-0.050} \pm 0.001 \pm 0.004 = 0.126^{+0.014}_{-0.051}, \tag{6.29a}$$

$$\mathcal{R}_{\chi_b(2P)} = 0.136^{+0.012}_{-0.044} \pm 0.002 \pm 0.004 = 0.136^{+0.013}_{-0.044}, \tag{6.29b}$$

$$\mathcal{R}_{\chi_b(3P)} = 0.144^{+0.012}_{-0.039} \pm 0.002 \pm 0.004 = 0.144^{+0.013}_{-0.040}. \tag{6.29c}$$

Here, the first uncertainties come from variation of μ_R between $2\,\mathrm{GeV}$ and $8\,\mathrm{GeV}$, and the second and third uncertainties come from uncalculated corrections of order $\Lambda_{\mathrm{QCD}}^2/m^2$ and v^3, which we estimate to be $(500\,\mathrm{MeV}/m)^2$ and 0.05 times the central values, respectively. We include uncertainties of order v^3, because in the case of bottomonia, v^3 can be larger than $\Lambda_{\mathrm{QCD}}^2/m^2$. We add the uncertainties in quadrature. The correction at order α_s coming from the short-distance coefficients at one loop is about -0.4 times the leading-order value, while the higher order corrections are about -0.2 times the leading-order value. The effect of the order-v^2 corrections is small, amounting to less than 10% of the leading-order value. We see that the uncertainties are dominated by the dependence on μ_R, which is a sign of poor convergence of the perturbative expansion. The fact that the convergence of the perturbative corrections is poor can also be seen from the fact that the values of $\mathcal{R}_{\chi_b}$ computed from the results in eq. (6.28), which are about 0.17–0.20, disagree with the results in eq. (6.29). That is, the numerical results for $\mathcal{R}_{\chi_b}$ depend strongly on the way the corrections are organized. Hence, it is possible that the uncertainties in eq. (6.29) computed from varying μ_R underestimates the effect of loop corrections of higher orders in α_s.

Next, we compute the scalar decay constants of $\chi_{b0}(nP)$ by using eq. (6.25a). We obtain

$$m f_{\chi_{b0}(1P)}^{\mathrm{OS}} = 0.96^{+0.12}_{-0.02} \pm 0.10 \ \mathrm{GeV}^2 = 0.96^{+0.15}_{-0.10} \ \mathrm{GeV}^2, \tag{6.30a}$$

$$m f_{\chi_{b0}(2P)}^{\mathrm{OS}} = 1.12^{+0.11}_{-0.02} \pm 0.11 \ \mathrm{GeV}^2 = 1.12^{+0.15}_{-0.11} \ \mathrm{GeV}^2, \tag{6.30b}$$

$$m f_{\chi_{b0}(3P)}^{\mathrm{OS}} = 1.21^{+0.09}_{-0.02} \pm 0.12 \ \mathrm{GeV}^2 = 1.21^{+0.15}_{-0.12} \ \mathrm{GeV}^2. \tag{6.30c}$$

Similarly, we obtain the axialvector decay constant for $\chi_{b1}(nP)$ by using eq. (6.25b). We obtain

$$f_{\chi_{b1}(1P)} = 0.156^{+0.014}_{-0.003} \pm 0.016 \text{ GeV} = 0.156^{+0.021}_{-0.016} \text{ GeV}, \tag{6.31a}$$

$$f_{\chi_{b1}(2P)} = 0.181^{+0.014}_{-0.003} \pm 0.018 \text{ GeV} = 0.181^{+0.023}_{-0.018} \text{ GeV}, \tag{6.31b}$$

$$f_{\chi_{b1}(3P)} = 0.198^{+0.013}_{-0.003} \pm 0.020 \text{ GeV} = 0.198^{+0.024}_{-0.020} \text{ GeV}. \tag{6.31c}$$

In both scalar and axialvector decay constants, the corrections at one loop are about 30% of the leading-order values, and the higher order corrections are about 10–15% of the leading-order values. Even though the corrections are milder compared to decay rates, the central values of our results are still larger than tree-level results by 40–50%. By using the bottom quark mass in the $\overline{\text{MS}}$ scheme $\overline{m} = m_{\overline{\text{MS}}}(\overline{m}) = 4.18^{+0.03}_{-0.02} \text{ GeV}$ [62], we obtain the $\overline{\text{MS}}$-renormalized scalar decay constant at scale $\mu = \overline{m}$:

$$f^{\overline{\text{MS}}}_{\chi_{b0}(1P)}(\mu = \overline{m}) = 0.229^{+0.036}_{-0.023} \text{ GeV}, \tag{6.32a}$$

$$f^{\overline{\text{MS}}}_{\chi_{b0}(2P)}(\mu = \overline{m}) = 0.267^{+0.037}_{-0.027} \text{ GeV}, \tag{6.32b}$$

$$f^{\overline{\text{MS}}}_{\chi_{b0}(3P)}(\mu = \overline{m}) = 0.290^{+0.037}_{-0.029} \text{ GeV}. \tag{6.32c}$$

Similarly to the charmonium case, our numerical results have been computed by using the RS$'$ bottom quark mass at $\nu_f = 2 \text{ GeV}$. Even though the bottom quark is heavier than the charm quark, so that we expect weaker dependence on the bottom quark mass in our calculation of decay rates and decay constants, it is still worth investigating the ν_f dependence. We find that our numerical results change by less than 3% if we use $\nu_f = 1 \text{ GeV}$ instead of $\nu_f = 2 \text{ GeV}$. Hence, the heavy quark mass dependences in our results are under good control.

6.4 Numerical results from Padé approximants

The numerical results for P-wave charmonia and bottomonia in the previous sections show bad convergence of the loop corrections from short-distance coefficients and corrections to the wavefunctions at the origin. This is in stark contrast with the previous work on S-wave quarkonia in ref. [16], where the poor convergence of the perturbative expansion of short-distance coefficients was significantly improved by inclusion of the corrections to the S-wave wavefunctions at the origin. It is known that in many cases, the Padé approximant of a function often gives a better approximation than a truncated Taylor series. Padé approximants have been successfully applied to studies of QCD perturbation series, where the convergence is often only asymptotic [74–78]. It would therefore be interesting to see how the use of Padé approximants affects P-wave quarkonium decay and production rates. Common uses of Padé approximants are to predict the size of unknown corrections of higher orders, and also to estimate the size of a (possibly divergent) perturbation series. We will primarily be interested in the latter; however, the former can serve as a test of the applicability of Padé approximants by comparing known higher order corrections beyond next-to-next-to-leading order with what Padé approximants predict without knowledge of the correct result.

In general, it is not clear whether Padé approximants are applicable to short-distance coefficients of NRQCD factorization formulae, which depend explicitly on the NRQCD factorization scheme and scale. If Padé approximants are used just for short-distance coefficients, the exact order by order cancellations of NRQCD factorization scheme and scale dependences that occur in series expansions in α_s can break down, which is unfavorable given the strong dependence on the factorization scale of short-distance coefficients and LDMEs. Before we tackle the problem of P-wave decay and production rates, let us put Padé approximants to the test: we consider the vector decay constant f_V of a S-wave vector quarkonium V, for which the short-distance coefficient is known to three-loop accuracy [10, 11, 79–81]:

$$f_V = \sqrt{\frac{2}{m_V}} c_v \langle 0|\chi^\dagger \boldsymbol{\epsilon} \cdot \boldsymbol{\sigma} \psi|V\rangle + O(v^2), \tag{6.33}$$

where $\boldsymbol{\epsilon}$ is the polarization vector of the quarkonium V, and $c_v = 1 + c_v^{(1)}\alpha_s + c_v^{(2)}\alpha_s^2 + c_v^{(3)}\alpha_s^3 + O(\alpha_s^4)$. Explicit expressions for $c_v^{(1)}$, $c_v^{(2)}$, and $c_v^{(3)}$ in the $\overline{\text{MS}}$ scheme can be found in refs. [10, 11, 79–81]. The two-loop coefficient $c_v^{(2)}$ contains $\log \Lambda$, and the three-loop coefficient $c_v^{(3)}$ contains $\log^2 \Lambda$ and $\log \Lambda$ terms, where Λ is the scale at which the LDME $\langle 0|\chi^\dagger \boldsymbol{\epsilon} \cdot \boldsymbol{\sigma} \psi|V\rangle$ is renormalized. The big question is whether Padé approximants can correctly predict $c_v^{(3)}$ only from knowledge of $c_v^{(1)}$ and $c_v^{(2)}$. From the expression for c_v to two-loop accuracy, we obtain the Padé approximant of order $[1/1]$ given by

$$\left[1 + c_v^{(1)}\alpha_s + c_v^{(2)}\alpha_s^2\right]_{[1/1]} = \frac{1 + (c_v^{(1)} - c_v^{(2)}/c_v^{(1)})\alpha_s}{1 - (c_v^{(2)}/c_v^{(1)})\alpha_s}. \tag{6.34}$$

Here, the order $[M/N]$ of a Padé approximant denotes the orders M and N of the polynomials in α_s in the numerator and the denominator, respectively. The denominator implies a finite radius of convergence of the series expansion, given by $|(c_v^{(2)}/c_v^{(1)})\alpha_s| < 1$. Expanding the right-hand side of eq. (6.34) to order α_s^3 gives the prediction from the Padé approximant $c_v^{(3)}|_{\text{Padé}} = (c_v^{(2)})^2/c_v^{(1)}$. By comparing this with the actual calculation of $c_v^{(3)}$ from ref. [81], we find that the prediction is completely wrong, giving $c_v^{(3)}|_{\text{Padé}} = -24.0$ while the correct result is $c_v^{(3)} = -52.2$, at scales $\Lambda = \mu_R = m$ and $n_f = 4$. The discrepancy increases for smaller values of Λ, as $c_v^{(3)}|_{\text{Padé}}$ predicts the wrong sign for the $\log^2 \Lambda$ term; that is, the Padé approximant incorrectly predicts the Λ dependence of the three-loop coefficient. Clearly, applying Padé approximants directly to the scheme and scale dependent short-distance coefficients will not do.

There may yet be a chance that Padé approximants could work if applied to correction factors that are scheme and scale independent. The calculation of the S-wave wavefunctions at the origin in ref. [16] makes construction of such correction factors possible. In ref. [16], the LDME $\langle 0|\chi^\dagger \boldsymbol{\epsilon} \cdot \boldsymbol{\sigma} \psi|V\rangle$ was computed in the $\overline{\text{MS}}$ scheme, in the form

$$\langle 0|\chi^\dagger \boldsymbol{\epsilon} \cdot \boldsymbol{\sigma} \psi|V\rangle = \sqrt{2N_c}|\Psi_V(0)| \left[1 + O(v^2, \Lambda_{\text{QCD}}^2/m^2)\right], \tag{6.35}$$

where $\Psi_V(r)$ is the wavefunction for the quarkonium V, and

$$\Psi_V(0) = \Psi_V^{\text{LO}}(0) \left[1 + \delta_\Psi^{\text{C}} + \delta_\Psi^{\text{NC}} + \delta_\Psi^{\text{RS}'} + O(v^3, \Lambda_{\text{QCD}}^2/m^2)\right], \tag{6.36}$$

where $\Psi_V^{\rm LO}(r)$ is a S-wave solution to the LO Schrödinger equation [eq. (4.3)], and $\delta_\Psi^{\rm C}$, $\delta_\Psi^{\rm NC}$, and $\delta_\Psi^{\rm RS'}$ are corrections at first order in the Rayleigh-Schrödinger perturbation theory from the loop corrections to the static potential, the potentials of higher orders in $1/m$, and the RS' subtraction term, respectively. The non-Coulombic correction $\delta_\Psi^{\rm NC}$ contains a UV divergence, which is renormalized in the $\overline{\rm MS}$ scheme at scale Λ. While the Coulombic correction $\delta_\Psi^{\rm C}$ and the correction from the RS' subtraction term $\delta_\Psi^{\rm RS'}$ cancel the μ_R and ν_f dependences of $\Psi_V^{\rm LO}(0)$, $\delta_\Psi^{\rm NC}$ cancels the Λ dependence in $c_v^{(2)}$ to two-loop accuracy; hence, if we write

$$f_V = \sqrt{\frac{2}{m_V}} \left[|\Psi_V^{\rm LO}(0)| \left(1 + \delta_\Psi^{\rm C} + \delta_\Psi^{\rm RS'} \right) \right]$$
$$\times \left[1 + c_v^{(1)} \alpha_s + c_v^{(2)} \alpha_s^2 + \delta_\Psi^{\rm NC} + O(\alpha_s^3) \right] + O(v^2), \quad (6.37)$$

every factor in the square brackets is separately invariant under variations of μ_R, Λ, and ν_f. We neglect the three-loop coefficient $c_v^{(3)}$ here, because the calculation of the non-Coulombic correction to matching accuracy requires calculation of the second order corrections in the Rayleigh-Schrödinger perturbation theory, which has only been done in perturbative QCD. In order to compare with the available order-α_s^3 correction computed in perturbative QCD in ref. [82], we compute the Padé approximant of the last correction factor as

$$\left[1 + c_v^{(1)} \alpha_s + c_v^{(2)} \alpha_s^2 + \delta_\Psi^{\rm NC} + O(\alpha_s^3) \right]_{[1/1]} = \frac{1 + \left[c_v^{(1)} - (c_v^{(2)} + \alpha_s^{-2}\delta_\Psi^{\rm NC})/c_v^{(1)} \right] \alpha_s}{1 - \left[(c_v^{(2)} + \alpha_s^{-2}\delta_\Psi^{\rm NC})/c_v^{(1)} \right] \alpha_s}, \quad (6.38)$$

from which we obtain the prediction $\alpha_s^3(c_v^{(2)} + \alpha_s^{-2}\delta_\Psi^{\rm NC})^2/c_v^{(1)}$ for the scheme and scale invariant order-α_s^3 term. Here, we used the fact that in perturbative QCD, $\delta_\Psi^{\rm NC}$ is of order α_s^2. This result can be compared with the perturbative QCD calculation of the leptonic decay rate of $1S$ quarkonium in ref. [82]. By computing $\delta_\Psi^{\rm NC}$ in perturbative QCD[11] at $\alpha_s(\mu_R = 3.5\,{\rm GeV}) = 0.2411$, $m = 4.911\,{\rm GeV}$, and $n_f = 4$, as were taken in ref. [82], we obtain $\delta_\Psi^{\rm NC} = 0.496$ for the $1S$ state at $\Lambda = m$, which leads to $\alpha_s^3(c_v^{(2)} + \alpha_s^{-2}\delta_\Psi^{\rm NC})^2/c_v^{(1)} \approx -24.6\alpha_s^3$. The correct result for the order-α_s^3 correction term can be obtained from the calculation of the leptonic decay rate of the $1S$ state in ref. [82], by subtracting the Coulombic corrections to three-loop accuracy [93], and also subtracting the correction from the binding energy [93–96], taking the square root, and expanding in powers of α_s, which gives $-21.5\alpha_s^3$. The prediction from the Padé approximant is in fair agreement with the correct result.

Following the example of the S-wave quarkonium vector decay constant, we construct correction factors to P-wave quarkonium decay and production rates that are independent on the renormalization, factorization, and mass renormalon subtraction scales by using the corrections to the wavefunctions computed in the previous section. We write the decay

---

[11]We note that the analytical results for $\delta_\Psi^{\rm NC}$ in perturbative QCD can be obtained at order α_s^2 indirectly from the calculations in refs. [10, 11, 83–92]. The numerical calculation in ref. [16] reproduces the analytical results (see appendix D of ref. [16]).

rate $\Gamma(\chi_{c0} \to \gamma\gamma)$ as

$$\Gamma(\chi_{c0} \to \gamma\gamma) = \frac{12\pi e_c^4 \alpha^2}{m_{\chi_{c0}}} \frac{3N_c}{2\pi} \left[|R'_{\mathrm{LO}}(0)|(1 + \delta_\Psi^{\mathrm{C}} + \delta_\Psi^{\mathrm{RS'}}) \right]^2 \left[\frac{1 - 3\delta m_{\mathrm{RS'}}/m_{\mathrm{RS'}}}{m_{\mathrm{RS'}}^3} \right]$$
$$\times \left[1 + 2\alpha_s c_{\gamma\gamma(00)}^{(1)} + \left(\alpha_s c_{\gamma\gamma(00)}^{(1)} \right)^2 + 2\alpha_s^2 \operatorname{Re}(c_{\gamma\gamma(00)}^{(2)}) + 2\delta_\Psi^{\mathrm{NC}}|_{^3P_0} \right]$$
$$+ O(\alpha_s^3, v^2), \tag{6.39}$$

where we rearranged the corrections to the wavefunctions at the origin and the loop corrections to the short-distance coefficients so that each factor in the square brackets is separately invariant under variations of μ_R, Λ, and also ν_f, up to corrections of order α_s^3. In the first factor in the square brackets, the μ_R and ν_f dependence of $|R'_{\mathrm{LO}}(0)|$ is cancelled by $\delta_\Psi^{\mathrm{C}} + \delta_\Psi^{\mathrm{RS'}}$. In the second factor, the dependence of $m_{\mathrm{RS'}}$ on ν_f is cancelled by the correction term $3\delta m_{\mathrm{RS'}}/m_{\mathrm{RS'}}$. Finally, in the third factor, the μ_R dependence in $\alpha_s c_{\gamma\gamma(00)}^{(1)}$ is cancelled explicitly by the $\log \mu_R$ term in $c_{\gamma\gamma(00)}^{(2)}$, and the Λ dependence cancels exactly between $\alpha_s^2 c_{\gamma\gamma(00)}^{(2)}$ and $\delta_\Psi^{\mathrm{NC}}|_{^3P_0}$ at two-loop level. Since the corrections in the first two factors are mild and converge rapidly, we examine the Padé approximant for the dimensionless correction factor that includes the loop corrections to the short-distance coefficients. If we consider the $\delta_\Psi^{\mathrm{NC}}|_{^3P_0}$ term to be of same order as the order-α_s^2 terms, which is necessary in establishing the exact two-loop level cancellation of the Λ dependence, we obtain the Padé approximant of order $[1/1]$ given by

$$\left[1 + 2\alpha_s c_{\gamma\gamma(00)}^{(1)} + \left(\alpha_s c_{\gamma\gamma(00)}^{(1)} \right)^2 + 2\alpha_s^2 \operatorname{Re}(c_{\gamma\gamma(00)}^{(2)}) + 2\delta_\Psi^{\mathrm{NC}}|_{^3P_0} \right]_{[1/1]} = \frac{1 + (A - B/A)\alpha_s}{1 - (B/A)\alpha_s}, \tag{6.40}$$

where $A = 2c_{\gamma\gamma(00)}^{(1)}$ and $B = (c_{\gamma\gamma(00)}^{(1)})^2 + 2\operatorname{Re}(c_{\gamma\gamma(00)}^{(2)}) + 2\alpha_s^{-2}\delta_\Psi^{\mathrm{NC}}|_{^3P_0}$. Even though the Padé approximant in eq. (6.40) has the same series expansion as the third correction factor in eq. (6.39) to order α_s^2, their numerical values are very different; while the last correction factor in eq. (6.39) is about 1.51, the numerical value of the Padé approximant is about 1.00. If we replace the last correction factor in eq. (6.39) by its Padé approximant, we obtain the following numerical result:

$$\Gamma(\chi_{c0} \to \gamma\gamma)|_{\mathrm{Padé}} = 3.08^{+0.32}_{-0.67} \pm 0.92 \text{ keV} = 3.08^{+0.98}_{-1.14} \text{ keV}, \tag{6.41}$$

where the first uncertainty comes from varying μ_R between $1.5\,\mathrm{GeV}$ and $4\,\mathrm{GeV}$, and the second uncertainty comes from uncalculated corrections of order v^2. We add the uncertainties in quadrature. This result is in much better agreement with the BESIII measurement of the decay rate $\Gamma(\chi_{c0} \to \gamma\gamma) = 2.33 \pm 0.20 \pm 0.22\,\mathrm{keV}$ from ref. [71] than the fixed-order calculation in the previous section.

We can also perform a similar analysis for the decay rate $\Gamma(\chi_{c2} \to \gamma\gamma)$, which can be written as

$$\Gamma(\chi_{c2} \to \gamma\gamma) = \frac{16\pi e_c^4 \alpha^2}{5m_{\chi_{c2}}} \frac{3N_c}{2\pi} \left[|R'_{\mathrm{LO}}(0)|(1 + \delta_\Psi^{\mathrm{C}} + \delta_\Psi^{\mathrm{RS'}}) \right]^2 \left[\frac{1 - 3\delta m_{\mathrm{RS'}}/m_{\mathrm{RS'}}}{m_{\mathrm{RS'}}^3} \right]$$

$$\times \left[1 + 2\alpha_s c^{(1)}_{\gamma\gamma(22)} + \left(\alpha_s c^{(1)}_{\gamma\gamma(22)} \right)^2 + \left(\alpha_s c^{(1)}_{\gamma\gamma(20)} \right)^2 \right.$$

$$\left. + 2\alpha_s^2 \operatorname{Re}(c^{(2)}_{\gamma\gamma(22)}) + 2\delta^{\mathrm{NC}}_{\Psi}|_{{}^3P_2} \right] + O(\alpha_s^3, v^2), \tag{6.42}$$

where each factor in the square brackets is again invariant under variations of μ_R, Λ, and ν_f up to corrections of order α_s^3. By replacing the last correction factor in eq. (6.42) by its Padé approximant, we obtain the numerical result

$$\Gamma(\chi_{c2} \to \gamma\gamma)|_{\mathrm{Padé}} = 0.61^{+0.10}_{-0.17} \pm 0.18 \text{ keV} = 0.61^{+0.21}_{-0.25} \text{ keV}, \tag{6.43}$$

where the uncertainties are as in eq. (6.41). This result is again in better agreement than the fixed-order calculation with the BESIII measurement of the decay rate $\Gamma(\chi_{c2} \to \gamma\gamma) = 0.63 \pm 0.04 \pm 0.06 \,\mathrm{keV}$ [71].

By dividing eq. (6.43) by eq. (6.40), and multiplying a factor of $1 + E^{\mathrm{LO}}/(3m)$ coming from the order-v^2 correction [8, 18], we obtain $\mathcal{R}_{\chi_c} = 0.24 \pm 0.04$, where the uncertainties come from variations of μ_R and uncalculated corrections of order $\Lambda^2_{\mathrm{QCD}}/m^2$. This is in good agreement with the BESIII result $\mathcal{R}_{\chi_c} = 0.27 \pm 0.04$ [71].

We repeat the analysis for the the $\chi_{cJ} + \gamma$ production rates in e^+e^- collisions at $\sqrt{s} = 10.58 \,\mathrm{GeV}$, for which we obtain

$$\sigma(e^+e^- \to \chi_{c0} + \gamma)|_{\mathrm{Padé}} = 1.29^{+0.25}_{-0.55} \pm 0.39 \text{ fb} = 1.29^{+0.46}_{-0.67} \text{ fb}, \tag{6.44a}$$

$$\sigma(e^+e^- \to \chi_{c1} + \gamma)|_{\mathrm{Padé}} = 14.3^{+1.7}_{-3.2} \pm 4.3 \text{ fb} = 14.3^{+4.6}_{-5.4} \text{ fb}, \tag{6.44b}$$

$$\sigma(e^+e^- \to \chi_{c2} + \gamma)|_{\mathrm{Padé}} = 2.80^{+1.02}_{-1.97} \pm 0.84 \text{ fb} = 2.80^{+1.33}_{-2.14} \text{ fb}, \tag{6.44c}$$

where the uncertainties are as in eq. (6.41). While effects of the use of Padé approximants are milder than the two-photon decay rates, the central value for $\sigma(e^+e^- \to \chi_{c1} + \gamma)$ obtained from the Padé approximant is in better agreement with the Belle measurement $\sigma(e^+e^- \to \chi_{c1} + \gamma) = 17.3^{+4.2}_{-3.9} \pm 1.7$ fb [72], and the numerical result for the $\chi_{c2} + \gamma$ production rate is smaller than the upper limit $\sigma(e^+e^- \to \chi_{c2} + \gamma) < 5.7$ fb from Belle [72].

The use of Padé approximants give the following results for the decay constants

$$m f^{\mathrm{OS}}_{\chi_{c0}}|_{\mathrm{Padé}} = 0.392^{+0.120}_{-0.118} \text{ GeV}^2, \tag{6.45a}$$

$$f_{\chi_{c1}}|_{\mathrm{Padé}} = 0.206 \pm 0.062 \text{ GeV}, \tag{6.45b}$$

where the uncertainties are as in eq. (6.41). By dividing $m f^{\mathrm{OS}}_{\chi_{c0}}$ by $\overline{m} = 1.27 \pm 0.02 \,\mathrm{GeV}$, we obtain $f^{\overline{\mathrm{MS}}}_{\chi_{c0}}(\mu = \overline{m})|_{\mathrm{Padé}} = 0.308^{+0.95}_{-0.93} \,\mathrm{GeV}$. In the case of decay constants, the effects of the use of Padé approximants are mild, and the numerical results are in agreement with the fixed-order calculations within uncertainties.

It is remarkable that by using Padé approximants, we obtain values of decay and production rates of P-wave charmonia that can deviate considerably from the fixed-order calculations at two-loop level. That is, we find sizable differences between the correction factors computed by using Padé approximants and values obtained from truncated series expansions in powers of α_s. In these cases, the Padé approximants have very small radii

of convergence when expanded as series in α_s. On the other hand, in the calculations of S-wave heavy quarkonium decay rates and decay constants in ref. [16], by combining the loop corrections to the short-distance coefficients with the corrections to the wavefunctions at the origin, we find that the NRQCD factorization scheme and scale invariant corrections become rapidly convergent. As a result, Padé approximants give values of S-wave heavy quarkonium decay rates and decay constants that differ by at most about 5% compared to the numerical results in ref. [16]. However, even in these cases, the Padé approximants predict series in α_s that do not converge for usual values of α_s, although the situation is much less severe than the P-wave case.

We note that, without the corrections to the wavefunctions at the origin computed in this work, the Padé approximants of the scheme and scale dependent short-distance coefficients give numerical results that are very different from what we have obtained above, and sometimes lead to unphysical, negative values of the rates. This is consistent with the poor behavior of the Padé approximant of the short-distance coefficient c_v of the S-wave quarkonium vector decay constant.

In the case of P-wave bottomonia, the effects of the use of Padé approximants are small for decay rates and decay constants, and we obtain numerical results that are consistent with the results in the previous section within uncertainties.

While it is interesting that by using Padé approximants, we obtain two-photon decay rates of χ_{c0} and χ_{c2} and $\chi_{c1} + \gamma$ production cross sections that are in good agreement with the BESIII and Belle measurements, implications of these agreements are limited because perturbative corrections are available only up to next-to-next-to leading order accuracy in α_s, and so, we can only obtain Padé approximants of the lowest possible order. For example, the value of $\mathcal{R}_{\chi_c}$ obtained by using the Padé approximant of the expression in eq. (6.21) agrees with what we obtain by dividing eq. (6.43) by eq. (6.40), only when we include corrections of higher orders in α_s that the Padé approximants predict.

7 Summary and discussion

In this work, we obtained P-wave heavy quarkonium wavefunctions at the origin in the $\overline{\text{MS}}$ scheme based on the pNRQCD effective field theory formalism. The results allow computation of $\overline{\text{MS}}$-renormalized NRQCD LDMEs for P-wave charmonia and bottomonia, which are necessary in making scheme-independent predictions of decay and production rates at two-loop level. The definitions of the NRQCD LDMEs and wavefunctions in d spacetime dimensions, which are necessary for carrying out renormalization in the $\overline{\text{MS}}$ scheme, are given in sections 2 and 3. The wavefunctions are computed from a potential that is determined by lattice QCD at long distances, while its short-distance behavior is given by perturbative QCD. We include corrections to the wavefunctions at subleading orders in $1/m$, which produce singularities at the origin. By generalizing the calculation of S-wave quarkonium wavefunctions in ref. [16], we compute the wavefunctions at the origin in position space by regulating the singularity by using finite-r regularization. The position-space expressions for the corrections to the wavefunctions are given in section 4. The finite-r regularized wavefunctions at the origin are then converted to the $\overline{\text{MS}}$ scheme by comput-

ing the scheme conversion in section 5. We use the results to make first-principles based, model-independent predictions of electromagnetic decay rates and exclusive electromagnetic production cross sections of P-wave charmonia and bottomonia in section 6.

Because the P-wave wavefunctions at the origin that we obtain have the correct dependences on the scale and scheme at which they are renormalized, we obtain predictions of decay and production rates that are independent of the NRQCD factorization scheme and scale, which has not been possible so far. Our first-principles based calculation also makes possible a proper treatment of the heavy quark pole mass, whose ambiguity can be removed by the use of renormalon subtracted masses. We also resum the logarithms that appear in the perturbative QCD corrections to the static potential, which significantly improves the convergence, as shown in refs. [16, 25]. These allow making much more refined predictions of physical quantities compared to existing model-dependent methods. Unlike potential-model based phenomenological studies in refs. [14, 15, 24], our first-principles based predictions of decay and production rates are robust under variations of input parameters such as renormalization and factorization scales, and heavy quark masses.

The corrections to the wavefunctions at the origin computed in this work allows us to investigate the corrections to the decay and production rates of P-wave heavy quarkonia in a scheme-independent manner. The calculation of the S-wave quarkonium wavefunctions at the origin in ref. [16] showed that the poor convergence of the scale dependent short-distance coefficients in the $\overline{\text{MS}}$ scheme is significantly improved by including the corrections to the wavefunctions at the origin, which remove the scheme and scale dependences. In the P-wave case, however, we find that the convergence of the corrections are still poor even after including the corrections to the P-wave wavefunctions at the origin, especially for decay and production rates of charmonia. In order to quantitatively assess the convergence of the corrections, we examine the Padé approximants of the scheme and scale-invariant corrections. While in the case of S-wave heavy quarkonia, the Padé approximants of the corrections to the decay rates and decay constants in ref. [16] have values that are consistent with the truncated series, we find significant differences between Padé approximants and truncated series of the scale and scheme independent corrections to P-wave charmonium decay and production rates. This suggests that the behaviors of perturbative corrections to decay and production rates differ between S-wave and P-wave heavy quarkonia.

Interestingly, we find that the Padé approximants lead to values of two-photon decay rates of χ_{c0} and χ_{c2} and exclusive electromagnetic production rates of χ_{c1} that agree well with measurements from BESIII [71] and Belle [72], while the truncated series give values that are in tension with experimental values. We also note that inclusion of the corrections to the P-wave wavefunctions at the origin is important in computing the Padé approximants. We find, from the available three-loop calculations of the vector decay constant of S-wave heavy quarkonia, that Padé approximants can give poor descriptions of scheme and scale dependent short-distance coefficients. In the P-wave case, using Padé approximants for the two-loop level short-distance coefficients in the $\overline{\text{MS}}$ scheme can sometimes lead to unphysical, negative values of the rates, and generally give values that are very different from what we obtain from the scheme-independent calculations in this work. However, we note that this analysis is limited to Padé approximants of the lowest possible orders,

because the perturbative corrections to the short-distance coefficients are available only up to two-loop accuracies.

We note that except for the ratio of decay rates, the accuracies of the phenomenological results involving P-wave heavy quarkonia in this work are limited to leading order in v. This is because the current level of accuracy of the pNRQCD expressions of the lowest dimensional NRQCD LDMEs is limited to first order in the expansion in powers of $1/m$, even though the higher dimensional LDMEs and the corresponding short-distance coefficients are already available [18, 24]. It is possible that the order-v^2 corrections are more important in P-wave quarkonium decay and production rates than the S-wave case. In order to fully incorporate the effect of the order-v^2 corrections, the order-v^2 corrections to the lowest dimensional LDMEs must be included, which requires calculation of the pN-RQCD matching coefficients $V_{\mathcal{O}}$ to second order in the expansion in powers of $1/m$ [22, 24]. We expect, however, the spin-dependent corrections in the matching coefficients to be suppressed by $\Lambda_{\mathrm{QCD}}^2/m^2$, and the leading spin-dependent corrections to the LDMEs to come from the corrections to the wavefunctions at the origin computed in this work.

The results presented in this work are relevant not only to precision studies of P-wave charmonium and bottomonium phenomenology, but also to calculations at tree and one-loop level. By comparing the first-principles calculations of the P-wave quarkonium wavefunctions at the origin at one-loop level with results from potential models, we have found that potential models can provide reasonable descriptions of the lowest dimensional LDMEs of P-wave heavy quarkonia; potential models can give central values of the LDMEs that are consistent with first-principles calculations, as long as the heavy quark mass is chosen consistently with the potential model employed. Nevertheless, due to large uncertainties coming from model dependences and the fact that the model calculations are incapable of reproducing the correct scheme and scale dependences of the NRQCD LDMEs, accurate QCD-based determinations of the LDMEs are essential for making improved predictions of decay and production rates, as we have done in this work.

Acknowledgments

A Short-distance coefficients

In this appendix, we list the NRQCD factorization formulae and short-distance coefficients for the decay rates, production cross sections, and decay constants that we consider in section 6. The NRQCD factorization formula for the two-photon decay rate of χ_{Q0} ($Q = c$ or b) is [4]

$$\Gamma(\chi_{Q0} \to \gamma\gamma) = \frac{12\pi e_Q^4 \alpha^2}{m_{\chi_{Q0}}} |c_{\gamma\gamma(00)}|^2 \frac{\langle \chi_{Q0}|\mathcal{O}(^3P_0)|\chi_{Q0}\rangle}{m^3} + O(v^2), \qquad (A.1)$$

where $m_{\chi_{Q0}}$ is the mass of the χ_{Q0}, e_Q is the fractional charge of the quark Q, and α is the QED coupling constant. A factor of $m_{\chi_{Q0}}$ in the denominator comes from the two-body phase space. The short-distance coefficient $c_{\gamma\gamma(00)}$ is given to two-loop accuracy in the $\overline{\text{MS}}$ scheme by [4, 14, 97, 98]

$$c_{\gamma\gamma(00)} = 1 + \alpha_s(\mu_R)c^{(1)}_{\gamma\gamma(00)} + \alpha_s^2(\mu_R)c^{(2)}_{\gamma\gamma(00)} + O(\alpha_s^3), \tag{A.2}$$

and

$$c^{(1)}_{\gamma\gamma(00)} = \frac{C_F}{\pi}\left(\frac{\pi^2}{8} - \frac{7}{6}\right), \tag{A.3a}$$

$$c^{(2)}_{\gamma\gamma(00)} = \frac{C_F}{\pi^2}\frac{\beta_0}{4}\left(\frac{\pi^2}{8} - \frac{7}{6}\right)\log\frac{\mu_R^2}{m^2} - \gamma^{(2)}_{3P_0}\log\frac{\Lambda}{m} + c^{(2),\text{fin}}_{\gamma\gamma(00)}, \tag{A.3b}$$

where $\beta_0 = \frac{11}{3}C_A - \frac{4}{3}T_F n_f$, n_f is the number of light quark flavors, $\alpha_s(\mu_R)$ is the strong coupling in the $\overline{\text{MS}}$ scheme at scale μ_R with n_f flavors, and $c^{(2),\text{fin}}_{\gamma\gamma(00)}$ is known numerically as [14]

$$c^{(2),\text{fin}}_{\gamma\gamma(00)}|_{n_f=3} = -2.40611 + 0.07997i, \tag{A.4a}$$

$$c^{(2),\text{fin}}_{\gamma\gamma(00)}|_{n_f=4} = -2.39666 + 0.11534i. \tag{A.4b}$$

The numerical results in eq. (A.4) include the contributions from the heavy quark loop.

The NRQCD factorization formula for the two-photon decay rate of χ_{Q2} ($Q = c$ or b) is [4]

$$\Gamma(\chi_{Q2} \to \gamma\gamma) = \frac{16\pi e_Q^4 \alpha^2}{5m_{\chi_{Q2}}}\left(|c_{\gamma\gamma(22)}|^2 + |c_{\gamma\gamma(20)}|^2\right)\frac{\langle\chi_{Q2}|\mathcal{O}(^3P_2)|\chi_{Q2}\rangle}{m^3} + O(v^2), \tag{A.5}$$

where $m_{\chi_{Q2}}$ is the mass of the χ_{Q2}. A factor of $m_{\chi_{Q0}}$ in the denominator comes from the two-body phase space. The short-distance coefficients $c_{\gamma\gamma(22)}$ and $c_{\gamma\gamma(20)}$ correspond to the two helicity amplitudes, which add at the squared amplitude level. They are given by [4, 14, 97, 98]

$$c_{\gamma\gamma(22)} = 1 + \alpha_s(\mu_R)c^{(1)}_{\gamma\gamma(22)} + \alpha_s^2(\mu_R)c^{(2)}_{\gamma\gamma(22)} + O(\alpha_s^3), \tag{A.6a}$$

$$c_{\gamma\gamma(20)} = \alpha_s(\mu_R)c^{(1)}_{\gamma\gamma(20)} + O(\alpha_s^2), \tag{A.6b}$$

and

$$c^{(1)}_{\gamma\gamma(22)} = -\frac{2C_F}{\pi}, \qquad c^{(1)}_{\gamma\gamma(20)} = -\frac{C_F}{\sqrt{6}\pi}\left(\frac{3\pi^2}{8} - 6\log 2 + 1\right), \tag{A.7a}$$

$$c^{(2)}_{\gamma\gamma(22)} = -\frac{2C_F}{\pi^2}\frac{\beta_0}{4}\log\frac{\mu_R^2}{m^2} - \gamma^{(2)}_{3P_2}\log\frac{\Lambda}{m} + c^{(2),\text{fin}}_{\gamma\gamma(22)}. \tag{A.7b}$$

The finite part $c^{(2),\text{fin}}_{\gamma\gamma(22)}$ is known numerically as [14]

$$c^{(2),\text{fin}}_{\gamma\gamma(22)}|_{n_f=3} = -3.11689 - 0.11467i, \tag{A.8a}$$

$$c^{(2),\text{fin}}_{\gamma\gamma(22)}|_{n_f=4} = -3.37915 - 0.83616i, \tag{A.8b}$$

which include the contributions from the heavy quark loop. While the order-α_s^2 correction to $c_{\gamma\gamma(20)}$ has also been computed in ref. [14], this contributes to the decay rate from order α_s^3, and hence, is neglected in this work. We also note that to order-α_s^2 accuracy, the numerical size of $c_{\gamma\gamma(20)}$ is tiny compared to $c_{\gamma\gamma(22)}$ [14].

The production cross sections $\sigma(e^+ e^- \to \chi_{QJ} + \gamma)$ for $J = 0$, 1, and 2 at the collision energy $\sqrt{s}$ are given at leading order in v by [5]

$$\sigma(e^+ e^- \to \chi_{QJ} + \gamma) = \sigma_{QJ}^{(0)}(s,m)\left[1 + \alpha_s(\mu_R)\hat{\sigma}_{QJ}^{(1)}(r) + \alpha_s^2(\mu_R)\hat{\sigma}_{QJ}^{(2)}(r) + O(\alpha_s^3)\right]$$
$$\times \langle \chi_{QJ}|\mathcal{O}(^3P_J)|\chi_{QJ}\rangle + O(v^2), \tag{A.9}$$

where the tree-level short-distance coefficients are given by [5]

$$\sigma_{Q0}^{(0)}(s,m) = \frac{(4\pi)^3 \alpha^3 e_Q^4 (1-3r)^2}{18\pi m^3 s^2 (1-r)}, \tag{A.10a}$$

$$\sigma_{Q1}^{(0)}(s,m) = \frac{(4\pi)^3 \alpha^3 e_Q^4 (1+r)}{3\pi m^3 s^2 (1-r)}, \tag{A.10b}$$

$$\sigma_{Q2}^{(0)}(s,m) = \frac{(4\pi)^3 \alpha^3 e_Q^4 (1+3r+6r^2)}{9\pi m^3 s^2 (1-r)}, \tag{A.10c}$$

where $r = 4m^2/s$. The order-α_s corrections are known analytically as [99]

$$\hat{\sigma}_{Q0}^{(1)}(r) = \frac{C_0^0(r)}{\pi}, \tag{A.11a}$$

$$\hat{\sigma}_{Q1}^{(1)}(r) = \frac{C_1^0(r) + rC_1^1(r)}{\pi(1+r)} \tag{A.11b}$$

$$\hat{\sigma}_{Q2}^{(1)}(r) = \frac{C_2^0(r) + 3rC_2^1(r) + 6r^2 C_2^2(r)}{\pi(1+3r+6r^2)}, \tag{A.11c}$$

where explicit expressions for $C_i^j(r)$ are given in ref. [99]. The order-α_s^2 corrections are given by

$$\hat{\sigma}_{QJ}^{(2)}(r) = \frac{\beta_0}{4\pi}\hat{\sigma}_{QJ}^{(1)}(r)\log\frac{\mu_R^2}{4m^2} - 2\gamma_{^3P_J}^{(2)}\log\frac{\Lambda}{m} + \hat{\sigma}_{QJ}^{(2),\text{fin}}(r), \tag{A.12}$$

where the $\hat{\sigma}_{QJ}^{(2),\text{fin}}(r)$ have been computed numerically in ref. [15] for $Q = c$ at $\sqrt{s} = 10.58\,\text{GeV}$ and $n_f = 3$ for two different choices of charm quark masses $m = 1.4\,\text{GeV}$ and $m = 1.68\,\text{GeV}$:

$$\hat{\sigma}_{c0}^{(2),\text{fin}}(r)|_{m=1.4\text{ GeV}} = -0.799, \tag{A.13a}$$

$$\hat{\sigma}_{c1}^{(2),\text{fin}}(r)|_{m=1.4\text{ GeV}} = -2.358, \tag{A.13b}$$

$$\hat{\sigma}_{c2}^{(2),\text{fin}}(r)|_{m=1.4\text{ GeV}} = -4.285, \tag{A.13c}$$

$$\hat{\sigma}_{c0}^{(2),\text{fin}}(r)|_{m=1.68\text{ GeV}} = -0.857, \tag{A.13d}$$

$$\hat{\sigma}_{c1}^{(2),\text{fin}}(r)|_{m=1.68\text{ GeV}} = -2.487, \tag{A.13e}$$

$$\hat{\sigma}_{c2}^{(2),\text{fin}}(r)|_{m=1.68\text{ GeV}} = -5.047, \tag{A.13f}$$

where the contribution from the heavy quark loop is included. We compute numerical values of $\hat{\sigma}_{cJ}^{(2),\text{fin}}(r)$ for other values of m by assuming that $\hat{\sigma}_{cJ}^{(2),\text{fin}}(r)$ changes linearly under

small variations of m. Unfortunately, the numerical results given in ref. [15] does not generalize to $\hat{\sigma}_{QJ}^{(2),\text{fin}}(r)$ at different values of $\sqrt{s}$ or for values of m that deviate too much from the charm quark mass.

The decay constants $f_{\chi Q0}$ and $f_{\chi Q1}$ are given in NRQCD by [13]

$$f_{\chi Q0}^{\text{OS}} = \frac{2}{\sqrt{m_{\chi Q0}}} \left(1 + \alpha_s(\mu_R)c_s^{(1)} + \alpha_s^2(\mu_R)c_s^{(2)} + O(\alpha_s^3) \right) \frac{\langle \chi_{Q0} | \mathcal{O}(^3P_0) | \chi_{Q0} \rangle}{m}, \quad \text{(A.14a)}$$

$$f_{\chi Q2} = \frac{\sqrt{6}}{\sqrt{m_{\chi Q1}}} \left(1 + \alpha_s(\mu_R)c_a^{(1)} + \alpha_s^2(\mu_R)c_a^{(2)} + O(\alpha_s^3) \right) \frac{\langle \chi_{Q1} | \mathcal{O}(^3P_1) | \chi_{Q1} \rangle}{m}, \quad \text{(A.14b)}$$

where the denominator factors $\sqrt{m_{\chi QJ}}$ come from the fact that the decay constants are defined in QCD with relativistically normalized states, while the NRQCD LDMEs are defined with nonrelativistic normalization. The superscript OS on $f_{\chi Q0}$ implies that the scalar decay constant has been renormalized in the on-shell scheme. The short-distance coefficients at order α_s and α_s^2 are given by [13]

$$c_s^{(1)} = \frac{C_F}{2\pi}, \quad \text{(A.15a)}$$

$$c_s^{(2)} = \frac{C_F}{2\pi^2} \frac{\beta_0}{4} \log \frac{\mu_R^2}{m^2} + \frac{C_F^2}{\pi^2} \left(\frac{5}{16} - \frac{37}{8}\zeta_2 + 3\zeta_2 \log 2 - \frac{11}{4}\zeta_3 - 2\zeta_2 \log \frac{\Lambda^2}{m^2} \right)$$

$$+ \frac{C_F C_A}{\pi^2} \left(\frac{49}{144} + \frac{1}{8}\zeta_2 - 3\zeta_2 \log 2 - \frac{5}{4}\zeta_3 - \frac{1}{2}\zeta_2 \log \frac{\Lambda^2}{m^2} \right)$$

$$+ \frac{C_F T_F}{\pi^2} \left(-\frac{5}{36}n_f + \frac{121}{36} - 2\zeta_2 + X_{\text{sing}}^{(s)} \right), \quad \text{(A.15b)}$$

$$c_a^{(1)} = -\frac{C_F}{\pi}, \quad \text{(A.15c)}$$

$$c_a^{(2)} = -\frac{C_F}{\pi^2} \frac{\beta_0}{4} \log \frac{\mu_R^2}{m^2} + \frac{C_F^2}{\pi^2} \left(\frac{23}{24} - \frac{27}{4}\zeta_2 + \frac{19}{4}\zeta_2 \log 2 - \frac{27}{16}\zeta_3 - \frac{5}{4}\zeta_2 \log \frac{\Lambda^2}{m^2} \right)$$

$$+ \frac{C_F C_A}{\pi^2} \left(-\frac{101}{72} + \frac{35}{24}\zeta_2 - \frac{7}{2}\zeta_2 \log 2 - \frac{9}{8}\zeta_3 - \frac{1}{2}\zeta_2 \log \frac{\Lambda^2}{m^2} \right)$$

$$+ \frac{C_F T_F}{\pi^2} \left(\frac{7}{18}n_f + \frac{20}{9} - \frac{4}{3}\zeta_2 + X_{\text{sing}}^{(a)} \right), \quad \text{(A.15d)}$$

where $\zeta_s = \sum_{n=1}^{\infty} \frac{1}{n^s}$, and

$$X_{\text{sing}}^{(s)} = \frac{2}{3} - \frac{29}{12}\zeta_2 + 4\zeta_2 \log 2 - \log 2 + \frac{\pi i}{2}, \quad \text{(A.16a)}$$

$$X_{\text{sing}}^{(a)} = -\frac{23}{12}\zeta_2 + 4\zeta_2 \log 2 - 2\log 2 + \frac{2}{3}\log^2 2 + i\pi \left(1 - \frac{2}{3}\log 2 \right). \quad \text{(A.16b)}$$

We note that the results for $c_a^{(1)}$ and $c_a^{(2)}$ in eqs. (A.15) are computed in naïve dimensional regularization, where γ_5 commutes with every γ matrix, except in $X_{\text{sing}}^{(a)}$, where the t'Hooft-Veltman scheme was used [13].

B Potentials in perturbative QCD

In this appendix, we list the short-distance behaviors of the potentials, which are obtained from perturbative QCD. In perturbative QCD, the static potential is given at leading order in α_s by

$$V^{(0)}(r)\big|_{\text{pert}} = -\frac{\alpha_s(\mu)C_F}{r} + O(\alpha_s^2). \tag{B.1}$$

where $\alpha_s = \alpha_s(\mu)$ is the $\overline{\text{MS}}$-renormalized QCD coupling constant at scale μ. Corrections of relative order α_s and α_s^2 have been computed in [57, 58], and corrections of relative order α_s^3 are given in refs. [41, 100–104]. In this paper, we include corrections to the static potential up to relative order α_s^2.

The forms of the $1/m$ and $1/m^2$ potentials generally depend on the matching scheme in which the potentials are determined. In on-shell matching, where we match on-shell S-matrix elements in NRQCD and pNRQCD in momentum space, we obtain [89, 105–111]

$$V^{(1)}(r)\big|_{\text{pert}}^{\text{OS}} = \frac{\alpha_s^2 C_F(\frac{1}{2}C_F - C_A)}{2r^2} + O(\alpha_s^3), \tag{B.2a}$$

$$V_r^{(2)}(r)\big|_{\text{pert}}^{\text{OS}} = 0 + O(\alpha_s^2), \tag{B.2b}$$

$$V_{p^2}^{(2)}(r)\big|_{\text{pert}}^{\text{OS}} = -\frac{\alpha_s C_F}{r} + O(\alpha_s^2), \tag{B.2c}$$

$$V_{L^2}^{(2)}(r)\big|_{\text{pert}}^{\text{OS}} = 0 + O(\alpha_s^2), \tag{B.2d}$$

$$V_{S^2}^{(2)}(r)\big|_{\text{pert}}^{\text{OS}} = \frac{4\pi\alpha_s C_F}{3}\delta^{(3)}(\boldsymbol{r}) + O(\alpha_s^2), \tag{B.2e}$$

$$V_{S_{12}}^{(2)}(r)\big|_{\text{pert}}^{\text{OS}} = \frac{\alpha_s C_F}{4r^3} + O(\alpha_s^2), \tag{B.2f}$$

$$V_{so}^{(2)}(r)\big|_{\text{pert}}^{\text{OS}} = \frac{3\alpha_s C_F}{2r^3} + O(\alpha_s^2). \tag{B.2g}$$

We use the superscript OS to denote the on-shell matching scheme.

In Wilson-loop matching, the potentials are given in terms of the rectangular Wilson loop $W_{r \times T}$ with spatial size r and time extension T, with insertions of gluon fields [33, 39]. The short-distance behavior of the potentials in Wilson loop matching can be obtained by computing the nonperturbative definitions in perturbative QCD [46]. We list the results at leading nonvanishing orders in α_s:

$$V^{(1)}(r)\big|_{\text{pert}}^{\text{WL}} = -\frac{\alpha_s^2 C_F C_A}{2r^2} + O(\alpha_s^3), \tag{B.3a}$$

$$V_r^{(2)}(r)\big|_{\text{pert}}^{\text{WL}} = \pi\alpha_s C_F \delta^{(3)}(\boldsymbol{r}) + O(\alpha_s^2), \tag{B.3b}$$

$$V_{p^2}^{(2)}(r)\big|_{\text{pert}}^{\text{WL}} = -\frac{\alpha_s C_F}{r} + O(\alpha_s^2), \tag{B.3c}$$

$$V_{L^2}^{(2)}(r)\big|_{\text{pert}}^{\text{WL}} = \frac{\alpha_s C_F}{2r^3} + O(\alpha_s^2), \tag{B.3d}$$

$$V_{S^2}^{(2)}(r)\big|_{\text{pert}}^{\text{WL}} = \frac{4\pi\alpha_s C_F}{3}\delta^{(3)}(\boldsymbol{r}) + O(\alpha_s^2), \tag{B.3e}$$

$$V_{S_{12}}^{(2)}(r)\big|_{\text{pert}}^{\text{WL}} = \frac{\alpha_s C_F}{4r^3} + O(\alpha_s^2), \tag{B.3f}$$

$$V_{so}^{(2)}(r)\big|_{\text{pert}}^{\text{WL}} = \frac{3\alpha_s C_F}{2r^3} + O(\alpha_s^2). \tag{B.3g}$$

The superscript WL denotes that the potential is obtained in Wilson loop matching.

The potentials from on-shell matching in eq. (B.2) and the potentials from Wilson loop matching in eq. (B.3) are related by unitary transformations. The effect of the unitary transformations on P-wave wavefunctions are described in section 5.4.

The momentum-space potentials in the on-shell matching scheme can be computed in d dimensions, which are suitable for calculations in DR. For calculations in this work, we only need the color singlet projection of the potential. If we include the $1/m$ and $1/m^2$ potentials at leading nonvanishing orders in α_s, we obtain [89, 111]

$$\begin{aligned} V(\boldsymbol{p}', \boldsymbol{p}) = {} & -\frac{4\pi\alpha_s C_F}{\boldsymbol{q}^2} + \delta\tilde{V}_C(\boldsymbol{q}^2) + \frac{\pi^2\alpha_s^2 C_F}{m|\boldsymbol{q}|}\left(\frac{\Lambda^2}{\boldsymbol{q}^2}\right)^\epsilon \left(\frac{C_F}{2}(1-2\epsilon) - C_A(1-\epsilon)\right) c_\epsilon \\ & -\frac{2\pi\alpha_s C_F(\boldsymbol{p}^2 + \boldsymbol{p}'^2)}{m^2\boldsymbol{q}^2} + \frac{2\pi\alpha_s C_F}{m^2} + \frac{\pi\alpha_s C_F}{4m^2\boldsymbol{q}^2}[\sigma_i,\sigma_j]q_j \otimes [\sigma_i,\sigma_k]q_k \\ & -\frac{3\pi\alpha_s C_F}{2m^2\boldsymbol{q}^2}\left([\sigma_i,\sigma_j]q_i p_j \otimes 1 - 1 \otimes [\sigma_i,\sigma_j]q_i p_j\right) - (2\pi)^{d-1}\delta^{(d-1)}(\boldsymbol{q})\frac{\boldsymbol{p}^4}{4m^3}, \end{aligned} \tag{B.4}$$

where $\boldsymbol{q} = \boldsymbol{p}' - \boldsymbol{p}$ and

$$c_\epsilon = \frac{e^{\gamma_E \epsilon}\Gamma(\frac{1}{2}-\epsilon)^2\Gamma(\frac{1}{2}+\epsilon)}{\pi^{3/2}\Gamma(1-2\epsilon)}. \tag{B.5}$$

The Λ in eq. (B.4) comes from associating a factor of $\left(\Lambda^2\frac{e^{\gamma_E}}{4\pi}\right)^\epsilon$ with each loop integral. The last term in eq. (B.4) comes from the relativistic correction to the kinetic energy. The term $\delta\tilde{V}_C(\boldsymbol{q}^2)$ encodes the loop corrections to the static potential, whose explicit expressions are not needed in this paper. We identify the spin-dependent terms proportional to $[\sigma_i,\sigma_j]q_j \otimes [\sigma_i,\sigma_k]q_k$ and $[\sigma_i,\sigma_j]q_i p_j \otimes 1 - 1 \otimes [\sigma_i,\sigma_j]q_i p_j$ as the hyperfine and spin-orbit terms, respectively. It can be shown that eq. (B.4) reproduces the position-space expressions in eqs. (B.2) in the on-shell scheme (the $\boldsymbol{p}$ and $\boldsymbol{p}'$-independent term and the isotropic part of the hyperfine term combine to give the $\boldsymbol{S}^2$ term in the position-space expression).

Now we obtain the d-dimensional expression for $\delta\tilde{\mathcal{V}}(\boldsymbol{p}', \boldsymbol{p})$ from eq. (B.4) by reducing the $\boldsymbol{p}^2$ and $\boldsymbol{p}'^2$ by using the d-dimensional Lippmann-Schwinger equation and the Schrödinger equation. We obtain

$$\begin{aligned} \delta\tilde{\mathcal{V}}(\boldsymbol{p}', \boldsymbol{p}) = {} & \frac{\pi^2\alpha_s^2 C_F}{m|\boldsymbol{q}|}\left(\frac{\Lambda^2}{\boldsymbol{q}^2}\right)^\epsilon \left(\frac{C_F}{2}(1-2\epsilon) - C_A(1-\epsilon)\right) c_\epsilon \\ & + \frac{1}{m}\int_{\boldsymbol{k}} \frac{4\pi\alpha_s C_F}{\boldsymbol{k}^2}\tilde{V}_{\text{LO}}(\boldsymbol{k}-\boldsymbol{q}) - \frac{1}{4m}\int_{\boldsymbol{k}}\tilde{V}_{\text{LO}}(\boldsymbol{k})\tilde{V}_{\text{LO}}(\boldsymbol{k}-\boldsymbol{q}) \\ & + \frac{2\pi\alpha_s C_F}{m^2} + \frac{\pi\alpha_s C_F}{4m^2\boldsymbol{q}^2}[\sigma_i,\sigma_j]q_j \otimes [\sigma_i,\sigma_k]q_k \\ & -\frac{3\pi\alpha_s C_F}{2m^2\boldsymbol{q}^2}\left([\sigma_i,\sigma_j]q_i p_j \otimes 1 - 1 \otimes [\sigma_i,\sigma_j]q_i p_j\right), \end{aligned} \tag{B.6}$$

where $\tilde{V}_{\text{LO}}(\boldsymbol{q}) = -4\pi\alpha_s C_F/\boldsymbol{q}^2$ in perturbative QCD.

C Matrix elements of the spin-spin potential

In this section we discuss the angular matrix elements of the spin-spin potential on P-wave states. While the angular matrix elements of S_{12} are generally known, we focus on its action on P-wave LO wavefunctions $\Psi_n^{\rm LO}(\boldsymbol{r})$ in the Cartesian basis, which is also useful in analytical calculations of the scheme conversion coefficient. In the Cartesian basis, the dependencies of P-wave wavefunctions on the angles of $\boldsymbol{r}$ and $Q\bar{Q}$ spin can be written as $1_{2\times2}\hat{\boldsymbol{r}}$, $\hat{\boldsymbol{r}}\cdot\boldsymbol{\sigma}$, $\hat{\boldsymbol{r}}^{[i}\sigma^{j]}$, and $\hat{\boldsymbol{r}}^{(i}\sigma^{j)}$ for the $^1P_1$, $^3P_0$, $^3P_1$, and $^3P_2$ states, respectively. Then, the application of S_{12} on a $^1P_1$ state can be computed as

$$S_{12}\hat{\boldsymbol{r}} = -(3\hat{\boldsymbol{r}}\cdot\boldsymbol{\sigma}\hat{\boldsymbol{r}}\cdot\boldsymbol{\sigma} - \boldsymbol{\sigma}\cdot\boldsymbol{\sigma})\hat{\boldsymbol{r}} = 0. \tag{C.1}$$

For $^3P_0$ and $^3P_1$ states, we have

$$S_{12}\hat{\boldsymbol{r}}\cdot\boldsymbol{\sigma} = -3\hat{\boldsymbol{r}}\cdot\boldsymbol{\sigma}(\hat{\boldsymbol{r}}\cdot\boldsymbol{\sigma})\hat{\boldsymbol{r}}\cdot\boldsymbol{\sigma} + \sigma^i(\hat{\boldsymbol{r}}\cdot\boldsymbol{\sigma})\sigma^i = -4\hat{\boldsymbol{r}}\cdot\boldsymbol{\sigma}, \tag{C.2}$$

$$S_{12}\hat{\boldsymbol{r}}^{[i}\sigma^{j]} = -3\hat{\boldsymbol{r}}\cdot\boldsymbol{\sigma}(\hat{\boldsymbol{r}}^{[i}\sigma^{j]})\hat{\boldsymbol{r}}\cdot\boldsymbol{\sigma} + \sigma^k(\hat{\boldsymbol{r}}^{[i}\sigma^{j]})\sigma^k = 2\hat{\boldsymbol{r}}^{[i}\sigma^{j]}. \tag{C.3}$$

Finally, for a $^3P_2$ state, we have

$$\begin{aligned} S_{12}\hat{\boldsymbol{r}}^{(i}\sigma^{j)} &= -3\hat{\boldsymbol{r}}\cdot\boldsymbol{\sigma}(\hat{\boldsymbol{r}}^{(i}\sigma^{j)})\hat{\boldsymbol{r}}\cdot\boldsymbol{\sigma} + \sigma^k(\hat{\boldsymbol{r}}^{(i}\sigma^{j)})\sigma^k \\ &= -\frac{2}{5}\hat{\boldsymbol{r}}^{(i}\boldsymbol{\sigma}^{j)} + \frac{6}{5}f^{ij}(\hat{\boldsymbol{r}},\boldsymbol{\sigma}), \end{aligned} \tag{C.4}$$

where

$$f^{ij}(\hat{\boldsymbol{r}},\boldsymbol{\sigma}) = (\delta^{ij} - 5\hat{\boldsymbol{r}}^i\hat{\boldsymbol{r}}^j)\boldsymbol{\sigma}\cdot\hat{\boldsymbol{r}} + \hat{\boldsymbol{r}}^i\sigma^j + \hat{\boldsymbol{r}}^j\sigma^i \tag{C.5}$$

is a F-wave contribution of total spin 2. This contribution is orthogonal to the P-wave wavefunctions, that is, $\delta^{ij}f^{ij}(\hat{\boldsymbol{r}},\boldsymbol{\sigma}) = \hat{\boldsymbol{r}}^{[i}\sigma^{j]}f^{ij}(\hat{\boldsymbol{r}},\boldsymbol{\sigma}) = \hat{\boldsymbol{r}}^{(i}\sigma^{j)}f^{ij}(\hat{\boldsymbol{r}},\boldsymbol{\sigma}) = 0$. While S_{12} induces transitions between states with different orbital angular momentum, S_{12} is diagonal within the P-wave block, with diagonal elements $0, 4, -2$, and $2/5$ for angular momentum states with quantum numbers $^1P_1$, $^3P_0$, $^3P_1$, and $^3P_2$, respectively. As we have argued in section 4, the F-wave contribution does not affect the LDMEs to first order in the QMPT, and so the off-diagonal matrix elements of S_{12} can be neglected in our calculation of the wavefunctions at the origin.

D Logarithmically divergent tensor integrals

In this appendix, we compute the logarithmically divergent two-loop tensor integrals in eqs. (5.51) and (5.52). We compute the two-loop integrals as nested one-loop integrals, by first integrating over $\boldsymbol{p}$, and then integrating over $\boldsymbol{p}'$. We note that the integration over $\boldsymbol{p}$ can be done in the same way in DR and in finite-r regularization, as long as we work in $d-1$ spatial dimensions and expand in powers of ϵ for the finite-r regularized integral. The integrals can be simplified by using the fact that we only need the difference between DR and finite-r regularization, so that any UV-finite contribution that appear commonly in both regularizations can be neglected. Since the tensor integrals are at most

logarithmically divergent, we can make any changes in the integrands as long as the large $\boldsymbol{p}$ and $\boldsymbol{p}'$ behaviors are kept unaltered. We note that in the integral over $\boldsymbol{p}$,

$$\frac{1}{E - \boldsymbol{p}^2/m} = -\frac{m}{\boldsymbol{p}^2} - \frac{m}{\boldsymbol{p}^4/(mE) - \boldsymbol{p}^2}. \tag{D.1}$$

Since the second term does not produce UV divergences, it can be neglected in our calculation of the integrals. This removes the scale E from the integration over $\boldsymbol{p}$, and leaves only the scale $\boldsymbol{p}'^2$, which simplifies the calculation. We do not make similar modifications for the $\boldsymbol{p}'$ integral, because if we set $E = 0$ everywhere, the tensor integrals develop logarithmic IR divergences, which must be regulated in the same way in both DR and finite-r regularization. While this is in principle possible, for example by regulating the IR divergences in DR, this requires computing the finite-r regularized integral in $d - 1$ spatial dimensions, which is more difficult than keeping E nonzero in the $\boldsymbol{p}'$ integral.

In J_{3b} and J_{3c}, the integration over $\boldsymbol{p}$ contains power IR divergences. We regulate the IR divergences dimensionally in both DR and finite-r regularized integrals. Unlike logarithmic divergences, power divergences are subtracted automatically by expanding in powers of ϵ, and so, we can compute the finite-r regularized integral over $\boldsymbol{p}'$ in 3 spatial dimensions.

D.1 J_{3a}

We compute the integral over $\boldsymbol{p}$ using Feynman parametrization.

$$\begin{aligned}
\int_{\boldsymbol{p}} \frac{1}{(\boldsymbol{p} - \boldsymbol{p}')^2} \frac{\boldsymbol{p}^j \boldsymbol{p}^k \boldsymbol{p}^l}{(\boldsymbol{p}^2)^3} &= 3 \int_0^1 dx\,(1-x)^2 \int_{\boldsymbol{p}} \frac{\boldsymbol{p}^j \boldsymbol{p}^k \boldsymbol{p}^l}{[\boldsymbol{p}^2 - 2x\boldsymbol{p} \cdot \boldsymbol{p}' + x\boldsymbol{p}'^2]^4} \\
&= 3 \int_0^1 dx\,(1-x)^2 \int_{\boldsymbol{p}} \frac{\frac{x}{d-1}(\boldsymbol{p}'^j \delta^{kl} + \boldsymbol{p}'^k \delta^{jl} + \boldsymbol{p}'^l \delta^{jk})\boldsymbol{p}^2 + x^3 \boldsymbol{p}'^j \boldsymbol{p}'^k \boldsymbol{p}'^l}{[\boldsymbol{p}^2 + x(1-x)\boldsymbol{p}'^2]^4} \\
&= \Lambda^{2\epsilon} e^{\epsilon\gamma_{\mathrm{E}}} \frac{2^{2\epsilon-6}\Gamma(\frac{1}{2}-\epsilon)\Gamma(\frac{3}{2}+\epsilon)}{\pi\Gamma(1-\epsilon)} \\
&\quad \times \left[(3+2\epsilon)\frac{\boldsymbol{p}'^j \boldsymbol{p}'^k \boldsymbol{p}'^l}{(\boldsymbol{p}'^2)^{5/2+\epsilon}} + \frac{\boldsymbol{p}'^j \delta^{kl} + \boldsymbol{p}'^k \delta^{jl} + \boldsymbol{p}'^l \delta^{jk}}{(\boldsymbol{p}'^2)^{3/2+\epsilon}}\right]. \tag{D.2}
\end{aligned}$$

The integrals over $\boldsymbol{p}'$ in DR are evaluated as

$$\begin{aligned}
\int_{\boldsymbol{p}'} \frac{\boldsymbol{p}'^i \boldsymbol{p}'^j \boldsymbol{p}'^k \boldsymbol{p}'^l}{(\boldsymbol{p}'^2 - mE)(\boldsymbol{p}'^2)^{5/2+\epsilon}} &= \frac{\Gamma(7/2+\epsilon)}{\Gamma(5/2+\epsilon)} \int_0^1 dz \int_{\boldsymbol{p}'} \frac{z^{3/2+\epsilon} \boldsymbol{p}'^i \boldsymbol{p}'^j \boldsymbol{p}'^k \boldsymbol{p}'^l}{[\boldsymbol{p}'^2 - (1-z)mE]^{7/2+\epsilon}} \tag{D.3} \\
&= (\delta^{ij}\delta^{kl} + \delta^{ik}\delta^{jl} + \delta^{il}\delta^{jk}) \frac{\Lambda^{2\epsilon} e^{\epsilon\gamma_{\mathrm{E}}}}{4(4\pi)^{3/2}} \frac{\Gamma(2\epsilon)\Gamma(1-2\epsilon)}{\Gamma(7/2-\epsilon)(-mE)^{-2\epsilon}},
\end{aligned}$$

and

$$\int_{\boldsymbol{p}'} \frac{\boldsymbol{p}'^i \boldsymbol{p}'^j}{(\boldsymbol{p}'^2 - mE)(\boldsymbol{p}'^2)^{3/2+\epsilon}} = \delta^{ij} \frac{\Lambda^{2\epsilon} e^{\epsilon\gamma_{\mathrm{E}}}}{2(4\pi)^{3/2}} \frac{\Gamma(2\epsilon)\Gamma(1-2\epsilon)}{\Gamma(5/2-\epsilon)(-mE)^{-2\epsilon}}, \tag{D.4}$$

so that

$$\begin{aligned}
\int_{\boldsymbol{p}'} \int_{\boldsymbol{p}} \frac{\boldsymbol{p}'^i \boldsymbol{p}^j \boldsymbol{p}^k \boldsymbol{p}^l}{(\boldsymbol{p}'^2 - mE)(\boldsymbol{p} - \boldsymbol{p}')^2 (\boldsymbol{p}^2)^3} &= \frac{\delta^{ij}\delta^{kl} + \delta^{ik}\delta^{jl} + \delta^{il}\delta^{jk}}{1920\pi^2} \\
&\quad \times \left[\frac{1}{\epsilon_{\mathrm{UV}}} + 2\log\left(-\frac{\Lambda^2}{mE}\right) + \frac{76}{15} + O(\epsilon)\right]. \tag{D.5}
\end{aligned}$$

On the other hand, the finite-r regulated integrals over $\boldsymbol{p}'$ are computed as

$$\left(-i\frac{\partial}{\partial r}\right)\int_{\boldsymbol{p}'}\frac{e^{i\boldsymbol{p}'\cdot\boldsymbol{r}}\boldsymbol{p}'^j\boldsymbol{p}'^k\boldsymbol{p}'^l}{(\boldsymbol{p}'^2-mE)(\boldsymbol{p}'^2)^{5/2}}\Bigg|_{|\boldsymbol{r}|=r_0}$$

$$=\left(-i\frac{\partial}{\partial r}\right)\frac{\Gamma(7/2)}{\Gamma(5/2)}\int_0^1 dz\, z^{3/2}\int_{\boldsymbol{p}'}\frac{e^{i\boldsymbol{p}'\cdot\boldsymbol{r}}\boldsymbol{p}'^j\boldsymbol{p}'^k\boldsymbol{p}'^l}{[\boldsymbol{p}'^2-(1-z)mE]^{7/2}} \tag{D.6}$$

$$=-\frac{1}{30\pi^2}\left\{\hat{\boldsymbol{r}}^j\hat{\boldsymbol{r}}^k\hat{\boldsymbol{r}}^l+(\hat{\boldsymbol{r}}^j\delta^{kl}+\hat{\boldsymbol{r}}^k\delta^{lj}+\hat{\boldsymbol{r}}^l\delta^{jk})\left[-\frac{8}{15}+\gamma_{\mathrm{E}}+\frac{1}{2}\log(-r_0^2 mE)\right]\right\},$$

and

$$\left(-i\frac{\partial}{\partial r}\right)\int_{\boldsymbol{p}'}\frac{e^{i\boldsymbol{p}'\cdot\boldsymbol{r}}\boldsymbol{p}'^j}{(\boldsymbol{p}'^2-mE)(\boldsymbol{p}'^2)^{3/2}}\Bigg|_{|\boldsymbol{r}|=r_0}=-\frac{1}{6\pi^2}\hat{\boldsymbol{r}}^j\left[-\frac{1}{3}+\gamma_{\mathrm{E}}+\frac{1}{2}\log(-r_0^2 mE)\right], \tag{D.7}$$

which give

$$\int_{\boldsymbol{p}'}\int_{\boldsymbol{p}}\frac{e^{i\boldsymbol{p}'\cdot\boldsymbol{r}}\hat{\boldsymbol{r}}\cdot\boldsymbol{p}'\boldsymbol{p}^j\boldsymbol{p}^k\boldsymbol{p}^l}{(\boldsymbol{p}'^2-mE)(\boldsymbol{p}-\boldsymbol{p}')^2(\boldsymbol{p}^2)^3}\Bigg|_{|\boldsymbol{r}|=r_0} \tag{D.8}$$

$$=-\frac{(\hat{\boldsymbol{r}}^j\delta^{kl}+\hat{\boldsymbol{r}}^k\delta^{jl}+\hat{\boldsymbol{r}}^l\delta^{jk})}{1920\pi^2}\left[-\frac{49}{30}+4\gamma_{\mathrm{E}}+2\log(-r_0^2 mE)\right]-\frac{\hat{\boldsymbol{r}}^i\hat{\boldsymbol{r}}^j\hat{\boldsymbol{r}}^k}{1280\pi^2}+O(r_0).$$

From these we obtain

$$\frac{1}{m^2}\hat{\boldsymbol{r}}^i\left(J_{3a}^{ijkl}\big|_{(r_0)}-J_{3a}^{ijkl}\big|_{\mathrm{DR}}\right)=-\frac{(\hat{\boldsymbol{r}}^j\delta^{kl}+\hat{\boldsymbol{r}}^k\delta^{jl}+\hat{\boldsymbol{r}}^l\delta^{jk})}{480\pi^2}\left[\frac{1}{4\epsilon_{\mathrm{UV}}}+\frac{103}{120}+\log(\Lambda r_0 e^{\gamma_{\mathrm{E}}})\right]$$

$$-\frac{1}{1280\pi^2}\hat{\boldsymbol{r}}^j\hat{\boldsymbol{r}}^k\hat{\boldsymbol{r}}^l. \tag{D.9}$$

D.2 J_{3b}

We first integrate over $\boldsymbol{p}$. This integral contains a power IR divergence, which we regulate in DR.

$$\int_{\boldsymbol{p}}\frac{(\boldsymbol{p}'-\boldsymbol{p})^j(\boldsymbol{p}'-\boldsymbol{p})^k\boldsymbol{p}^l}{[(\boldsymbol{p}'-\boldsymbol{p})^2](\boldsymbol{p}^2)^3}$$

$$=\frac{\Gamma(4)}{\Gamma(3)}\int_0^1 dx\int_{\boldsymbol{p}}\frac{(1-x)^2(\boldsymbol{p}'-\boldsymbol{p})^j(\boldsymbol{p}'-\boldsymbol{p})^k\boldsymbol{p}^l}{[\boldsymbol{p}^2-2x\boldsymbol{p}\cdot\boldsymbol{p}'+x\boldsymbol{p}'^2]^4}$$

$$=\frac{\Lambda^{2\epsilon}e^{\epsilon\gamma_{\mathrm{E}}}}{(4\pi)^{3/2}}\frac{\Gamma(5/2+\epsilon)}{\Gamma(3)}\int_0^1 dx\frac{x(1-x)^4\boldsymbol{p}'^j\boldsymbol{p}'^k\boldsymbol{p}'^l}{[x(1-x)\boldsymbol{p}'^2]^{5/2+\epsilon}}$$

$$+\frac{\Lambda^{2\epsilon}e^{\epsilon\gamma_{\mathrm{E}}}}{2(4\pi)^{3/2}}\frac{\Gamma(3/2+\epsilon)}{\Gamma(3)}\int_0^1 dx(1-x)^2\frac{x\delta^{jk}\boldsymbol{p}'^l-(1-x)\boldsymbol{p}'^k\delta^{jl}-(1-x)\boldsymbol{p}'^j\delta^{kl}}{[x(1-x)\boldsymbol{p}'^2]^{3/2+\epsilon}}$$

$$=\Lambda^{2\epsilon}e^{\epsilon\gamma_{\mathrm{E}}}\frac{2^{2\epsilon-7}\Gamma(1/2+\epsilon)\Gamma(1/2-\epsilon)}{\pi\Gamma(1-\epsilon)}$$

$$\times\left[(4\epsilon^2-9)\frac{\boldsymbol{p}'^j\boldsymbol{p}'^k\boldsymbol{p}'^l}{[\boldsymbol{p}'^2]^{5/2+\epsilon}}+\frac{(1+2\epsilon)\delta^{jk}\boldsymbol{p}'^l+(3-2\epsilon)[\boldsymbol{p}'^k\delta^{jl}+\boldsymbol{p}'^j\delta^{kl}]}{[\boldsymbol{p}'^2]^{3/2+\epsilon}}\right]. \tag{D.10}$$

Since this expression does not contain poles when expanded in powers of ϵ, there are no logarithmic IR divergences, and we can set $\epsilon=0$ in calculations in finite-r regularization,

which subtracts the power IR divergence. By using eqs. (D.3) and (D.4), we obtain in DR

$$
\int_{\boldsymbol{p}'} \int_{\boldsymbol{p}} \frac{\boldsymbol{p}'^i (\boldsymbol{p}' - \boldsymbol{p})^j (\boldsymbol{p}' - \boldsymbol{p})^k \boldsymbol{p}^l}{(\boldsymbol{p}^2 - mE)(\boldsymbol{p}' - \boldsymbol{p})^2 (\boldsymbol{p}^2)^3}
$$
$$
= \frac{3\delta^{ij}\delta^{kl} + 3\delta^{ik}\delta^{jl} - 2\delta^{il}\delta^{jk}}{7680\pi^2 \epsilon_{\text{UV}}} + \frac{(\delta^{ij}\delta^{kl} + \delta^{ik}\delta^{jl})}{6400\pi^2} \left[1 + 5\log\left(-\frac{\Lambda^2}{mE}\right) \right]
$$
$$
- \frac{\delta^{il}\delta^{jk}}{28800\pi^2} \left[8 + 15\log\left(-\frac{\Lambda^2}{mE}\right) \right] + O(\epsilon), \tag{D.11}
$$

where the $1/\epsilon_{\text{UV}}$ pole comes from the UV divergence of the $\boldsymbol{p}'$ integral. Similarly, by using eqs. (D.6) and (D.7) we obtain in finite-r regularization

$$
\int_{\boldsymbol{p}'} \int_{\boldsymbol{p}} \frac{e^{i\boldsymbol{p}' \cdot \boldsymbol{r}} \hat{\boldsymbol{r}} \cdot \boldsymbol{p}' (\boldsymbol{p}' - \boldsymbol{p})^j (\boldsymbol{p}' - \boldsymbol{p})^k \boldsymbol{p}^l}{(\boldsymbol{p}^2 - mE)(\boldsymbol{p}' - \boldsymbol{p})^2 (\boldsymbol{p}^2)^3} \bigg|_{|\boldsymbol{r}| = r_0}
$$
$$
= \frac{\hat{\boldsymbol{r}}^j \delta^{kl} + \hat{\boldsymbol{r}}^k \delta^{jl}}{6400\pi^2} \left[\frac{1}{3} - 10\gamma_{\text{E}} - 5\log\left(-r_0^2 mE\right) \right]
$$
$$
- \frac{\hat{\boldsymbol{r}}^l \delta^{jk}}{28800\pi^2} \left[\frac{47}{2} - 30\gamma_{\text{E}} - 15\log\left(-r_0^2 mE\right) \right] + \frac{3}{1280\pi^2} \hat{\boldsymbol{r}}^j \hat{\boldsymbol{r}}^k \hat{\boldsymbol{r}}^l + O(r_0). \tag{D.12}
$$

By subtracting eq. (D.11) from eq. (D.12) we obtain

$$
\frac{1}{m^2} \hat{\boldsymbol{r}}^i \left(J_{3b}^{ijkl} \big|_{(r_0)} - J_{3b}^{ijkl} \big|_{\text{DR}} \right)
$$
$$
= -\frac{3\hat{\boldsymbol{r}}^j \delta^{kl} + 3\hat{\boldsymbol{r}}^k \delta^{jl} - 2\hat{\boldsymbol{r}}^l \delta^{jk}}{7680\pi^2 \epsilon_{\text{UV}}} + \frac{\hat{\boldsymbol{r}}^j \delta^{kl} + \hat{\boldsymbol{r}}^k \delta^{jl}}{6400\pi^2} \left[-\frac{2}{3} - 10\log\left(\Lambda r_0 e^{\gamma_{\text{E}}}\right) \right]
$$
$$
- \frac{\hat{\boldsymbol{r}}^l \delta^{jk}}{28800\pi^2} \left[\frac{31}{2} - 30\log\left(\Lambda r_0 e^{\gamma_{\text{E}}}\right) \right] + \frac{3}{1280\pi^2} \hat{\boldsymbol{r}}^j \hat{\boldsymbol{r}}^k \hat{\boldsymbol{r}}^l + O(\epsilon, r_0). \tag{D.13}
$$

D.3 J_{3c}

We again first integrate over $\boldsymbol{p}$, and we regulate the power IR divergence in DR.

$$
\int_{\boldsymbol{p}} \frac{(\boldsymbol{p}' - \boldsymbol{p})^j \boldsymbol{p}^k \boldsymbol{p}^l}{[(\boldsymbol{p}' - \boldsymbol{p})^2](\boldsymbol{p}^2)^3}
$$
$$
= \frac{\Gamma(4)}{\Gamma(3)} \int_0^1 dx \int_{\boldsymbol{p}} \frac{(1-x)^2 (\boldsymbol{p}' - \boldsymbol{p})^j \boldsymbol{p}^k \boldsymbol{p}^l}{[\boldsymbol{p}^2 - 2x\boldsymbol{p} \cdot \boldsymbol{p}' + x\boldsymbol{p}'^2]^4}
$$
$$
= -\frac{\Lambda^{2\epsilon} e^{\epsilon \gamma_{\text{E}}}}{(4\pi)^{3/2}} \frac{\Gamma(5/2 + \epsilon)}{\Gamma(3)} \int_0^1 dx \frac{x(1-x)^4 \boldsymbol{p}'^j \boldsymbol{p}'^k \boldsymbol{p}'^l}{[x(1-x)\boldsymbol{p}'^2]^{5/2+\epsilon}}
$$
$$
- \frac{\Lambda^{2\epsilon} e^{\epsilon \gamma_{\text{E}}}}{2(4\pi)^{3/2}} \frac{\Gamma(3/2 + \epsilon)}{\Gamma(3)} \int_0^1 dx (1-x)^2 \frac{x\delta^{jk}\boldsymbol{p}'^l + x\boldsymbol{p}'^k \delta^{jl} - (1-x)\boldsymbol{p}'^j \delta^{kl}}{[x(1-x)\boldsymbol{p}'^2]^{3/2+\epsilon}}
$$
$$
= -\Lambda^{2\epsilon} e^{\epsilon \gamma_{\text{E}}} \frac{2^{2\epsilon - 7} \Gamma(1/2 + \epsilon) \Gamma(1/2 - \epsilon)}{\pi \Gamma(1 - \epsilon)}
$$
$$
\times \left[(4\epsilon^2 - 9) \frac{\boldsymbol{p}'^j \boldsymbol{p}'^k \boldsymbol{p}'^l}{[\boldsymbol{p}'^2]^{5/2+\epsilon}} + \frac{(1+2\epsilon)(\delta^{jk}\boldsymbol{p}'^l + \boldsymbol{p}'^k \delta^{jl}) + (3-2\epsilon)\boldsymbol{p}'^j \delta^{kl}}{[\boldsymbol{p}'^2]^{3/2+\epsilon}} \right]. \tag{D.14}
$$

Again, this expression does not contain poles in ϵ, so that we can set $\epsilon = 0$ in the finite-r regularized integral, which subtracts the power IR divergence. By using eqs. (D.3) and (D.4),

we obtain in DR

$$
\begin{aligned}
\int_{\boldsymbol{p'}} \int_{\boldsymbol{p}} & \frac{\boldsymbol{p'}^i (\boldsymbol{p'} - \boldsymbol{p})^j \boldsymbol{p}^k \boldsymbol{p}^l}{(\boldsymbol{p}^2 - mE)(\boldsymbol{p'} - \boldsymbol{p})^2 (\boldsymbol{p}^2)^3} \\
&= -\frac{3\delta^{ij}\delta^{kl} - 2\delta^{ik}\delta^{jl} - 2\delta^{il}\delta^{jk}}{7680\pi^2 \epsilon_{\mathrm{UV}}} + \frac{\delta^{ik}\delta^{jl} + \delta^{il}\delta^{jk}}{28800\pi^2} \left[8 + 15\log\left(-\frac{\Lambda^2}{mE}\right)\right] \\
&\quad - \frac{\delta^{ij}\delta^{kl}}{6400\pi^2}\left[1 + 5\log\left(-\frac{\Lambda^2}{mE}\right)\right] + O(\epsilon).
\end{aligned}
\tag{D.15}
$$

Similarly, by using eqs. (D.6) and (D.7) we obtain in finite-r regularization

$$
\begin{aligned}
\int_{\boldsymbol{p'}} \int_{\boldsymbol{p}} & \frac{e^{i\boldsymbol{p'}\cdot\boldsymbol{r}}\hat{\boldsymbol{r}}\cdot\boldsymbol{p'}(\boldsymbol{p'}-\boldsymbol{p})^j \boldsymbol{p}^k \boldsymbol{p}^l}{(\boldsymbol{p}^2 - mE)(\boldsymbol{p'}-\boldsymbol{p})^2(\boldsymbol{p}^2)^3}\bigg|_{|\boldsymbol{r}|=r_0} \\
&= \frac{\hat{\boldsymbol{r}}^k \delta^{jl} + \hat{\boldsymbol{r}}^l \delta^{jk}}{28800\pi^2}\left[\frac{47}{2} - 30\gamma_{\mathrm{E}} - 15\log\left(-r_0^2 mE\right)\right] \\
&\quad - \frac{\hat{\boldsymbol{r}}^j \delta^{kl}}{6400\pi^2}\left[\frac{1}{3} - 10\gamma_{\mathrm{E}} - 5\log\left(-r_0^2 mE\right)\right] - \frac{3}{1280\pi^2}\hat{\boldsymbol{r}}^j\hat{\boldsymbol{r}}^k\hat{\boldsymbol{r}}^l + O(r_0).
\end{aligned}
\tag{D.16}
$$

By subtracting eq. (D.15) from eq. (D.16) we obtain

$$
\begin{aligned}
\frac{1}{m^2}\hat{\boldsymbol{r}}^i & \left(J_{3c}^{ijkl}|_{(r_0)} - J_{3c}^{ijkl}|_{\mathrm{DR}}\right) \\
&= \frac{3\hat{\boldsymbol{r}}^j \delta^{kl} - 2\hat{\boldsymbol{r}}^k \delta^{jl} - 2\hat{\boldsymbol{r}}^l \delta^{jk}}{7680\pi^2 \epsilon} + \frac{\hat{\boldsymbol{r}}^k \delta^{jl} + \hat{\boldsymbol{r}}^l \delta^{jk}}{28800\pi^2}\left[\frac{31}{2} - 30\log\left(\Lambda r_0 e^{\gamma_{\mathrm{E}}}\right)\right] \\
&\quad - \frac{\hat{\boldsymbol{r}}^j \delta^{kl}}{6400\pi^2}\left[-\frac{2}{3} - 10\log\left(\Lambda r_0 e^{\gamma_{\mathrm{E}}}\right)\right] - \frac{3}{1280\pi^2}\hat{\boldsymbol{r}}^j\hat{\boldsymbol{r}}^k\hat{\boldsymbol{r}}^l.
\end{aligned}
\tag{D.17}
$$

E   Convergence of $1/m$ corrections to wavefunctions

In this appendix, we test the validity of the Rayleigh-Schrödinger perturbation theory at first order in computation of the corrections from the $1/m$ potential to S- and P-wave wavefunctions. The radial equation that includes the $1/m$ potential reads

$$
\left[-\frac{1}{m}\left(\frac{\partial^2}{\partial r^2} + \frac{2}{r}\frac{\partial}{\partial r}\right) + V_{\mathrm{LO}}(r) + \frac{V^{(1)}(r)}{m} + \frac{L(L+1)}{mr^2}\right]R(r) = E\, R(r),
\tag{E.1}
$$

where $L = 0$ and 1 for S and P-wave states, respectively. To first order in the Rayleigh-Schrödinger perturbation theory, $R(r)$ is computed from

$$
R(r)|_{\text{first order}} = R_{\mathrm{LO}}(r) - \int_0^\infty dr'\, r'^2\, \hat{G}_n^L(r,r')\frac{V^{(1)}(r')}{m}R_{\mathrm{LO}}(r'),
\tag{E.2}
$$

where $\hat{G}_n^L(r,r')$ is the contribution to the reduced Green's function from orbital angular momentum L defined through the relation

$$
\hat{G}_n(\boldsymbol{r},\boldsymbol{r'}) = \sum_{L=0}^\infty \sum_{M=-L}^{+L} \hat{G}_n^L(r,r')Y_L^M(\hat{\boldsymbol{r}})Y_L^{M*}(\hat{\boldsymbol{r'}}),
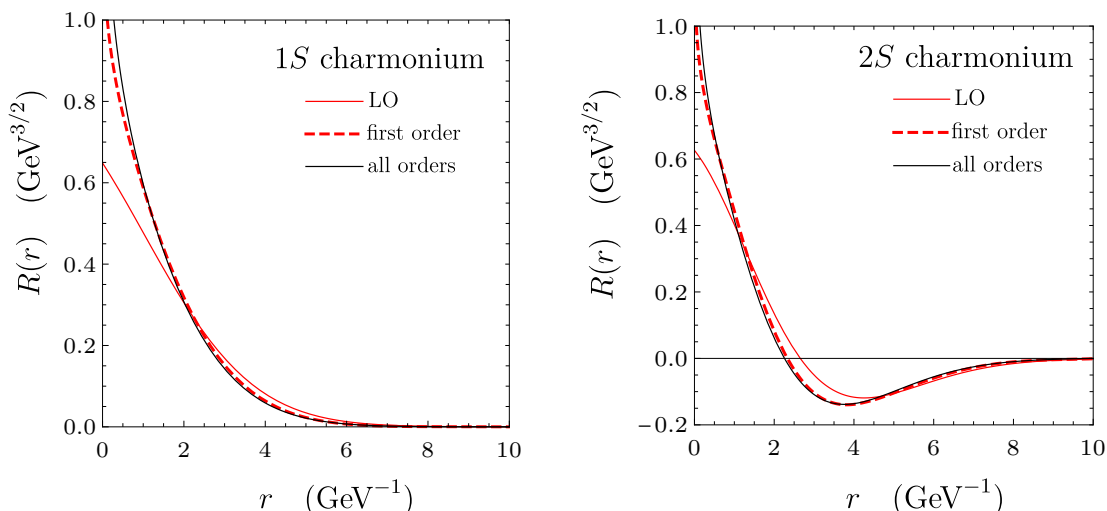\tag{E.3}
$$

Figure 4. Radial wavefunctions for $1S$ and $2S$ states including the effect of the $1/m$ potential to first order in Rayleigh-Schrödinger perturbation theory (red dashed lines) compared to the all-orders calculation (black solid lines). The LO radial wavefunctions are shown as red solid lines for comparison.

and $R_{\text{LO}}(r)$ is the bound-state solution of the LO radial equation

$$\left[-\frac{1}{m}\left(\frac{\partial^2}{\partial r^2} + \frac{2}{r}\frac{\partial}{\partial r} \right) + V_{\text{LO}}(r) + \frac{L(L+1)}{mr^2} \right] R_{\text{LO}}(r) = E_n^{\text{LO}}\, R_{\text{LO}}(r). \qquad \text{(E.4)}$$

The validity of eq. (E.2) can be tested by comparing it with the solution of eq. (E.1). We find the two lowest S-wave and P-wave bound-state solutions of eq. (E.1) by using the modified Crank-Nicolson method in ref. [61]. We use $m = 1.316\,\text{GeV}$ and $\alpha_s = \alpha_s(\mu_R = 2.5\ \text{GeV})$, which are used in our numerical calculations of charmonium wavefunctions. We use the expression for $V^{(1)}(r)$ given in the Wilson-loop matching scheme in eq. (6.3b). For the computation of eq. (E.2), we use the method developed in section 6.1.3 to compute the radial integral.

We show the radial wavefunctions for the $1S$ and $2S$ states in figure 4. For both $1S$ and $2S$ states, the radial wavefunctions computed to first order in the Rayleigh-Schrödinger perturbation theory agree well with the all-orders calculation, showing that the corrections at first order reproduce the bulk of the all-orders correction from the $1/m$ potential. The small deviations at $r \lesssim 1/m$ arise from the fact that the all-orders calculation includes the logarithmic divergences of the form $(\alpha_s^2 \log r)^n$ coming from the $1/m$ potential to higher orders in α_s, while the first-order calculation includes the short-distance divergences only at leading order (order α_s^2). As these are short-distance effects that must be subtracted order by order in α_s through renormalization, the agreements in the region $r > 1/m$ is sufficient to confirm the validity of the Rayleigh-Schrödinger perturbation theory at first order.

Similarly to the S-wave case, we show the radial wavefunctions for the $1P$ and $2P$ states in figure 5. Again, for both $1P$ and $2P$ states, the radial wavefunctions computed to first order in the Rayleigh-Schrödinger perturbation theory agree well with the all-orders calculation, showing that also for the P-wave states, the corrections at first order reproduce the bulk of the all-orders corrections from the $1/m$ potential.
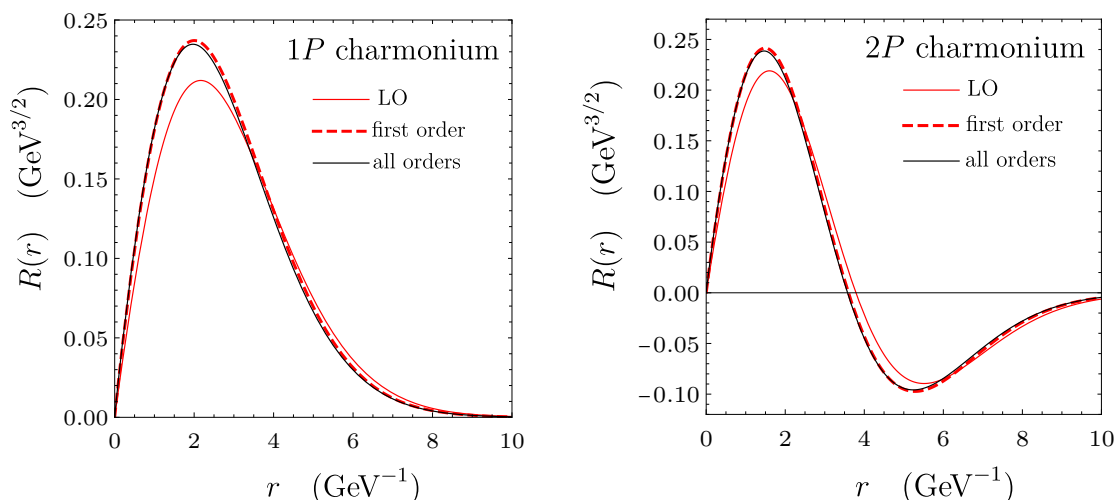
Figure 5. Radial wavefunctions for $1P$ and $2P$ states including the effect of the $1/m$ potential to first order in Rayleigh-Schrödinger perturbation theory (red dashed lines) compared to the all-orders calculation (black solid lines). The LO radial wavefunctions are shown as red solid lines for comparison.

By repeating the same analysis for $m = 4.743\,\text{GeV}$ and $\alpha_s = \alpha_s(\mu_R = 5\text{ GeV})$, we find that the agreements between first-order calculations and all-orders calculations are even better for heavier quark mass. Therefore, we conclude that computing the effect of the $1/m$ potential by using Rayleigh-Schrödinger perturbation theory order by order in the $1/m$ expansion is well justified.

F *P*-wave wavefunctions in perturbative QCD

If we work strictly in perturbative QCD, the LO potential is just the Coulomb potential $V_{\text{LO}}(r) = -\alpha_s C_F/r$, and in this case, the solutions of the LO Schrödinger equation, as well as the Green's function, can be found analytically [112]. For the $L = 1$ case, the P-wave Green's function is given by

$$G^{L=1}(r', r; E) = \frac{2\alpha_s C_F m^3 E}{3}(1 - \lambda)\Gamma(-\lambda)\, r_< r_> \exp\left(-\frac{1}{2\lambda}\alpha_s C_F m(r_< + r_>)\right)$$

$$\times {}_1F_1(2 - \lambda; 4; \alpha_s C_F m r_</\lambda)\, U(2 - \lambda; 4; \alpha_s C_F m r_>/\lambda), \tag{F.1}$$

where $r_< = \min(r, r')$, $r_> = \max(r, r')$, $\lambda = \alpha_s C_F/\sqrt{-4E/m}$, and

$$_1F_1(a; b; z) = \sum_{k=0}^{\infty} \frac{(a)_k}{(b)_k}\frac{z^k}{k!}, \tag{F.2a}$$

$$U(a; b; z) = \frac{1}{\Gamma(a)}\int_0^\infty dt\, e^{-zt} t^{a-1}(1 + t)^{b-a-1}. \tag{F.2b}$$

This result can be obtained from eq. (6.9) by using the expressions for $u_<(r)$ and $u_>(r)$ that are given in terms of the two linearly independent Whittaker functions. The P-wave

α_s	State	$\delta_\Psi^{\rm NC}|_{^3P_0}$	$\delta_\Psi^{\rm NC}|_{^3P_1}$	$\delta_\Psi^{\rm NC}|_{^3P_2}$	$\delta_\Psi^{\rm NC}|_{^1P_1}$
	1P	0.318	0.258	0.201	0.236
0.20	2P	0.296	0.243	0.190	0.222
	3P	0.286	0.236	0.185	0.216
	1P	0.376	0.306	0.238	0.279
0.22	2P	0.350	0.287	0.225	0.263
	3P	0.338	0.279	0.219	0.255
	1P	0.438	0.357	0.278	0.326
0.24	2P	0.407	0.335	0.262	0.306
	3P	0.392	0.324	0.255	0.297
	1P	0.504	0.412	0.320	0.376
0.26	2P	0.468	0.385	0.302	0.353
	3P	0.450	0.373	0.293	0.341
	1P	0.574	0.469	0.365	0.428
0.28	2P	0.532	0.439	0.344	0.402
	3P	0.511	0.424	0.334	0.388
	1P	0.648	0.530	0.413	0.484
0.30	2P	0.599	0.495	0.389	0.453
	3P	0.575	0.478	0.376	0.438
	1P	0.725	0.594	0.463	0.542
0.32	2P	0.669	0.554	0.435	0.507
	3P	0.642	0.534	0.421	0.490
	1P	0.805	0.660	0.515	0.603
0.34	2P	0.742	0.615	0.484	0.564
	3P	0.711	0.593	0.468	0.544
	1P	0.889	0.730	0.570	0.667
0.36	2P	0.818	0.679	0.535	0.623
	3P	0.784	0.654	0.517	0.600

Table 3. Perturbative QCD results for non-Coulombic corrections to the P-wave wavefunctions at the origin $\delta_\Psi^{\rm NC}$ in the $\overline{\rm MS}$ scheme at scale $\Lambda = m$ for $1P$, $2P$, and $3P$ states.

bound states can be identified by the singularities at $\lambda - 1 = 1, 2, 3, \ldots$. The reduced Green's function can be obtained from eq. (F.1), for example by computing the subtraction term in eq. (4.9) from the residue of eq. (F.1) at positive integer values of $\lambda - 1$, which also provides the corresponding LO radial wavefunction. Once the expressions for the reduced Green's functions are obtained, it is in principle possible to compute the perturbative QCD corrections to the P-wave wavefunctions at the origin, especially the $\overline{\rm MS}$-renormalized non-Coulombic corrections $\delta_\Psi^{\rm NC}$, by evaluating the position-space integrals in eq. (6.16). While an analytical calculation of $\delta_\Psi^{\rm NC}$ is outside the scope of this paper, it is a simple task to compute numerically the position-space integrals and obtain values for $\delta_\Psi^{\rm NC}$ in perturbative QCD. We tabulate values of $\delta_\Psi^{\rm NC}$ at the $\overline{\rm MS}$ scale $\Lambda = m$ for various values of the strong coupling α_s in table 3. Note that in perturbative QCD, $\delta_\Psi^{\rm NC}$ is independent of m when $\Lambda = m$. These results can be useful in two-loop calculations of decay and production rates of P-wave bound states in perturbative QCD and in weakly coupled pNRQCD.

References

[1] G.T. Bodwin, E. Braaten and G.P. Lepage, *Rigorous QCD predictions for decays of P wave quarkonia*, *Phys. Rev. D* **46** (1992) R1914 [`hep-lat/9205006`] [INSPIRE].

[2] G.T. Bodwin, E. Braaten, T.C. Yuan and G.P. Lepage, *P wave charmonium production in B meson decays*, *Phys. Rev. D* **46** (1992) R3703 [`hep-ph/9208254`] [INSPIRE].

[3] G.T. Bodwin, E. Braaten and G.P. Lepage, *Rigorous QCD predictions for decays of p wave quarkonia*, `hep-ph/9211253` [INSPIRE].

[4] G.T. Bodwin, E. Braaten and G.P. Lepage, *Rigorous QCD analysis of inclusive annihilation and production of heavy quarkonium*, *Phys. Rev. D* **51** (1995) 1125 [*Erratum ibid.* **55** (1997) 5853] [`hep-ph/9407339`] [INSPIRE].

[5] H.S. Chung, J. Lee and C. Yu, *Exclusive heavy quarkonium + gamma production from e^+e^- annihilation into a virtual photon*, *Phys. Rev. D* **78** (2008) 074022 [`arXiv:0808.1625`] [INSPIRE].

[6] N. Brambilla et al., *Heavy quarkonium: progress, puzzles, and opportunities*, *Eur. Phys. J. C* **71** (2011) 1534 [`arXiv:1010.5827`] [INSPIRE].

[7] N. Brambilla et al., *QCD and strongly coupled gauge theories: challenges and perspectives*, *Eur. Phys. J. C* **74** (2014) 2981 [`arXiv:1404.3723`] [INSPIRE].

[8] N. Brambilla, H.S. Chung and A. Vairo, *Inclusive hadroproduction of P-wave heavy quarkonia in potential nonrelativistic QCD*, *Phys. Rev. Lett.* **126** (2021) 082003 [`arXiv:2007.07613`] [INSPIRE].

[9] N. Brambilla, H.S. Chung and A. Vairo, *Inclusive production of heavy quarkonia in pNRQCD*, *JHEP* **09** (2021) 032 [`arXiv:2106.09417`] [INSPIRE].

[10] A. Czarnecki and K. Melnikov, *Two loop QCD corrections to the heavy quark pair production cross-section in e^+e^- annihilation near the threshold*, *Phys. Rev. Lett.* **80** (1998) 2531 [`hep-ph/9712222`] [INSPIRE].

[11] M. Beneke, A. Signer and V.A. Smirnov, *Two loop correction to the leptonic decay of quarkonium*, *Phys. Rev. Lett.* **80** (1998) 2535 [`hep-ph/9712302`] [INSPIRE].

[12] A. Czarnecki and K. Melnikov, *Charmonium decays: $J/\psi \to e^+e^-$ and $\eta_c \to \gamma\gamma$*, *Phys. Lett. B* **519** (2001) 212 [`hep-ph/0109054`] [INSPIRE].

[13] B.A. Kniehl, A. Onishchenko, J.H. Piclum and M. Steinhauser, *Two-loop matching coefficients for heavy quark currents*, *Phys. Lett. B* **638** (2006) 209 [`hep-ph/0604072`] [INSPIRE].

[14] W.-L. Sang, F. Feng, Y. Jia and S.-R. Liang, *Next-to-next-to-leading-order QCD corrections to $\chi_{c0,2} \to \gamma\gamma$*, *Phys. Rev. D* **94** (2016) 111501 [`arXiv:1511.06288`] [INSPIRE].

[15] W.-L. Sang, F. Feng and Y. Jia, *Next-to-next-to-leading-order radiative corrections to $e^+e^- \to \chi_{cJ} + \gamma$ at B factory*, *JHEP* **10** (2020) 098 [`arXiv:2008.04898`] [INSPIRE].

[16] H.S. Chung, $\overline{MS}$ *renormalization of S-wave quarkonium wavefunctions at the origin*, *JHEP* **12** (2020) 065 [`arXiv:2007.01737`] [INSPIRE].

[17] A.H. Hoang, *Perturbative $O(\alpha_S^2)$ corrections to the hadronic cross-section near heavy quark-anti-quark thresholds in e^+e^- annihilation*, *Phys. Rev. D* **56** (1997) 5851 [hep-ph/9704325] [INSPIRE].

[18] N. Brambilla, W. Chen, Y. Jia, V. Shtabovenko and A. Vairo, *Relativistic corrections to exclusive $\chi_{cJ} + \gamma$ production from e^+e^- annihilation*, *Phys. Rev. D* **97** (2018) 096001 [*Erratum ibid.* **101** (2020) 039903] [arXiv:1712.06165] [INSPIRE].

[19] A. Pineda and J. Soto, *Effective field theory for ultrasoft momenta in NRQCD and NRQED*, *Nucl. Phys. B Proc. Suppl.* **64** (1998) 428 [hep-ph/9707481] [INSPIRE].

[20] N. Brambilla, A. Pineda, J. Soto and A. Vairo, *Potential NRQCD: an effective theory for heavy quarkonium*, *Nucl. Phys. B* **566** (2000) 275 [hep-ph/9907240] [INSPIRE].

[21] N. Brambilla, D. Eiras, A. Pineda, J. Soto and A. Vairo, *New predictions for inclusive heavy quarkonium P wave decays*, *Phys. Rev. Lett.* **88** (2002) 012003 [hep-ph/0109130] [INSPIRE].

[22] N. Brambilla, D. Eiras, A. Pineda, J. Soto and A. Vairo, *Inclusive decays of heavy quarkonium to light particles*, *Phys. Rev. D* **67** (2003) 034018 [hep-ph/0208019] [INSPIRE].

[23] N. Brambilla, A. Pineda, J. Soto and A. Vairo, *Effective field theories for heavy quarkonium*, *Rev. Mod. Phys.* **77** (2005) 1423 [hep-ph/0410047] [INSPIRE].

[24] N. Brambilla, H.S. Chung, D. Müller and A. Vairo, *Decay and electromagnetic production of strongly coupled quarkonia in pNRQCD*, *JHEP* **04** (2020) 095 [arXiv:2002.07462] [INSPIRE].

[25] Y. Kiyo, A. Pineda and A. Signer, *New determination of inclusive electromagnetic decay ratios of heavy quarkonium from QCD*, *Nucl. Phys. B* **841** (2010) 231 [arXiv:1006.2685] [INSPIRE].

[26] A.H. Hoang and P. Ruiz-Femenia, *Heavy pair production currents with general quantum numbers in dimensionally regularized NRQCD*, *Phys. Rev. D* **74** (2006) 114016 [hep-ph/0609151] [INSPIRE].

[27] E. Braaten and Y.-Q. Chen, *Helicity decomposition for inclusive J/ψ production*, *Phys. Rev. D* **54** (1996) 3216 [hep-ph/9604237] [INSPIRE].

[28] E. Braaten and Y.-Q. Chen, *Dimensional regularization in quarkonium calculations*, *Phys. Rev. D* **55** (1997) 2693 [hep-ph/9610401] [INSPIRE].

[29] J.H. Kuhn, J. Kaplan and E.G.O. Safiani, *Electromagnetic annihilation of e^+e^- into quarkonium states with even charge conjugation*, *Nucl. Phys. B* **157** (1979) 125.

[30] B. Guberina, J.H. Kühn, R.D. Peccei and R. Ruckl, *Rare decays of the Z0*, *Nucl. Phys. B* **174** (1980) 317 [INSPIRE].

[31] F. Feng, Y. Jia and W.-L. Sang, *Can nonrelativistic QCD explain the $\gamma\gamma^* \to \eta_c$ transition form factor data?*, *Phys. Rev. Lett.* **115** (2015) 222001 [arXiv:1505.02665] [INSPIRE].

[32] A. Petrelli, M. Cacciari, M. Greco, F. Maltoni and M.L. Mangano, *NLO production and decay of quarkonium*, *Nucl. Phys. B* **514** (1998) 245 [hep-ph/9707223] [INSPIRE].

[33] A. Pineda and A. Vairo, *The QCD potential at $O(1/m^2)$: complete spin dependent and spin independent result*, *Phys. Rev. D* **63** (2001) 054007 [*Erratum ibid.* **64** (2001) 039902] [hep-ph/0009145] [INSPIRE].

[34] K.G. Wilson, *Confinement of quarks*, *Phys. Rev. D* **10** (1974) 2445 [INSPIRE].

[35] L. Susskind, *Coarse grained quantum chromodynamics*, in the proceedings of the *Ecole d'Ete de Physique Theorique — Weak and Electromagnetic Interactions at High Energy*, July 5–Augsut 14, Les Houches, France (1976), p. 207.

[36] L.S. Brown and W.I. Weisberger, *Remarks on the static potential in quantum chromodynamics*, *Phys. Rev. D* **20** (1979) 3239 [InSPIRE].

[37] A. Pineda, *Is there a linear potential at short distances?*, *Nucl. Phys. B Proc. Suppl.* **133** (2004) 190 [hep-ph/0310135] [InSPIRE].

[38] A. Bazavov, N. Brambilla, X.G. Tormo, I, P. Petreczky, J. Soto and A. Vairo, *Determination of α_s from the QCD static energy: An update*, *Phys. Rev. D* **90** (2014) 074038 [*Erratum ibid.* **101** (2020) 119902] [arXiv:1407.8437] [InSPIRE].

[39] N. Brambilla, A. Pineda, J. Soto and A. Vairo, *The QCD potential at O(1/m)*, *Phys. Rev. D* **63** (2001) 014023 [hep-ph/0002250] [InSPIRE].

[40] M. Beneke and V.A. Smirnov, *Asymptotic expansion of Feynman integrals near threshold*, *Nucl. Phys. B* **522** (1998) 321 [hep-ph/9711391] [InSPIRE].

[41] A. Pineda, *Review of heavy quarkonium at weak coupling*, *Prog. Part. Nucl. Phys.* **67** (2012) 735 [arXiv:1111.0165] [InSPIRE].

[42] R. Mertig, M. Böhm and A. Denner, *FEYN CALC: computer algebraic calculation of Feynman amplitudes*, *Comput. Phys. Commun.* **64** (1991) 345 [InSPIRE].

[43] V. Shtabovenko, R. Mertig and F. Orellana, *New developments in FeynCalc 9.0*, *Comput. Phys. Commun.* **207** (2016) 432 [arXiv:1601.01167] [InSPIRE].

[44] V. Shtabovenko, R. Mertig and F. Orellana, *FeynCalc 9.3: new features and improvements*, *Comput. Phys. Commun.* **256** (2020) 107478 [arXiv:2001.04407] [InSPIRE].

[45] N. Brambilla, H.S. Chung, V. Shtabovenko and A. Vairo, *FeynOnium: using FeynCalc for automatic calculations in nonrelativistic effective field theories*, *JHEP* **11** (2020) 130 [arXiv:2006.15451] [InSPIRE].

[46] C. Peset, A. Pineda and M. Stahlhofen, *Potential NRQCD for unequal masses and the B_c spectrum at N^3LO*, *JHEP* **05** (2016) 017 [arXiv:1511.08210] [InSPIRE].

[47] S.J. Brodsky and G.P. Lepage, *Exclusive processes in quantum chromodynamics*, *Adv. Ser. Direct. High Energy Phys.* **5** (1989) 93 [InSPIRE].

[48] V.L. Chernyak and A.R. Zhitnitsky, *Asymptotic behavior of exclusive processes in QCD*, *Phys. Rept.* **112** (1984) 173 [InSPIRE].

[49] Y. Jia and D. Yang, *Refactorizing NRQCD short-distance coefficients in exclusive quarkonium production*, *Nucl. Phys. B* **814** (2009) 217 [arXiv:0812.1965] [InSPIRE].

[50] X.-P. Wang and D. Yang, *The leading twist light-cone distribution amplitudes for the S-wave and P-wave quarkonia and their applications in single quarkonium exclusive productions*, *JHEP* **06** (2014) 121 [arXiv:1401.0122] [InSPIRE].

[51] K.G. Chetyrkin, J.H. Kühn and M. Steinhauser, *RunDec: a Mathematica package for running and decoupling of the strong coupling and quark masses*, *Comput. Phys. Commun.* **133** (2000) 43 [hep-ph/0004189] [InSPIRE].

[52] F. Herren and M. Steinhauser, *Version 3 of RunDec and CRunDec*, *Comput. Phys. Commun.* **224** (2018) 333 [arXiv:1703.03751] [InSPIRE].

[53] C. Peset, A. Pineda and J. Segovia, *The charm/bottom quark mass from heavy quarkonium at N³LO*, *JHEP* **09** (2018) 167 [arXiv:1806.05197] [ɪɴSPIRE].

[54] A. Pineda, *Determination of the bottom quark mass from the Υ(1S) system*, *JHEP* **06** (2001) 022 [hep-ph/0105008] [ɪɴSPIRE].

[55] TXL, T(X)L collaboration, *Static potentials and glueball masses from QCD simulations with Wilson sea quarks*, *Phys. Rev. D* **62** (2000) 054503 [hep-lat/0003012] [ɪɴSPIRE].

[56] Y. Koma and M. Koma, *Heavy quarkonium spectroscopy in pNRQCD with lattice QCD input*, PoS(LATTICE2012)140 [arXiv:1211.6795] [ɪɴSPIRE].

[57] W. Fischler, *Quark-anti-quark potential in QCD*, *Nucl. Phys. B* **129** (1977) 157 [ɪɴSPIRE].

[58] Y. Schröder, *The static potential in QCD to two loops*, *Phys. Lett. B* **447** (1999) 321 [hep-ph/9812205] [ɪɴSPIRE].

[59] M.J. Strassler and M.E. Peskin, *The heavy top quark threshold: QCD and the Higgs*, *Phys. Rev. D* **43** (1991) 1500 [ɪɴSPIRE].

[60] J. Crank and P. Nicolson, *A practical method for numerical evaluation of solutions of partial differential equations of the heat-conduction type*, *Math. Proc. Cambridge Phil. Soc.* **43** (1947) 50.

[61] D. Kang and E. Won, *Precise numerical solutions of potential problems using Crank-Nicholson method*, *J. Comput. Phys.* **227** (2008) 2970 [physics/0609176] [ɪɴSPIRE].

[62] PARTICLE DATA GROUP collaboration, *Review of Particle Physics*, *PTEP* **2020** (2020) 083C01 [ɪɴSPIRE].

[63] G.T. Bodwin, K.-T. Chao, H.S. Chung, U.-R. Kim, J. Lee and Y.-Q. Ma, *Fragmentation contributions to hadroproduction of prompt J/ψ, χcJ, and ψ(2S) states*, *Phys. Rev. D* **93** (2016) 034041 [arXiv:1509.07904] [ɪɴSPIRE].

[64] W. Buchmüller and S.H.H. Tye, *Quarkonia and quantum chromodynamics*, *Phys. Rev. D* **24** (1981) 132 [ɪɴSPIRE].

[65] E.J. Eichten and C. Quigg, *Quarkonium wave functions at the origin*, *Phys. Rev. D* **52** (1995) 1726 [hep-ph/9503356] [ɪɴSPIRE].

[66] G.T. Bodwin, H.S. Chung, D. Kang, J. Lee and C. Yu, *Improved determination of color-singlet nonrelativistic QCD matrix elements for S-wave charmonium*, *Phys. Rev. D* **77** (2008) 094017 [arXiv:0710.0994] [ɪɴSPIRE].

[67] E.J. Eichten and C. Quigg, *Quarkonium wave functions at the origin: an update*, arXiv:1904.11542 [ɪɴSPIRE].

[68] E. Braaten and T.C. Yuan, *Gluon fragmentation into P wave heavy quarkonium*, *Phys. Rev. D* **50** (1994) 3176 [hep-ph/9403401] [ɪɴSPIRE].

[69] Y.-Q. Ma, K. Wang and K.-T. Chao, *QCD radiative corrections to χcJ production at hadron colliders*, *Phys. Rev. D* **83** (2011) 111503 [arXiv:1002.3987] [ɪɴSPIRE].

[70] B. Gong, L.-P. Wan, J.-X. Wang and H.-F. Zhang, *Polarization for prompt J/ψ and ψ(2s) production at the Tevatron and LHC*, *Phys. Rev. Lett.* **110** (2013) 042002 [arXiv:1205.6682] [ɪɴSPIRE].

[71] BESIII collaboration, *Two-photon widths of the χc0,2 states and helicity analysis for χc2 → γγ*, *Phys. Rev. D* **85** (2012) 112008 [ɪɴSPIRE].

[72] BELLE collaboration, *Observation of $e^+e^- \to \gamma\chi_{c1}$ and search for $e^+e^- \to \gamma\chi_{c0}, \gamma\chi_{c2}$, and $\gamma\eta_c$ at $\sqrt{s}$ near* 10.6 *GeV at Belle*, *Phys. Rev. D* **98** (2018) 092015 [`arXiv:1810.10291`] [INSPIRE].

[73] H.S. Chung, J. Lee and C. Yu, *NRQCD matrix elements for S-wave bottomonia and $\Gamma[\eta_b(nS) \to \gamma\gamma]$ with relativistic corrections*, *Phys. Lett. B* **697** (2011) 48 [`arXiv:1011.1554`] [INSPIRE].

[74] M.A. Samuel, G. Li and E. Steinfelds, *Estimating perturbative coefficients in quantum field theory using Pade approximants*, *Phys. Rev. D* **48** (1993) 869 [INSPIRE].

[75] M.A. Samuel, G. Li and E. Steinfelds, *Estimating perturbative coefficients in quantum field theory using Pade approximants. 2.*, *Phys. Lett. B* **323** (1994) 188 [INSPIRE].

[76] J.R. Ellis, M. Karliner, M.A. Samuel and E. Steinfelds, *The anomalous magnetic moments of the electron and the muon: Improved QED predictions using Pade approximants*, `hep-ph/9409376` [INSPIRE].

[77] J.R. Ellis, E. Gardi, M. Karliner and M.A. Samuel, *Pade approximants, Borel transforms and renormalons: the Bjorken sum rule as a case study*, *Phys. Lett. B* **366** (1996) 268 [`hep-ph/9509312`] [INSPIRE].

[78] M.A. Samuel, J.R. Ellis and M. Karliner, *Comparison of the Pade approximation method to perturbative QCD calculations*, *Phys. Rev. Lett.* **74** (1995) 4380 [`hep-ph/9503411`] [INSPIRE].

[79] R. Barbieri, R. Gatto, R. Kogerler and Z. Kunszt, *Meson hyperfine splittings and leptonic decays*, *Phys. Lett. B* **57** (1975) 455 [INSPIRE].

[80] W. Celmaster, *Lepton width suppression in vector mesons*, *Phys. Rev. D* **19** (1979) 1517 [INSPIRE].

[81] P. Marquard, J.H. Piclum, D. Seidel and M. Steinhauser, *Three-loop matching of the vector current*, *Phys. Rev. D* **89** (2014) 034027 [`arXiv:1401.3004`] [INSPIRE].

[82] M. Beneke et al., *Leptonic decay of the $\Upsilon(1S)$ meson at third order in QCD*, *Phys. Rev. Lett.* **112** (2014) 151801 [`arXiv:1401.3005`] [INSPIRE].

[83] A.H. Hoang and T. Teubner, *Top quark pair production at threshold: Complete next-to-next-to-leading order relativistic corrections*, *Phys. Rev. D* **58** (1998) 114023 [`hep-ph/9801397`] [INSPIRE].

[84] K. Melnikov and A. Yelkhovsky, *The b quark low scale running mass from Upsilon sum rules*, *Phys. Rev. D* **59** (1999) 114009 [`hep-ph/9805270`] [INSPIRE].

[85] A.A. Penin and A.A. Pivovarov, *Bottom quark pole mass and $|V_{cb}|$ matrix element from $R(e^+e^- \to b\bar{b})$ and $\Gamma_{sl}(b \to cl\nu)$ in the next to next-to-leading order*, *Nucl. Phys. B* **549** (1999) 217 [`hep-ph/9807421`] [INSPIRE].

[86] A.H. Hoang and T. Teubner, *Top quark pair production close to threshold: Top mass, width and momentum distribution*, *Phys. Rev. D* **60** (1999) 114027 [`hep-ph/9904468`] [INSPIRE].

[87] K. Melnikov and A. Yelkhovsky, *Top quark production at threshold with $O(\alpha_S^2)$ accuracy*, *Nucl. Phys. B* **528** (1998) 59 [`hep-ph/9802379`] [INSPIRE].

[88] O.I. Yakovlev, *Top quark production near threshold: NNLO QCD correction*, *Phys. Lett. B* **457** (1999) 170 [`hep-ph/9808463`] [INSPIRE].

[89] M. Beneke, A. Signer and V.A. Smirnov, *Top quark production near threshold and the top quark mass*, *Phys. Lett. B* **454** (1999) 137 [hep-ph/9903260] [INSPIRE].

[90] T. Nagano, A. Ota and Y. Sumino, $O(\alpha_s^2)$ *corrections to* $e^+e^- \to t\bar{t}$ *total and differential cross-sections near threshold*, *Phys. Rev. D* **60** (1999) 114014 [hep-ph/9903498] [INSPIRE].

[91] A.A. Penin and A.A. Pivovarov, *Analytical results for* $e^+e^- \to t\bar{t}$ *and* $\gamma\gamma \to t\bar{t}$ *observables near the threshold up to the next-to-next-to leading order of NRQCD*, *Phys. Atom. Nucl.* **64** (2001) 275 [hep-ph/9904278] [INSPIRE].

[92] A.A. Penin, A. Pineda, V.A. Smirnov and M. Steinhauser, *Spin dependence of heavy quarkonium production and annihilation rates: complete next-to-next-to-leading logarithmic result*, *Nucl. Phys. B* **699** (2004) 183 [*Erratum ibid.* **829** (2010) 398] [hep-ph/0406175] [INSPIRE].

[93] M. Beneke, Y. Kiyo and K. Schuller, *Third-order Coulomb corrections to the S-wave Green function, energy levels and wave functions at the origin*, *Nucl. Phys. B* **714** (2005) 67 [hep-ph/0501289] [INSPIRE].

[94] W.-Y. Keung and I.J. Muzinich, *Beyond the static limit for quarkonium decays*, *Phys. Rev. D* **27** (1983) 1518 [INSPIRE].

[95] M.E. Luke and M.J. Savage, *Power counting in dimensionally regularized NRQCD*, *Phys. Rev. D* **57** (1998) 413 [hep-ph/9707313] [INSPIRE].

[96] G.T. Bodwin, H.S. Chung, J. Lee and C. Yu, *Order-α_s corrections to the quarkonium electromagnetic current at all orders in the heavy-quark velocity*, *Phys. Rev. D* **79** (2009) 014007 [arXiv:0807.2634] [INSPIRE].

[97] R. Barbieri, M. Caffo, R. Gatto and E. Remiddi, *Strong QCD corrections to p wave quarkonium decays*, *Phys. Lett. B* **95** (1980) 93 [INSPIRE].

[98] R. Barbieri, M. Caffo, R. Gatto and E. Remiddi, *QCD corrections to P wave quarkonium decays*, *Nucl. Phys. B* **192** (1981) 61 [INSPIRE].

[99] W.-L. Sang and Y.-Q. Chen, *Higher order corrections to the cross section of* $e^+e^- \to$ *quarkonium + gamma*, *Phys. Rev. D* **81** (2010) 034028 [arXiv:0910.4071] [INSPIRE].

[100] N. Brambilla, A. Pineda, J. Soto and A. Vairo, *The infrared behavior of the static potential in perturbative QCD*, *Phys. Rev. D* **60** (1999) 091502 [hep-ph/9903355] [INSPIRE].

[101] B.A. Kniehl and A.A. Penin, *Ultrasoft effects in heavy quarkonium physics*, *Nucl. Phys. B* **563** (1999) 200 [hep-ph/9907489] [INSPIRE].

[102] A.V. Smirnov, V.A. Smirnov and M. Steinhauser, *Fermionic contributions to the three-loop static potential*, *Phys. Lett. B* **668** (2008) 293 [arXiv:0809.1927] [INSPIRE].

[103] C. Anzai, Y. Kiyo and Y. Sumino, *Static QCD potential at three-loop order*, *Phys. Rev. Lett.* **104** (2010) 112003 [arXiv:0911.4335] [INSPIRE].

[104] A.V. Smirnov, V.A. Smirnov and M. Steinhauser, *Three-loop static potential*, *Phys. Rev. Lett.* **104** (2010) 112002 [arXiv:0911.4742] [INSPIRE].

[105] S.N. Gupta, S.F. Radford and W.W. Repko, *Quarkonium spectra and quantum chromodynamics*, *Phys. Rev. D* **26** (1982) 3305 [INSPIRE].

[106] J.T. Pantaleone and S.H.H. Tye, *The hyperfine splitting of P states in heavy quarkonia*, *Phys. Rev. D* **37** (1988) 3337 [INSPIRE].

[107] S. Titard and F.J. Yndurain, *Rigorous QCD evaluation of spectrum and ground state properties of heavy $q\bar{q}$ systems: with a precision determination of $m_b M(\eta_b)$*, *Phys. Rev. D* **49** (1994) 6007 [hep-ph/9310236] [INSPIRE].

[108] A.V. Manohar and I.W. Stewart, *The QCD heavy quark potential to order v^2: one loop matching conditions*, *Phys. Rev. D* **62** (2000) 074015 [hep-ph/0003032] [INSPIRE].

[109] B.A. Kniehl, A.A. Penin, M. Steinhauser and V.A. Smirnov, *Non-Abelian $\alpha^3(s)/(m(q)R^2)$ heavy quark anti-quark potential*, *Phys. Rev. D* **65** (2002) 091503 [hep-ph/0106135] [INSPIRE].

[110] B.A. Kniehl, A.A. Penin, V.A. Smirnov and M. Steinhauser, *Potential NRQCD and heavy quarkonium spectrum at next-to-next-to-next-to-leading order*, *Nucl. Phys. B* **635** (2002) 357 [hep-ph/0203166] [INSPIRE].

[111] M. Beneke, Y. Kiyo and K. Schuller, *Third-order correction to top-quark pair production near threshold I. Effective theory set-up and matching coefficients*, arXiv:1312.4791 [INSPIRE].

[112] R. A. Mapleton, *Characteristic Coulomb Green's function and its eigenfunction expansion*, *J. Math. Phys.* **2** (1961) 478.